POSITRONS: PRACTICAL PLASMA PROBE?

by

UǦIS OSKARS ZIEMELIS
B.Sc., McMaster University, 1974

A THESIS SUBMITTED IN PARTIAL FULFILLMENT OF
THE REQUIREMENTS FOR THE DEGREE OF
MASTER OF SCIENCE

in

The Faculty of Graduate Studies
Department of Physics

We accept this thesis as conforming
to the required standard

The University of British Columbia
September, 1976

Department of Physics

The University of British Columbia
2075 Wesbrook Place
Vancouver, Canada
V6T 1W5

Date: September 27, 1976

ABSTRACT

The feasibility of using positrons to probe plasmas is investigated. Analysis of the γ rays resulting from the annihilation of positrons with plasma electrons may yield information about the momentum distribution, temperature and number density of these electrons.

A number of 'positron probe' success criteria are introduced and a wide range of positron-plasma systems are evaluated in light of these criteria. Of special importance are positron annihilation time (τ_a) and thermalization time (τ_t) calculations, which indicate that the most important success criterion, $\tau_t < \tau_a$, is satisfied by the class of plasmas characterized by $kT_e > 10$ eV. Two potential fusion plasmas, namely Tokamak and laser compression plasmas, belong to this class (where some positron diagnostic techniques may be practical). Detailed fractional thermalization calculations for positrons from a ^{22}Na source in hypothetical, fully ionized H_2 plasmas of these types indicate that most positrons will thermalize and annihilate while the plasma environment is in existence.

Positron sources, including pair creation, which is predicted to occur in both Tokamak and laser compression plasmas, and γ ray detectors are discussed. Annihilation γ ray counting rates are estimated under a variety of circumstances for both NaI(Tℓ) and Ge(Li) detectors to prepare the way for the assessment of specific positron diagnostic techniques. Four such techniques are evaluated with reference to both Tokamak and laser compression plasmas.

It is concluded that diagnostic techniques involving measurements of shift and broadening of the annihilation line appear most promising in both cases. The measurement of positron lifetimes may be possible in some Tokamak plasmas, but is not feasible in laser compression plasmas. 'Slow' positron probing of plasmas would be ideal, but slow positron sources of sufficient intensity do not yet exist. Angular correlation measurements do not appear feasible at this time.

TABLE OF CONTENTS

LIST OF TABLES

LIST OF FIGURES

ACKNOWLEDGMENTS

Writing a thesis is quite an experience - an experience that is enriched immensely by other people - at every stage. For this enrichment, thank you to all! But special thanks to Dr. Boye Ahlborn who suggested the four p's (plasma, positrons, practical, probe) and who has been a fine supervisor. Discussions were numerous and always helpful - hearty thanks to Dr. A.J. Barnard, Dr. G. Jones and Dr. A.T. Stewart.

The financial assistance of the National Research Council of Canada was definitely invaluable and is indeed appreciated. Some of this financial assistance ended up with Shari Haller, who in return did a superb job of typing this thesis.

There is one person in a far away place, who played a rather mystical role in all this . . . thank you, Mārīte.

Kas visu grib zināt . . . tas ātri paliek vecs

[He who wants to know it
all . . . quickly grows old.]

Latvian proverb

Chapter I

INTRODUCTION

"On 2 August 1932, Dr. Carl D. Anderson discovered the positive electron." This is indeed, as Hanson (1963) puts it, a statement whose "innocent, matter-of-fact tone conceals one of the most intricate and interesting chapters in the history of scientific discovery" - a chapter which is still being actively written. Anderson's 'positively charged electron' was identified soon after its discovery as the 'negative energy electron' of Dirac's hole theory (Dirac, 1930). The new particle, or positron, as it was named, became the focus of much basic research which continues even today to be fruitful.

Initial experiments were designed to determine the properties of the positron and in addition, to study its unique interaction with matter. Characteristic of this interaction is the annihilation reaction (between a colliding electron and positron) which generates one, two or three γ photons as illustrated schematically in Figure 1a.

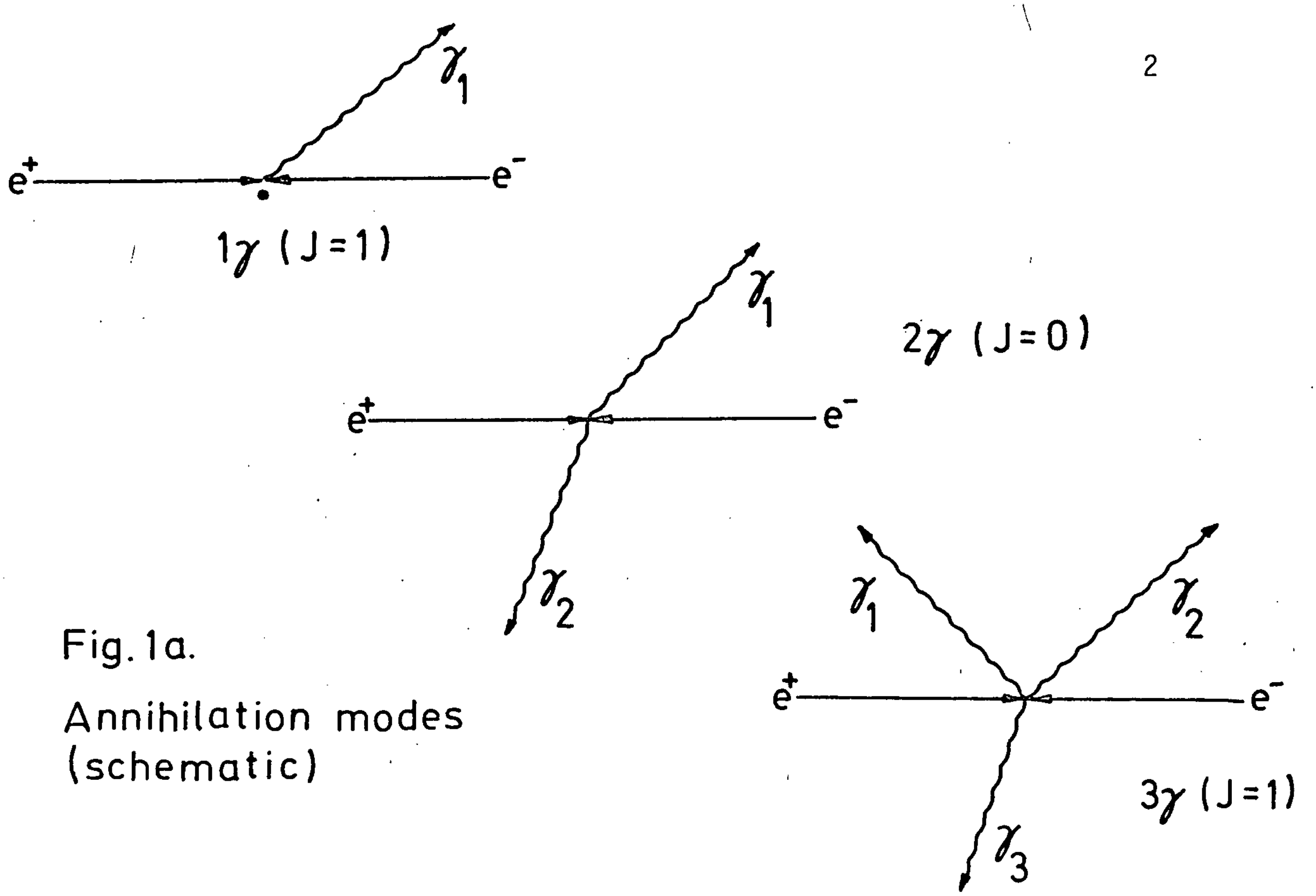

Fig. 1a.
Annihilation modes (schematic)

The momenta and energies of the annihilation γ photons are related, through the action of conservation laws, to the energy and centre of mass momentum of the pre-annihilation pair. It is possible to determine the distribution of electron-positron pair centre of mass velocities by observing the annihilation γ photons which escape the sample under scrutiny. Such observations form the basis of a number of intriguing 'positron probe' diagnostic techniques which have been used to study solids, liquids and gases.*

---

*It should be noted that during the course of the early positron experiments, a positron-electron bound state was identified (Deutsch, 1951) and a new line of positron research initiated. This bound state, whose existence was originally suggested by Mohorovicic (1934) came to be known as positronium (Ruark, 1945). In some cases positronium (Ps) plays a part in the diagnostic techniques which utilize 'free' or unbound positrons as probes.

The use of positrons to probe plasmas was proposed initially by V.I. Goldanskii (1961) and independently by B.P. Konstantinov (in Toptygin, 1962). However, with the exception of the work of Lohnert and Schneider (1971) no experimental investigations involving positrons and plasmas have been carried out (based on a 1975 literature search).* It is the purpose of this work to assess the feasibility of using positrons to probe plasmas.

The recent interest in positrons has various causes: first, the success of positron techniques in other states of matter; secondly, the possibility that positron techniques may be useful in the highly compressed laser plasma regime where standard optical diagnostic techniques fail because the plasma densities are greater than the cut-off densities for visible radiation (annihilation gamma photons penetrate these dense plasmas easily); thirdly, the possibility that positrons may be produced through natural pair production in some plasma devices (e.g. by run-away electrons in Tokamak type plasmas), thus raising the question of whether these positrons (as opposed to positrons introduced from an external source) or their annihilation products could reveal any information about

---

*The work of Lohnert and Schneider does not constitute a true positron approach because their technique does not demand the use of positrons; in fact, it is complicated by the use of positrons as opposed to electrons (to be discussed in Chapter VII).

the plasma itself; and fourthly, the recent development of high resolution gamma ray analysis techniques.

In scope, this thesis is meant to be a survey, yet it is also meant to present specific conclusions concerning the feasibility of using positrons to probe plasmas. It reviews the necessary theoretical material and discusses the basic aspects of plasma diagnostics using positrons, including objectives, success criteria, positron sources and gamma ray detectors. The feasibility of four positron diagnostic techniques (measurements involving: 2γ angular correlation, annihilation line broadening, positron lifetimes, and slow positron beam spread) is studied in detail and counting rate calculations are carried out for positrons annihilating in Tokamak and laser compression plasmas. Results indicate that specific techniques are feasible under certain plasma conditions. See Chapter VIII for a summary of the results.

Chapter II

POSITRON REVIEW

A. Positron Preview

This chapter details the physical characteristics of the positron with a special emphasis on those aspects which make it such a unique diagnostic tool. In this light, some established diagnostic techniques are described and a number of illustratory experiments cited. Those familiar with positron techniques may bypass this chapter without loss of continuity.

B. The Positron: Basic Physical Properties

The positron is the antiparticle of the electron, the anti-electron, thus annihilation can take place between the two. This annihilation results in the emission of one, two, or three γ photons, depending on the relative spin orientation of the interacting particles (Figure 1a). Various conservation requirements guarantee that annihilations where the respective spins are antiparallel (total angular momentum:

J = 0) result in the emission of an even number of gamma photons (2γ annihilation). On the other hand, the parallel spin situation (J = 1) must be accompanied by the emission of an odd number of quanta (1γ and 3γ annihilation). One γ annihilation can occur only in the presence of a third body capable of absorbing the recoil momentum associated with the emission of a single γ photon. The annihilation process can be either bound annihilation (bound state formed between the positron and the electron prior to annihilation) or free annihilation (no bound state formed).

The first calculation of an annihilation cross-section was carried out by Dirac (1930) for the 2γ-free annihilation case, with the result:

$$\sigma_{2\gamma} = \frac{\pi r_0^2}{\Gamma + 1}\left[\frac{\Gamma^2 + 4\Gamma + 1}{\Gamma^2 - 1} \ln\left(\Gamma + \sqrt{\Gamma^2 - 1}\right) - \frac{\Gamma + 3}{\sqrt{\Gamma^2 - 1}}\right] \qquad (1)$$

where $\Gamma = 1/\sqrt{1 - v^2/c^2}$, v is the relative positron-electron velocity (Dirac assumes the electron at rest); and $r_0 = e^2/mc^2$ is the classical electron radius. In the non-relativistic case where v << c expression (1) reduces to

$$\sigma_{2\gamma} = \frac{\pi r_0^2 c}{v} \qquad (2)$$

Since annihilation is a collision induced process (the positron and electron must be in the immediate vicinity of each other if it is to occur), the cross section can be written as

$$\sigma = \frac{\nu}{nv} \tag{2a}$$

It follows that the expression for the 2γ annihilation rate, $\nu_{2\gamma}$, is energy independent:

$$\nu_{2\gamma} = \frac{1}{\tau_{2\gamma}} = \pi r_0{}^2 cn \tag{3}$$

where $\tau_{2\gamma}$ is the time required for a 2γ annihilation to occur (positron lifetime)

and n is the electron number density of the medium in which the annihilation takes place.

The 2γ annihilation mode is the most probable, therefore detailed discussion will be restricted to this mode. (Specifically $\sigma_{\gamma}/\sigma_{2\gamma}$ is of order α^4 and $\sigma_{3\gamma}/\sigma_{2\gamma}$ is of order α where $\alpha = e^2/\hbar c \simeq 1/137$). A more complete discussion of annihilation modes can be found in Appendix A.*

In the case of 2γ annihilation from rest, the spectrum is a delta function at a γ energy of $E(\gamma) = mc^2$,

---

*As previously indicated, in some cases an electron-positron bound state (positronium) forms before annihilation occurs. This 'hydrogen-like atom' has a binding energy of 6.76 eV and exists in two states: singlet or para-positronium (particle spins opposed; J = 0) and triplet or ortho-positronium (particle spins parallel; J = 1). Although many factors can influence the lifetime (annihilation time) of positronium, it does not, like the free annihilation time (equation 3), depend on the electron number density of the medium in a straightforward way. Additional information can be found in Appendix A.

where m is the positron or electron rest mass. Each γ photon carries away one electron rest mass energy and to conserve linear momentum they exit from the annihilation site in opposite directions (separation angle ϕ = 180° - see Figure 1b). This, of course, is a specific case; in general, the positron-electron pair is moving when it annihilates. The c. of m. motion is reflected in the motions of the annihilation photons in that it introduces (among other effects) a departure from collinear emission of these photons; they exit from the annihilation site separated by some angle $\phi < 180°$.

Consider Figure 1c. As viewed from the laboratory reference frame, just prior to annihilation the positron and electron have a centre of mass momentum: $\underset{\sim}{p}(e^+ + e^-) = \underset{\sim}{p}(e^+) + \underset{\sim}{p}(e^-)$ and a total energy $\varepsilon_t(e^+ + e^-) = 2mc^2 + E(e^+) + E(e^-)$, where $\underset{\sim}{p}$ represents linear momentum and E, kinetic energy. After annihilation, the γ photons exit with momenta $\underset{\sim}{p}(\gamma_{1,2})$ and energies $E(\gamma_{1,2})$. In most cases the magnitude of the centre of mass momentum of the pair, $p(e^+ + e^-) << mc$ and hence θ, the angle of deviation from 180° photon separation is small. In such cases, it is a good approximation to write $p(\gamma_1) = p(\gamma_2) \simeq mc$. Under these circumstances,

$$p_{\perp}(e^+ + e^-) \simeq mc \sin\theta \qquad (4)$$

or

$$p_{\perp}(e^+ + e^-) \simeq mc\,\theta \qquad \text{(for small } \theta\text{)}, \qquad (5)$$

Fig. 1b. Annihilation from rest.

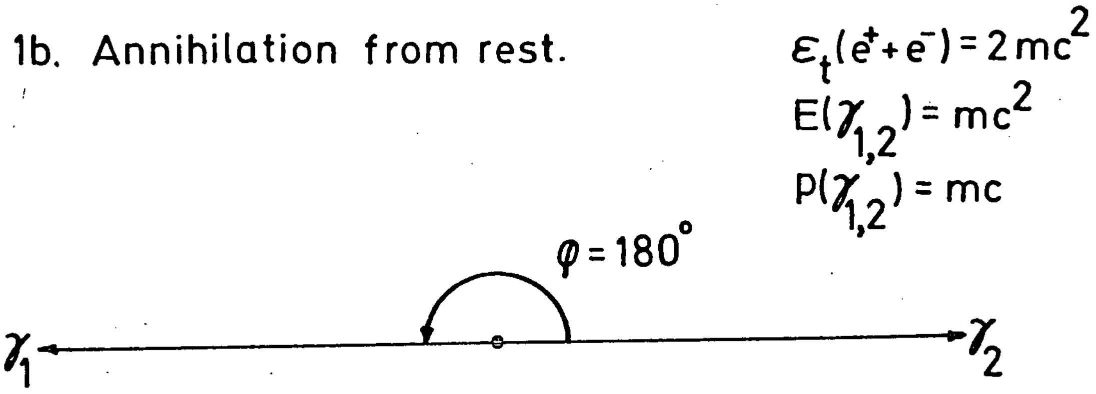

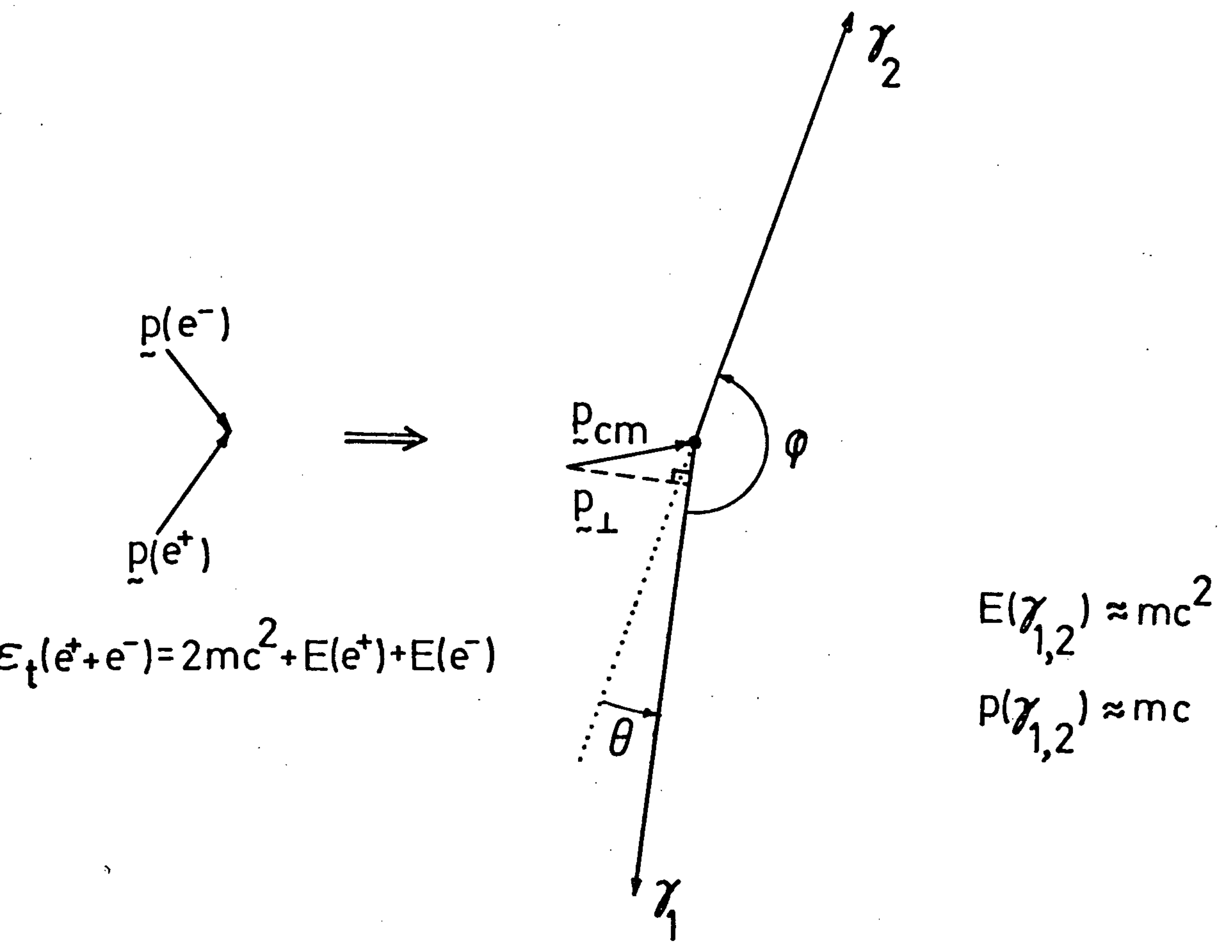

Fig. 1c. Annihilation in motion (not to scale).

where $\underset{\sim}{p}_{\perp}$ is the magnitude of the component of $\underset{\sim}{p}_{cm}$ perpendicular to the direction of emission of the γ photon under consideration (see Figure 1c).

Both photon energies remain almost equal to mc^2; deviations result from the initial positron-electron kinetic energy contributions: $E(e^+)$ and $E(e^-)$. Additional details and exact expressions for energy and momentum sharing between the two annihilation gamma photons can be found in Appendix B.

The energy spectrum associated with 3γ annihilation is shown in Figure 2 (Ore and Powell, 1949). (On this plot, the 2γ spectrum would be a delta function at $E(\gamma) = mc^2$). In a 3γ process, the energy divides three ways; any one given photon can carry away an energy ranging from zero to mc^2.

C. Established Diagnostic Techniques

Two diagnostic techniques become immediately obvious from the previous discussion. Positron lifetime analysis and 2γ angular correlation techniques are being applied sucessfully to study solids, liquids and gases.

(i) 2γ Angular Correlation

Measurements of the deviation angle, θ yield information about the positron-electron centre of mass momentum. The 2γ angular correlation technique involves 'coincidence counting' photons that have originated from a single annihilation

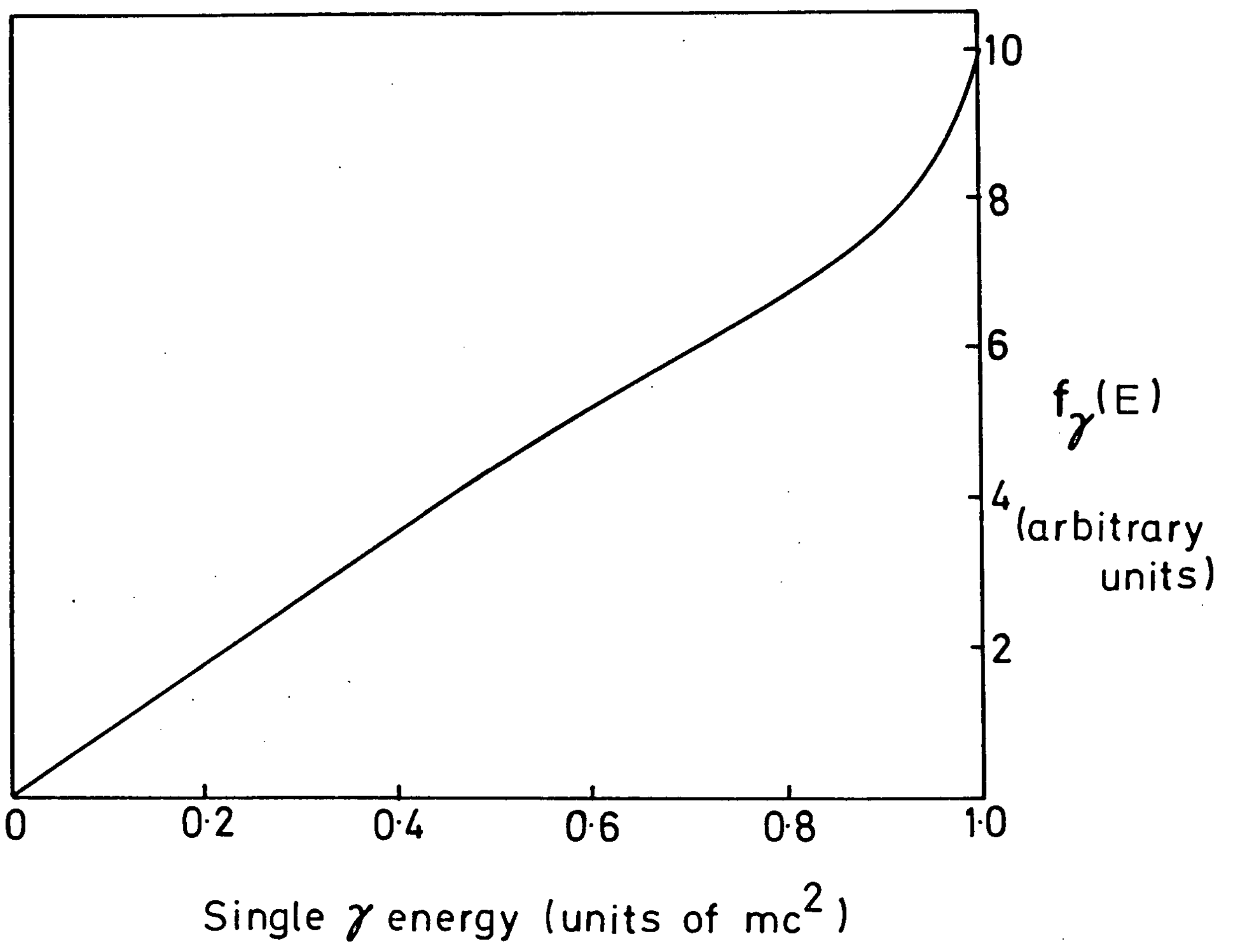

Fig. 2. Energy spectrum of photons from 3γ annihilation.

as a function of the deviation angle of one detector from colinearity with the other detector. (A typical arrangement is that of Lang and DeBeneditti (1957), see Figure 3). Note that the apparatus does not measure the deviation angle θ, but θ_z, the projection of θ on the yz plane. This and the vertical slit geometry make the instrument sensitive to only one centre of mass momentum component of the annihilating pair (in this case the z component, $\underset{\sim}{p}_z$). If the relation between the centre of mass momentum distribution in the z direction (which should be directly reflected by the coincidence counting rate, c) and θ_z is known, then N(p), the distribution in magnitude of centre of mass momentum can be found. Here, $p = |\underset{\sim}{p}(e^+ + e^-)|$, the magnitude of the positron-electron centre of mass momentum.

With the geometry sketched in Figure 3, the coincidence counting rate can be written as the following one-dimensional integral:

$$c(\theta_z) \propto \int_{p_z}^{\infty} \rho(p) p \, dp, \tag{6}$$

where $\rho(p)$ is the probability of finding an annihilating pair with momentum p in dp. The distribution in magnitude of momentum is usually expressed as:

$$N(p) = 4\pi \, p^2 \, \rho(p) \tag{7}$$

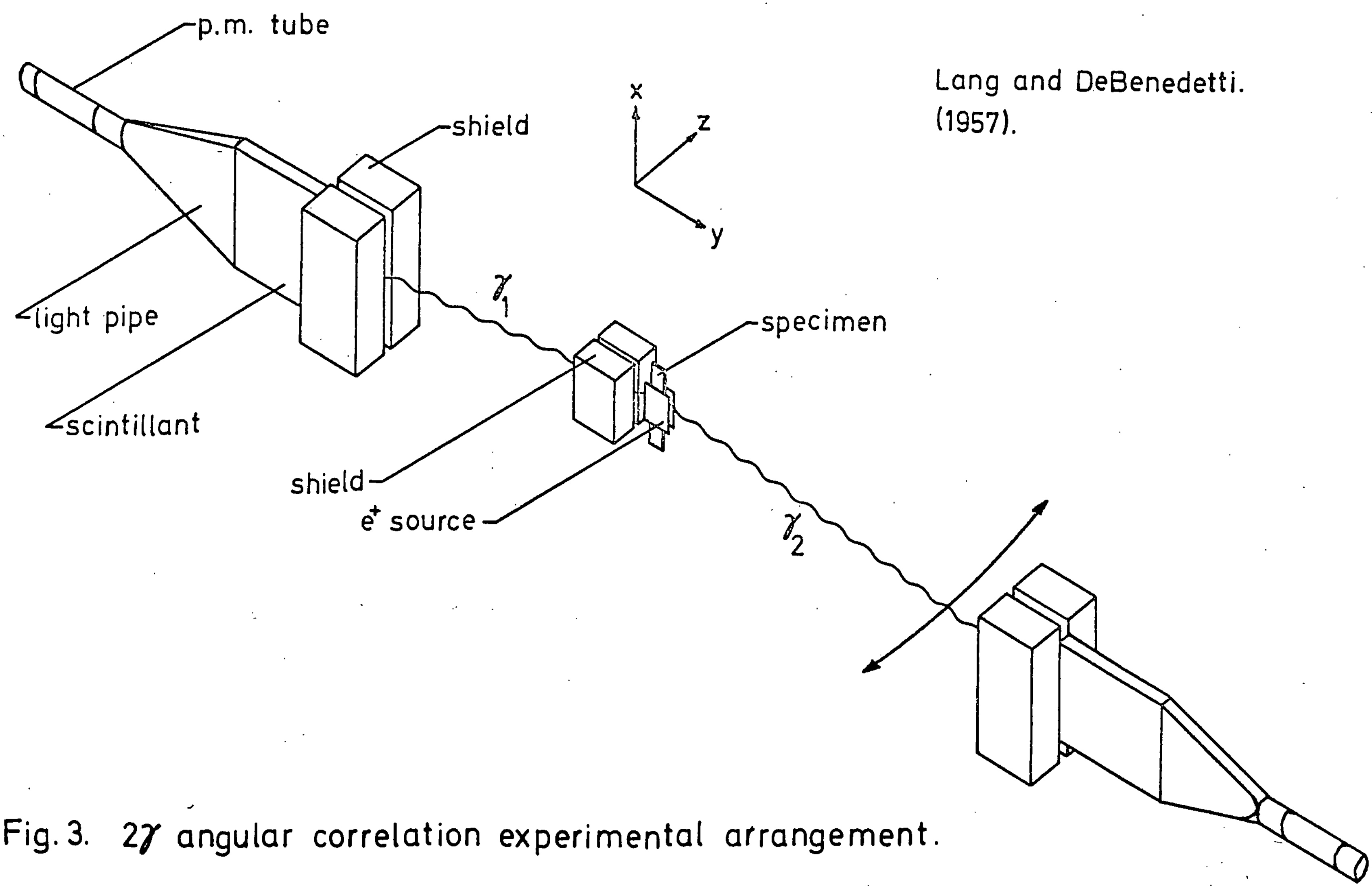

Fig. 3. 2γ angular correlation experimental arrangement.

Substituting for $\rho(p)$ in (6) and differentiating with respect to p yields:

$$N(p) \;\alpha\; p \frac{dc(\theta_z)}{dp}$$

or

$$N(p) \;\alpha\; \theta_z \frac{dc(\theta_z)}{d\theta_z} , \tag{8}$$

using expression (5) to relate p and θ_z. Thus, N(p) can be calculated in a straightforward manner once $c(\theta_z)$ has been measured.

In metals, where electron energies are of the order of electron volts, the deviation angle θ falls in the milliradian range. Even so, the 2γ angular correlation technique is powerful. An excellent example of the application of this technique is the early work of Stewart (1957) with metals. Figure 4 shows some results of this work: $\rho(k)$ and N(k) curves for annihilations in Period IVb metals (k α p here). Contributions from both low momentum conduction electrons (narrow component) and high momentum core electrons (broad component) are clearly visible. The Fermi energy, E_F, marks the boundary between these two components as expected.* With

*The momentum scale in Figure 4 should be interpreted as indicating electron momentum, although, strictly speaking it indicates positron-electron centre of mass momentum. This is a very good approximation because the positrons thermalize to mean energies of the order of 0.025 eV (at room temperature) and annihilate with electrons of the solid which are hundreds of times more energetic, with the result that almost all of the momentum passed on to the annihilation gamma photons comes from the electrons. This is not the case in plasmas, essentially because plasma electrons are not bound.

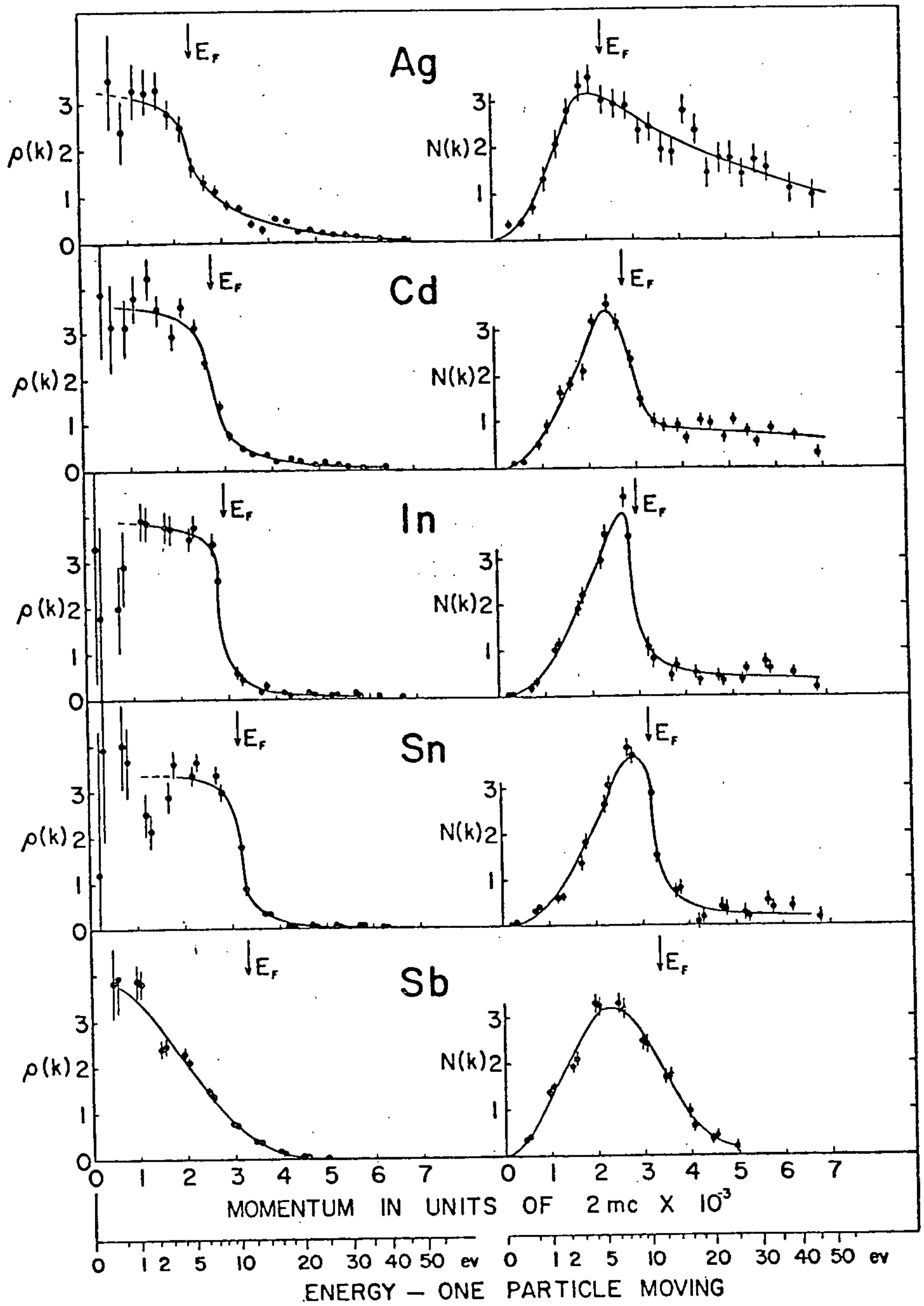

Fig. 4. Angular correlation results of Stewart (1957) for some Period IVb metals.

experimental results like these, Stewart and others have established 2γ angular correlation as a valuable diagnostic technique of the solid state.

(ii) Positron Lifetime Measurements

Dirac's expression (3) indicates that the positron lifetime (annihilation time) is inversely proportional to electron density, thus positron lifetime measurements should yield information about electron densities. Note that this is so because annihilation is a collision induced process which can be described by a cross section of the type defined in expression (2a). The first lifetime measurements (Shearer and Deutsch, 1949) and subsequent work (Deutsch, 1951) established the multi-component nature of positron lifetime spectra for a number of gases. One component was consistent with the Dirac expression (3) and was attributed to free annihilations; the others were attributed to annihilation of various bound states.*

Figure 5 shows Deutsch's apparatus (Deutsch, 1953). A gamma photon emitted almost simultaneously with each positron from the ^{22}Na source was used to trigger the counting circuitry and a stop pulse was supplied by one of the annihilation gamma photons. Deutsch employed a delayed coincidence counting

*It is generally considered that this work verified the existence of the bound state positronium.

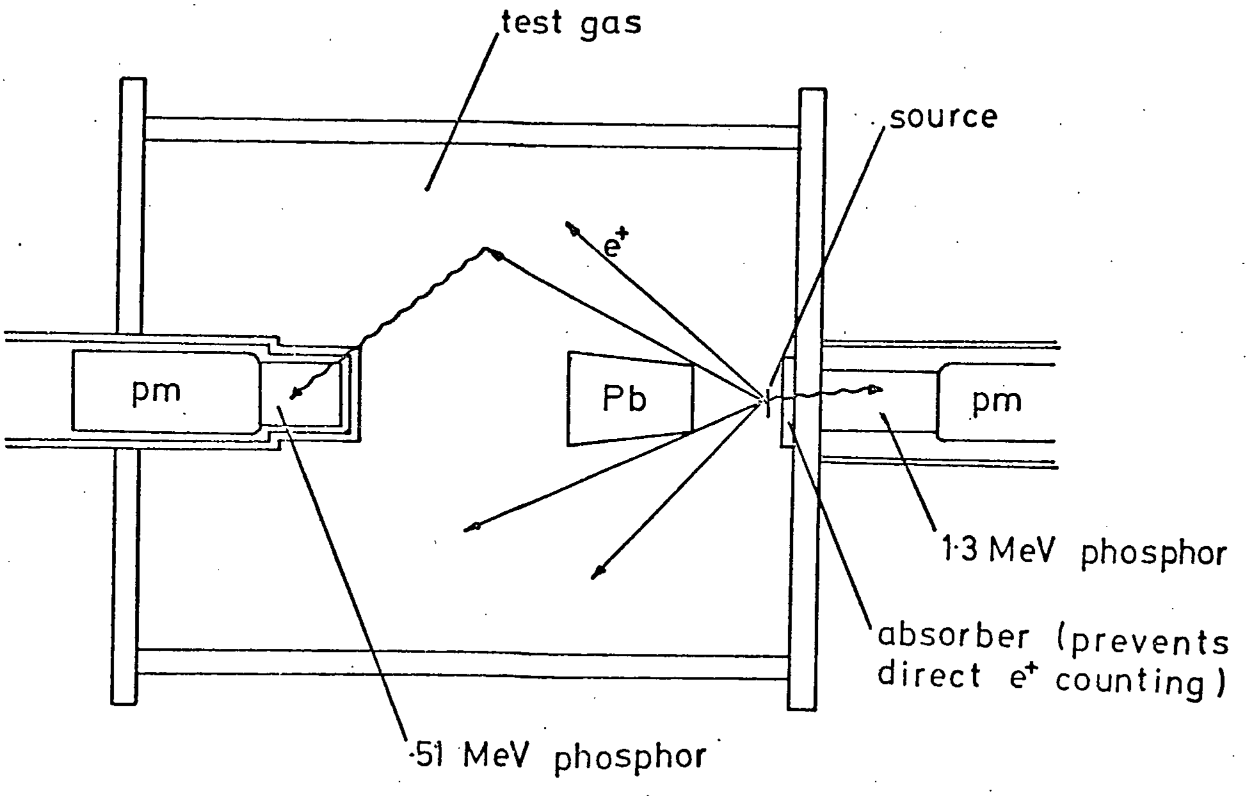

Fig. 5. Deutsch's positron lifetime apparatus.

technique to build up the lifetime spectra. With the advent of improved counting techniques, positron lifetimes have been measured in a very large number of substances in gaseous, solid and liquid states. Although quantitatively, some corrections have been applied to (3) to gain agreement with experimental results (Chapter IV, Section C), qualitatively, lifetimes do vary inversely with the electron density. In solids and liquids, free annihilation lifetimes are of the order of 10^{-10} sec as compared to 10^{-7} sec in gases. A lifetime listing can be found in Hogg *et al.* (1968).

A survey of techniques has not been attempted here.* The techniques mentioned are by way of example: to illustrate successful approaches and to establish physical correlates to the concepts introduced in Section B. These techniques and others will be examined in terms of their usefulness with respect to plasma diagnostics in Chapter VII.

---

*An up-to-date discussion of positron techniques being applied to probe the solid state can be found in a review article by West (1973).

Chapter III

POSITRONS IN PLASMAS

A. Positron-Plasma Survey

What are the basic plasma measurement objectives? What conditions must be satisfied if positrons are to be used to help realize these objectives? What is the fate of a positron in a plasma? Answers to these three questions form the basis of this chapter.

If positrons could somehow be introduced into a plasma (see Chapter V) their effective temperature (energy) would, in most cases, be much greater than the plasma electron temperature (energy). Thus, the positrons would be expected to lose energy to the plasma and in so doing, to slow to average plasma electron velocities in a characteristic thermalization time τ_t. The annihilation process, characterized by an annihilation time, τ_a, would compete as an energy loss mechanism with the thermalization process. The latter part of this chapter deals qualitatively and quantitatively with this multimechanism energy-loss process. A number of slowing down mechanisms are discussed and appropriate energy loss equations are introduced.

B. Plasma Measurement Objectives

Mean temperature and mean number density are the two prime parameters which characterize a given plasma. Due to the multicomponent nature of a plasma, there are in fact three mean temperatures and densities that must be considered - those describing the electrons, ions and neutrals. In some cases ('well-behaved plasmas') the mean component temperatures are identical, or almost so, and in others ('bad plasmas') this is not the case. More complete characterizations include information of varying spatial and temporal resolution on component velocity distributions (or the deviation thereof from the ideal Maxwell-Boltzmann distributions), particle collision frequencies (collision cross-sections) and some macroscopic properties (e.g. pressure).

Although it is not inconceivable that positrons could yield information about the ions and neutrals of a plasma (through annihilation with their electrons), they are uniquely suited to measure all of the above mentioned electron parameters: temperature, density, distribution of velocities and collision frequencies.

C. The Positron as a Plasma Probe: Feasibility Criteria

If a 'positron probe' method is to be an ideal plasma diagnostic technique, then it must satisfy a number of basic criteria. These fall into two categories: general (applicable to all diagnostic approaches) and specific (applicable to positron approaches only). A summary appears in Table I.

(i) General Criteria

a. $$\Delta\tau_{Macro} > \tau_i > \Delta\tau_{Micro} \tag{10}$$

The interrogation or sampling time (τ_i) should be shorter than $\Delta\tau_{Macro}$, the time that characterizes macroscopic plasma changes such as bulk flow, but longer than the characteristic microscopic change time (relaxation time), $\Delta\tau_{Micro}$. It is reasonable to demand the degree of time resolution suggested by the LHS (A) of the inequality to escape averaging over large scale fluctuations. The LHS can be written as $\tau_i < \frac{d_{plasma}}{c_s}$ where $\Delta\tau_{Macro}$ has been approximated by the ratio of the average plasma dimension(size), d_{plasma}, to the appropriate sound speed c_s.* The RHS (B) of the inequality

*This yields, for example, $\Delta\tau_{Macro} \simeq 10^{-8}$ sec with d = 1 mm and T_e (electron temperature) = 1KeV; $\Delta\tau_{Macro} \simeq 10^{-4}$ sec with d = 1 m and T_e = 100 eV.

Table I

Plasma Diagnostic Technique Feasibility Criteria

	General Criteria (All Diagnostic Techniques)	Specific Criteria (Positron Diagnostic Techniques)
Time	$\Delta\tau_{Macro} > \tau_i > \Delta\tau_{Micro}$	$\tau_{p\ell} > \tau_a > \tau_t$
Distance	$d_f > d_{Probe} > \lambda_D$	$R_t < d_{plasma}$
		Reasonable γ Ray Counting Rates

$\Delta\tau_{Macro}$: Characteristic Macroscopic Plasma Variation Time

$\Delta\tau_{Micro}$: " Microscopic " " "

τ_i : Plasma Interrogation (Sampling) Time

d_f : Characteristic Large Scale Plasma Fluctuation Dimension

d_{probe} : Probe Dimension

λ_D : Debye Length

$\tau_{p\ell}$: Plasma Lifetime

τ_a : Positron Lifetime (Annihilation Time)

τ_t : Positron Thermalization Time

R_t : Positron Range During Thermalization

d_{plasma} : Mean Plasma Size

guarantees that the system being 'interrogated' has achieved local uniformity and hence can be meaningfully described by a mean temperature parameter (T_e, for example). The time required for a few electron-electron collisions (say 10) is usually indicative of $\Delta\tau_{Micro}$.

With reference to positron techniques: each individual annihilation constitutes an instantaneous sampling event, however time averaging is to be expected due to the spread (in time) of annihilation events when more than one positron is being considered. The magnitude of the spread depends on the characteristics of the annihilation medium and the type of positron source being used (e.g. pulsed or continuous). This spread guarantees that the effective τ_i is greater in magnitude than $\Delta\tau_{Micro}$, thus satisfying requirement (B). In some cases the spread may be so large that the effective τ_i is in fact greater in magnitude than $\Delta\tau_{Macro}$, with the result: poor time resolution (requirement A not satisfied). This is a potential problem if good time resolution is required.

b. $$d_f > d_{Probe} > \lambda_D \qquad (11)$$

A B

The probe dimension, d_{Probe}, should be less than the characteristic dimension of large scale plasma fluctuations, d_f, but greater than the Debye length, λ_D. The LHS (A) of this inequality guarantees a spatial resolution finer than the large scale fluctuations, thus eliminating averaging over such fluctuations (characteristically of size ~ $d_{plasma}/10$). On the other hand, the RHS (B) insures that averaging will take place over distances shorter than the Debye length:

$$\lambda_D = \sqrt{\frac{kT_\alpha}{4\pi \sum_\alpha n_\alpha q_\alpha^2}} \quad , \tag{12}$$

where α is the component subscript (electrons or ions)

k is the Boltzman constant

T is the temperature

n is the number density

and q is the charge,

thus averaging out the non-uniformities that begin to appear on this size scale.

Again, with reference to positron approaches: although individual positrons, in annihilating with individual electrons, sample 'very small regions', a large number of positrons distributed throughout a plasma samples essentially the entire plasma. Thus, averaging over distances of the order λ_D certainly occurs; however, averaging also occurs over distances of the order d_f, making spatial resolution poor. The spatial resolution situation could be improved by localizing all the positrons to a particular region of the plasma or by looking at only those annihilation gamma rays originating from a specific volume of plasma. Of course, if situations arise where averaging over the plasma is desired, positron techniques are, in this respect, ideal.

(ii) <u>Specific Criteria</u>

a.

$$\underbrace{\tau_{p\ell} > \tau_a}_{A} > \tau_t \tag{13}$$

Obviously, the positron annihilation time τ_a must be less than the plasma lifetime, $\tau_{p\ell}$, (A) if positrons are to annihilate in plasma conditions. In addition, the positrons should be thermalized with the plasma electrons at the point of or prior to annihilation with these electrons (thermalization time less than annihilation time - B). This requirement that mean positron energies be of the order of (or less than) mean electron energies at annihilation insures that the perturbation of the annihilation gammas associated with electron motion is comparable in magnitude (and hence detectable) to the perturbation associated with the positron motion. If a 1 KeV positron annihilates with a 1 eV electron, the perturbation of the annihilation γ photons due to the pre-annihilation electron motion is certainly not detectable.

b.

$$R_t < d_{plasma} \tag{14}$$

In the most desirable situation, the majority of positrons introduced into a plasma for diagnostic purposes would annihilate in the plasma and not in surrounding materials. If this is to be the case, the positron range within the plasma (R_t) must be less than the average plasma dimension d_{plasma}.

c. All diagnostic techniques involving the use of positrons are based on the counting of the annihilation γ photons, using one of a number of methods (e.g. 2γ-coincidence), therefore, counting statistics must be considered. Such a consideration involves many factors (see Chapter VII), however the key requirement is that counting times be reasonably short (reasonably large counting rates). Precise limiting magnitudes will often be dictated by individual experimental arrangements.

Evaluation of various positron diagnostic techniques with reference to these 'specific feasibility criteria' forms the bulk of the latter part of this study.

D. The Life of a Positron in a Plasma

The life of an energetic positron in a plasma consists essentially of energy loss processes which it undergoes in an attempt to reach equilibrium with its surroundings. These processes will differ for positrons in a partially ionized environment and positrons in a fully ionized environment. Although later chapters deal only with fully ionized plasmas, a brief sketch of the partially ionized situation will be presented here.

(i) Partially Ionized Plasmas

A positron slowing down in a partially ionized plasma will pass through three characteristic interaction stages (Figure 6a). The first (I) involves a rapid energy loss through inelastic collisions, resulting in the degradation of the positron energy from the source level (0.5 to a few MeV) to ~50 or a few hundred eV. Most of the collisions that occur during this high energy stage result in ionization of neutral plasma particles or additional ionization of existing plasma ions. Positrons with energies less than a few hundred eV begin to undergo elastic collisions with the various species present in the plasma. In stage II (positron energies from a few hundred eV to the minimum excitation energy - all species considered), energy losses associated with elastic collisions are comparable to those associated with inelastic collisions. Positrons with energies less than V_i (minimum ionization energy - all species considered) can no longer initiate ionization reactions (where the ionization electron escapes). Energy loss in the energy gap: V_i to V_e (minimum excitation energy - all species considered) occurs by excitation collisions and elastic collisions.

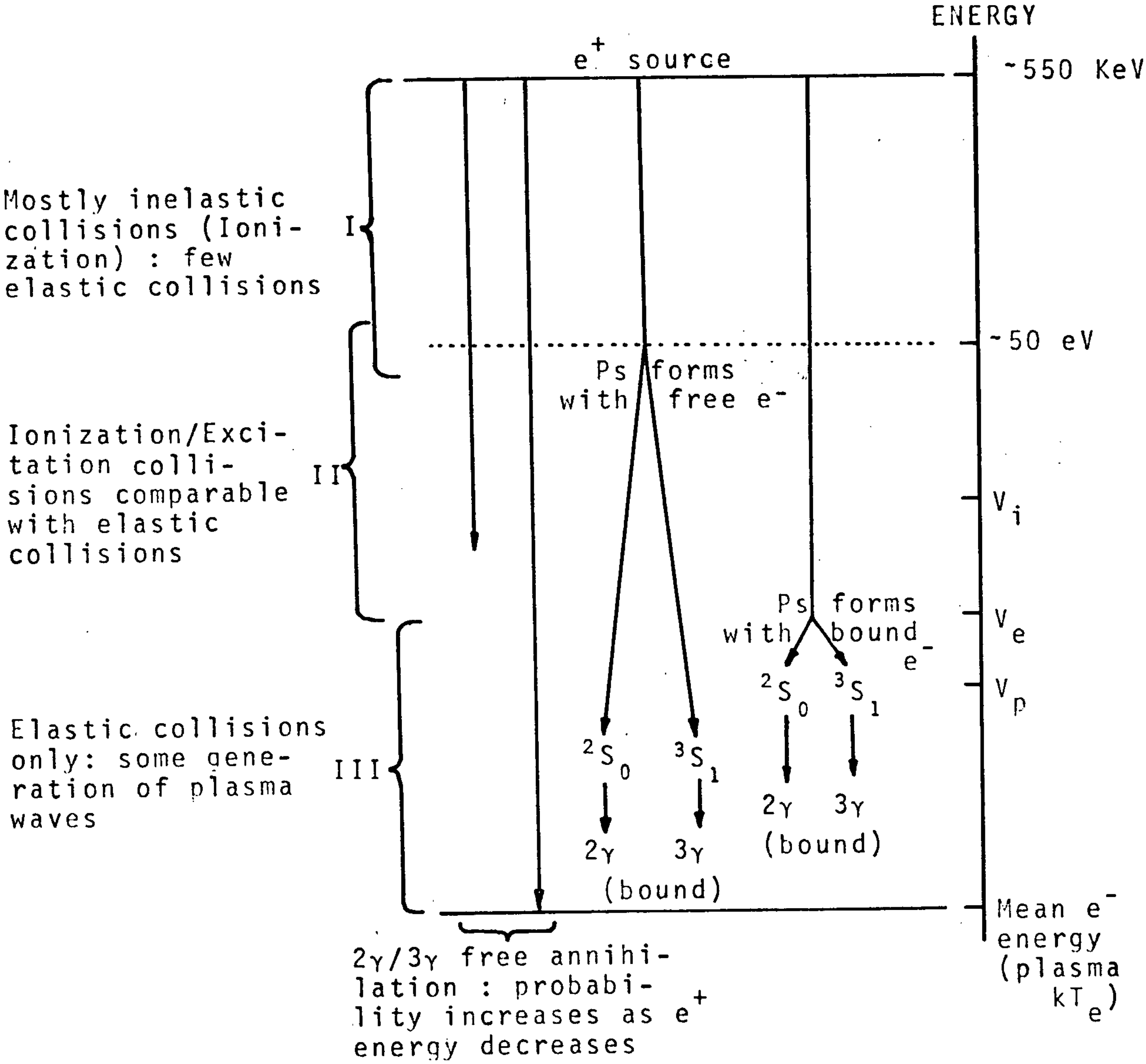

V_i: lowest ionization potential

V_e: lowest excitation potential

V_p: Ps formation threshold with bound e^-

Fig. 6a. e^+ in partially ionized plasmas.

Stage III (positron energies from V_e to the background electron temperature) is characterized by energy loss through elastic collisions, including a component attributable to excitation of plasma oscillations (for details see discussion of fully ionized plasmas).

Superimposed on this energy degradation scheme are the possible annihilation modes. At positron energies greater than roughly 50 eV, elastic and inelastic collision cross sections are much greater than annihilation cross sections, thus the former processes predominate almost exclusively.* Some free annihilation and positronium formation (this possibility is discussed in Appendix C) is expected to occur in the low energy stages II and III. The probability that these reactions will occur prior to thermalization (undesirable) as opposed to after thermalization (desirable), depends on the specific nature of the plasma in question (species present, T_e, n_e). This topic will be considered in detail in the next two chapters.

(ii) Fully Ionized Plasmas

A fully ionized plasma consists of only two species: free electrons and bare nuclei. A positron losing energy in

---

*For example: ionization cross sections in the KeV range are of the order of 10^{-16} to 10^{-17} cm^2 as compared to annihilation cross sections (Dirac) of the order of 10^{-25} to 10^{-24} cm^{-2}.

such a medium (Figure 6b) can do so only through elastic collisions, all inelastic energy loss options having been eliminated. As in the case of partially ionized plasmas, some pre-thermalization annihilation and positronium formation may take place (see also Appendix C).

Although the positron energy loss process consists essentially of elastic collisions, it is useful for the sake of analysis, to divide these collisions into two types. (I and II), according to the energy (momentum) transfer per collision. Type I are termed 'hard' or binary collisions, in the sense that they are characterized by a close (small impact parameter) interaction between two particles with large momentum transfer. Type II, on the other hand, are 'soft' collisions characterized by distant (large impact parameter) interactions between more than two particles, with a small total momentum transfer. A collision of the latter type corresponds to the creation of a plasma wave or waves (plasmons), that is, the creation of a quantum (or a number of quanta) of directed collective momentum (by some directed individual momentum). A rough dividing line between these two types of collision can be drawn at a momentum transfer of $\Delta p_D = \hbar k_D = \hbar/\lambda_D$ (where λ_D is the Debye radius), corresponding to the creation of a plasma wave described by a wavevector of magnitude $k_D = 1/\lambda_D$. The two regions thus defined are:

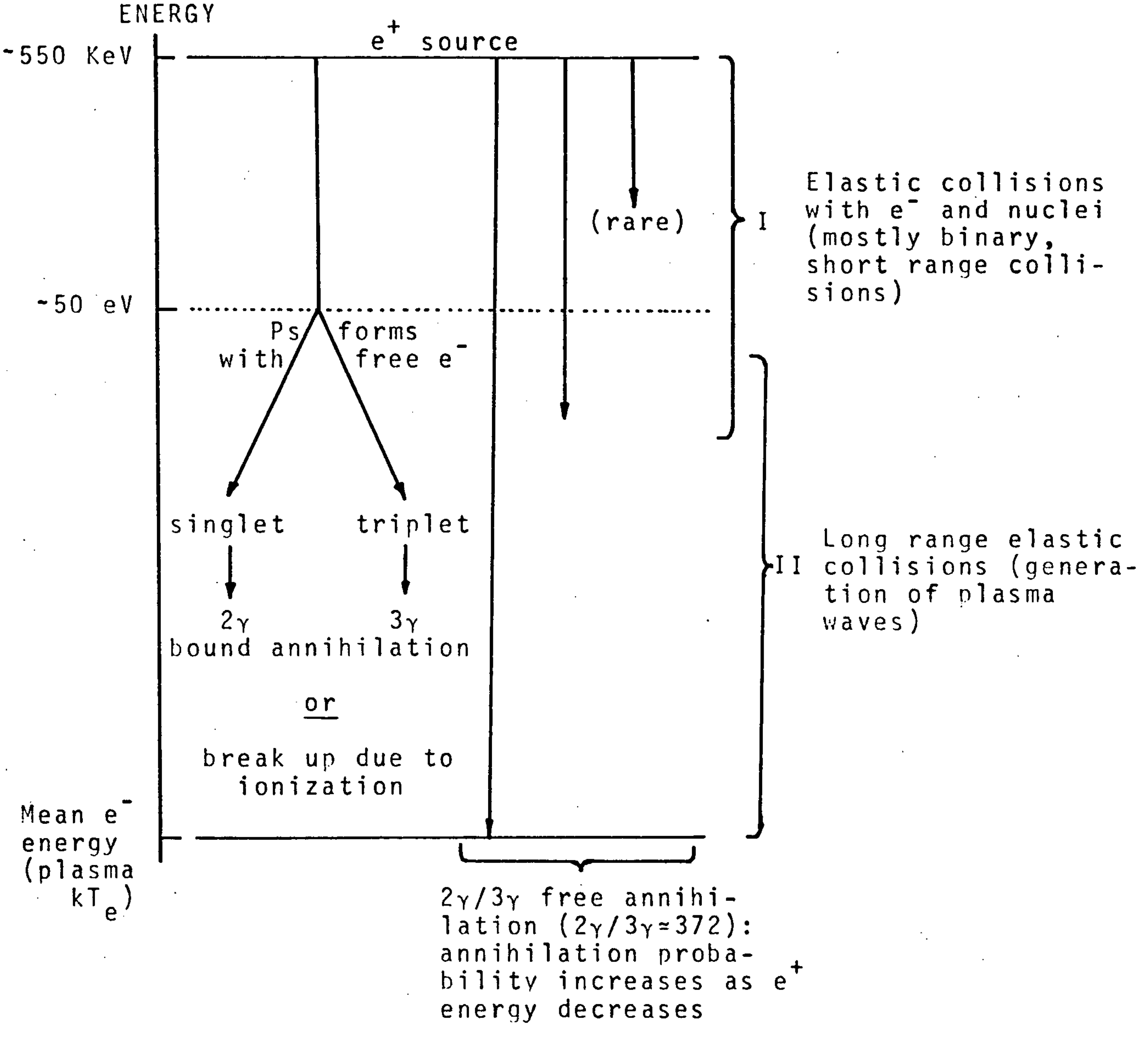

Fig. 6b. e^+ in fully ionized plasmas.

$$\Delta p_D < \Delta p < \Delta p_{max} \qquad \text{Type I} \tag{15}$$

Here, $k(=\Delta p/\hbar) > k_D$, corresponds to hard collisions. Actually, the wave idea breaks down for $\Delta p > \Delta p_D$, which corresponds to the creation of plasma waves shorter than the Debye radius - a physical impossibility since meaningful particle correlations (such as waves) are possible only on scales larger than λ_D. Δp_{max} represents the largest possible single-collision momentum transfer.

$$\Delta p_{min} < \Delta p < \Delta p_D \qquad \text{Type II} \tag{16}$$

Here, $k < k_D$, corresponds to soft collisions or the generation of plasma waves with wavelengths: $\lambda > \lambda_D$ (a meaningful situation). Δp_{min} represents the smallest possible momentum transfer.

E. Positron Energy Loss Rate

Calculation of the positron energy loss rate by summing the contributions of Type I and Type II collisions yields (details in Appendix D):

$$-\frac{dE}{dt} = \frac{e^2 \; \omega_e^2}{v} \ln\left(\frac{2mv^2}{\hbar \; \omega_e}\right) \tag{17}$$

where $\omega_e = \left(\frac{4\pi \; n \; e^2}{m}\right)^{\frac{1}{2}}$ is the plasma frequency,

n is the plasma electron number density,

e is the magnitude of the positron or electron elementary charge,

m is the mass of the electron or positron,

v is the velocity of the positron,

v_e is the velocity of the electron,

$\hbar = h/2\pi$ (h is Planck's constant),

and $v > v_e$.

This result was originally obtained by Bethe (1930) and is substantiated by the results obtained by Larkin (1959) using quantum field techniques. Note that the energy loss as expressed by (17) is independent of the plasma temperature. (mean plasma electron velocity). Husseiny and Forsen (1970), using an alternate technique (details in Appendix D), derive a plasma temperature dependent expression for the energy loss rate:

$$-\frac{dE}{dt} = \left(\frac{1}{4\pi\varepsilon_0}\right)^2 \frac{e^2\,\omega_e^{\,2}}{2\pi v} \ln\left[(4\pi\varepsilon_0)^{\frac{1}{2}} \frac{m\,v_e\,v}{2\hbar\,\omega_e}\right] \tag{18}$$

(rationalized MKS units - ε_0 is the permittivity of free space)

The appearance of $v_e v$ as opposed to v^2 in the argument of the logarithm does not greatly alter the energy loss rate (Figure 7), nor does it greatly alter thermalization time values based on expressions which follow from (17) and (18) by integration (Chapter IV).

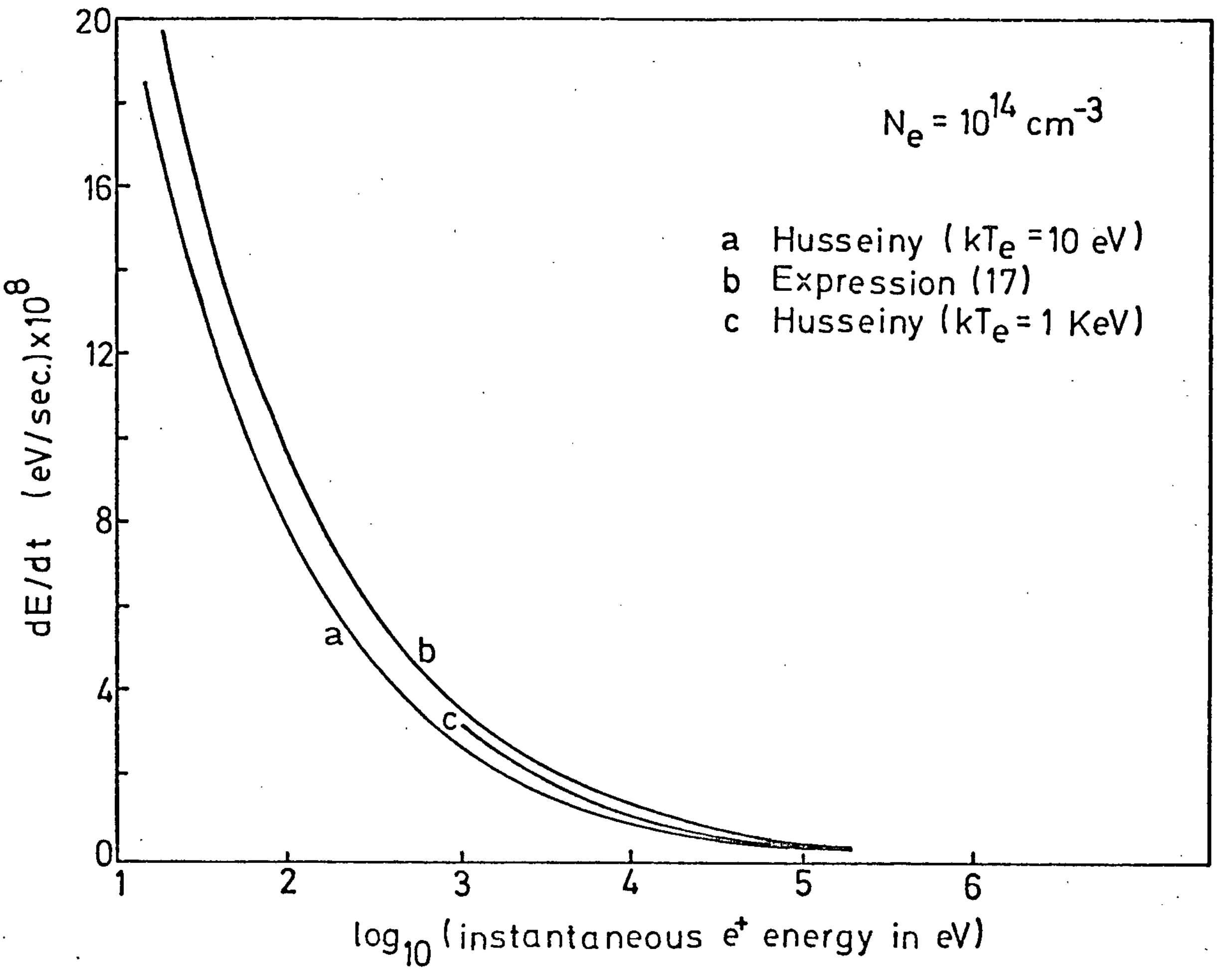

Fig. 7. Positron energy loss rate curves for fully ionized H_2.

A number of typical energy loss rate curves are plotted in Figure 7 for purposes of illustration and comparison. These calculations have been carried out for positrons (initial energy - 500 KeV) in a fully ionized hydrogen plasma, at various electron temperatures. The energy loss associated with positron-ion collisions is insignificant and has been ignored (see Appendix D).

Chapter IV

POSITRON ANNIHILATION/THERMALIZATION TIMES AND RANGES

A. Calculation Summary

Of the feasibility criteria mentioned in the previous chapter, those involving positron thermalization times and ranges are the most important. This chapter is devoted to detailed calculations of thermalization times (τ_t), annihilation time (τ_a) and thermalization ranges (R_t). Calculations are carried out over a wide range of plasma parameters, assuming a fully ionized hydrogen plasma:

$$10^{8} < n(\mathrm{cm}^{-3}) < 10^{26} \text{ and } 10^{-1} < Te(\mathrm{eV}) < 10^{4} \; *$$

Calculated values of τ_t and τ_a are used to delimit those regions of the n-T_e plane where positron diagnostics might be suitable (i.e. those regions where $\tau_t < \tau_a$). Two regions

---

*Strictly speaking, a fully ionized hydrogen plasma will not exist for the lowest T_e values being considered (T_e < ~ 5eV). In this range, the approximation of all collisions as elastic will yield upper limit values for thermalization times and ranges. Exact calculations for the partially ionized cases have not been carried out.

of interest are analyzed in detail, with reference to the thermalization behaviour of positrons from a ^{22}Na source and curves of per cent of positrons thermalized as a function of time and range are calculated.

B. Range and Time Expressions

The mean range and mean thermalization time of a positron with an initial energy E_i can be expressed in integral form as:

$$R_t = \int_{E_i}^{E_{th}} \frac{1}{\left(\frac{dE}{dx}\right)} dE , \tag{19}$$

$$\tau_t = \int_{E_i}^{E_{th}} \frac{1}{\left(\frac{dE}{dt}\right)} dE , \tag{20}$$

where E_{th} is the mean thermal energy of the plasma electrons. Substituting for dE/dt (expression 17) in (19) and (20) yields the following expressions for positron range and thermalization time:*

$$R_t = \frac{\hbar^2}{2\ m\ e^2} \left\{ li\left[\left(\frac{2\ E_i}{\hbar\ \omega_e}\right)^2\right] - li\left[\left(\frac{2\ E_{th}}{\hbar\ \omega_e}\right)^2\right] \right\} \tag{21}$$

---

*In these expressions li is the logarithmic integral, defined as follows:

$$li(x^{n+1}) = \int \frac{x^n\ dx}{\ln\ x}$$

and

$$\tau_t = \frac{1}{2e^2}\left(\frac{\hbar^3}{m\omega_e}\right)^{\frac{1}{2}}\left\{li\left[\left(\frac{2\ E_i}{\hbar\ \omega_e}\right)^{3/2}\right] - li\left[\left(\frac{2\ E_{th}}{\hbar\ \omega_e}\right)^{3/2}\right]\right\} \tag{22}$$

The analogous expressions based on the Husseiny equation (18) for dE/dt are:

$$R_t^H = n\pi\left(\frac{8\hbar^2}{mE_{th}}\right)^2\left\{li\left[(4\pi\varepsilon_o)^2\left(\frac{E_i\ E_{th}}{2\hbar^2\ \omega_e^2}\right)^2\right] - li\left[(4\pi\varepsilon_0)^2\left(\frac{E_{th}^2}{2\hbar^2\ \omega_e^2}\right)^2\right]\right\} \tag{23}$$

$$\tau_t^H = (4\pi\varepsilon_0)^{\frac{1}{2}}\ \frac{8\hbar^3\ \omega_e}{e^2(m\ E_{th}^3)^{\frac{1}{2}}}\left\{li\left[(4\pi\varepsilon_o)^{3/2}\left(\frac{E_i\ E_{th}}{2\hbar^2\ \omega_e^2}\right)^{3/2}\right.\right.$$

$$\left.\left. - li\left[(4\pi\varepsilon_o)^{3/2}\left(\frac{E_{th}^2}{2\hbar^2\ \omega_e^2}\right)^{3/2}\right]\right\} \tag{24}$$

Expressions (21) to (24) are valid for positrons thermalizing in a fully ionized hydrogen plasma.

The basic Dirac annihilation time (3) can be written in terms of ω_e as:

$$\tau_D = \frac{4c}{r_0\ \omega_e^2} \tag{25}$$

Comprehensive calculations were carried out by overlaying the T_e - n plane of interest with a grid and computing values of R_t, R_t^H, τ_t, τ_t^H and τ_D at each grid point. Equal time and equal range curves were constructed by joining grid points with identical values of the parameter of interest. Figure 8 shows curves of equal thermalization time based on expressions (22) and (24) as well as standard Fokker-Planck equal relaxation time curves for comparison.* The Dirac equal annihilation time curves are straight horizontal lines on this plot. In order to avoid confusion only the line levels are indicated along the right hand margin of the plot. Equal range curves based on expressions (21) and (23) appear in Figure 9. All curves have been calculated for positrons with initial energies: $E_i = 500$ KeV.

It is evident from Figures 8 and 9, that on the scales of interest, results based on the Husseiny expression (18) for dE/dt do not, on the whole, differ significantly from results based on expression (17) for dE/dt (nor do Fokker-Planck results differ greatly). Forthcoming thermalization time and range calculations will therefore be based on expression (17).

---

*The Fokker-Planck expression for the thermalization time: (this can also be termed a relaxation time, where the high energy positron distribution is considered to relax to the plasma electron distribution)

$$\tau_t^{FP} = \left(\frac{2}{m}\right)^{\frac{1}{2}} \frac{E_i^{3/2}}{e^2\ \omega_e^2}\ \frac{1}{\ln\Lambda}$$

where $\ln\Lambda$ is the Coulomb logarithm and

$$\Lambda = \frac{3\ E_{th}^{3/2}}{m^{\frac{1}{2}}\ e^2\ \omega_e}$$

follows from Fokker-Planck transport theory in fully ionized plasmas (see for example: Krall and Trivelpiece, 1973, Chapter 6).

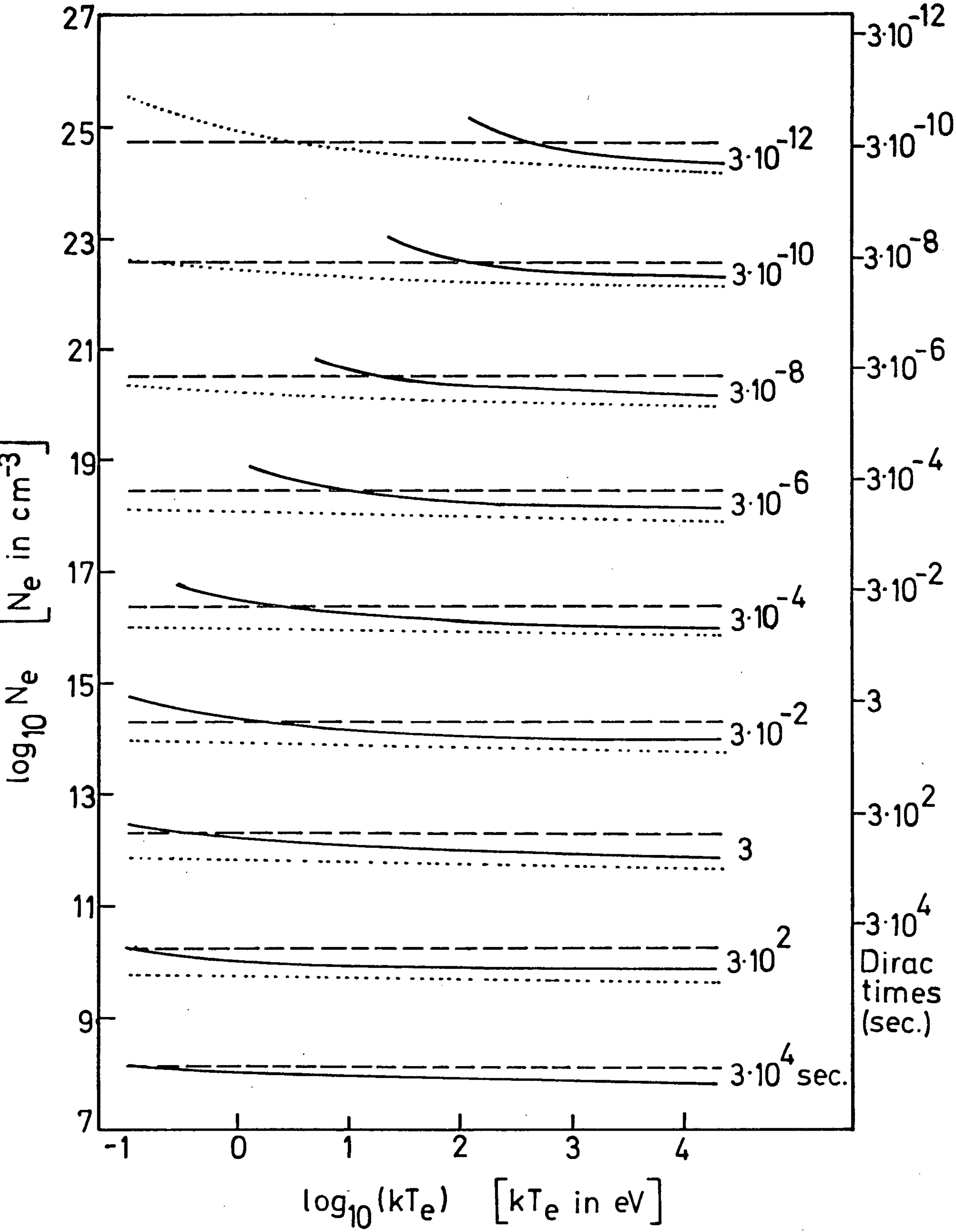

Fig. 8. Equal thermalization time curves for e^+ in fully ionized H_2.
------(22) ....(24) ——Fokker-Planck
Initial e^+ energy: 500 KeV.

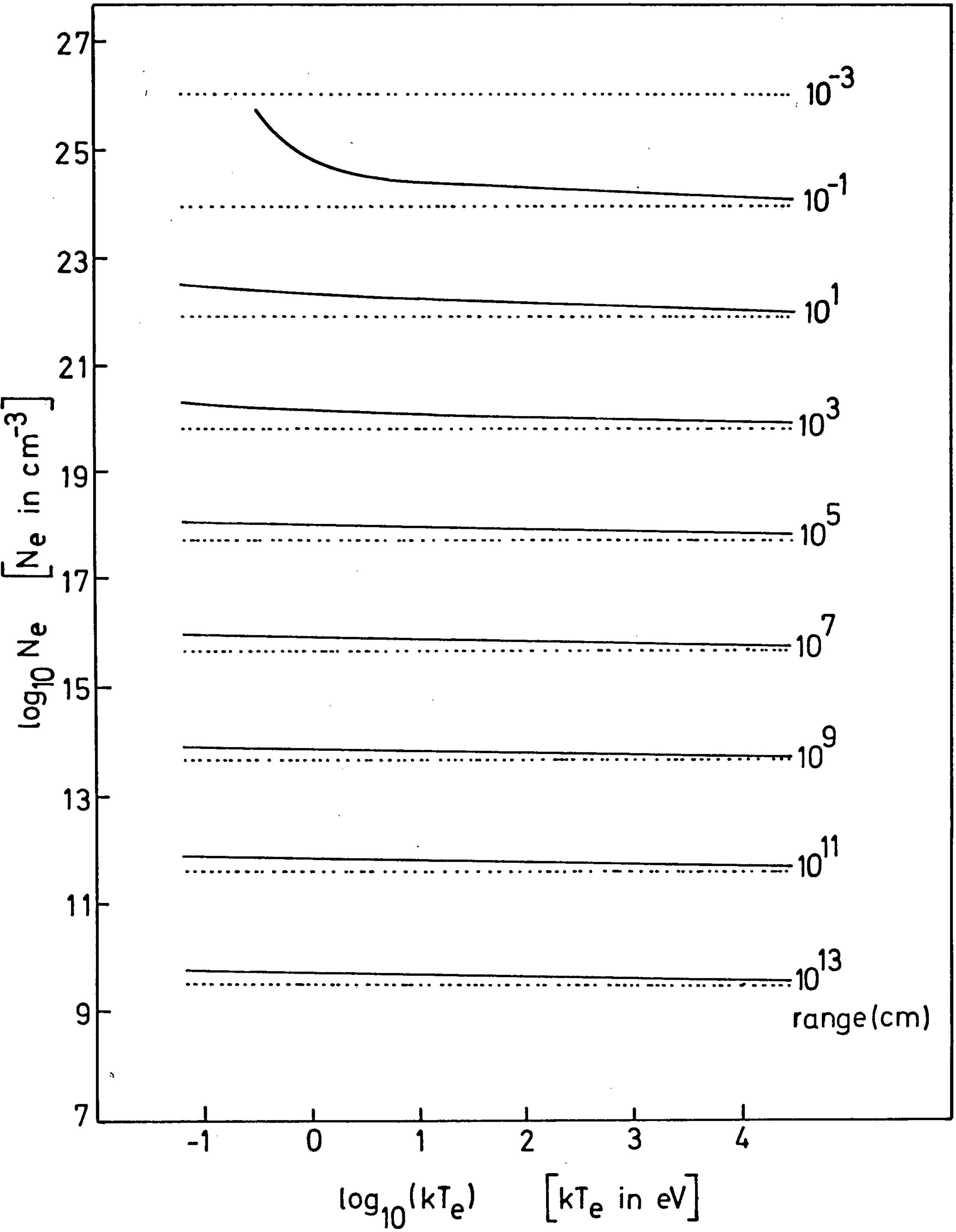

Fig. 9. Equal range curves for 500 KeV e^+ in fully ionized H_2.
·········(21) ——(23)

It is also clear from Figure 8 that

$$\tau_t < \tau_D \tag{26}$$

for all values of T_e and n. This is as expected from a comparison of the two cross sections involved: $\sigma_D = r_0{}^2c/v$, the Dirac annihilation cross section and $\sigma_c(90°) = \pi(\frac{e^2}{mv^2})^2$, the 90° Coulomb scattering cross section which describes (approximately) the typical thermalization interaction. Clearly,

$$\frac{\sigma_D}{\sigma_c} = \left(\frac{v}{c}\right)^3 << 1 \tag{27}$$

for the energy ranges of interest (recall that v is the relative positron-electron velocity).

C. Coulomb Correction

(i) Calculations

The key relation of the preceeding section (inequality (26)) is based on Dirac's first order expression for the annihilation cross section (and the annihilation time). The derivation of this expression is in turn based on a plane wave model for both positrons and electrons which ignores the distorting effects of long range Coulomb interactions.

Since long range Coulomb interactions are very important in plasmas - moreso than in other states of matter - the use of σ_D to calculate annihilation times is questionable. A number of attempts have been made to carry out annihilation rate calculations for fully ionized hydrogen plasmas, taking into account this long range Coulomb attraction between positrons and electrons (Toptygin, 1962; Wolfer, 1969). The results of these attempts are similar and indicate a very large enhancement of the annihilation rate at low plasma electron temperatures.

Wolfer derives the nonrelativistic Hamiltonian for a many-body system of positrons and electrons interacting via a Coulomb force and capable of annihilating with each other (i.e. capable of giving rise to annihilation photons). This Hamiltonian is then used to calculate, with the aid of Q.E.D. covariant perturbation formalism, the 2γ annihilation probability and the 2γ annihilation rate in a fully ionized hydrogen plasma. Wolfer's result for the annihilation rate can be written as:

$$\nu_W = 4r_0{}^2 cn\left(\frac{4\pi\ I}{k\ T_e}\right)^{3/2} f_1(T_e)\ e^{-4\left[\left(\frac{\hbar c}{e^2}\right)^2\frac{I}{kT_e} + f_2(T_e)\right]\frac{kT_e}{E_0}} \qquad (28)$$

where $I = \frac{me^4}{4\hbar^2}$ is the ionization potential of positronium,

n, T_e are plasma electron density and temperature respectively,

$f_1(T_e)$, $f_2(T_e)$ are complicated functions of T_e (see Wolfer, 1969).

and $E_0 = mc^2$

Both Wolfer's and Toptygin's results predict a drastic variation in the annihilation time with plasma electron temperature. Values of $\tau_w = 1/\nu_w$ are within an order of magnitude of the Dirac values, τ_D, for 50eV < kT_e < 10 KeV, however τ_w decreases almost six orders of magnitude with respect to τ_D in the range 1eV < kT_e < 50eV.

This dramatic effect is evident in Figure 10, where curves of equal annihilation time (constructed using Wolfer's expression (28)) are plotted on the T_e - n plane. It is obvious after comparing Figures 8 and 10 that thermalization times are no longer less than annihilation times for all T_e and n values. The T_e - n plane can be divided into regions where $\tau_t < \tau_w$ and $\tau_t > \tau_w$ by superimposing the plots of Figure 8 and 10. The results of such a division, for positrons with initial energy: 500 KeV, annihilating in a fully ionized hydrogen plasma are shown in Figure 11. Under these conditions, the region of interest ($\tau_t < \tau_w$) is defined by the line $\tau_w = \tau_t$ at $kT_e \simeq$ 10eV. Thus 'hot' positrons introduced into plasmas where kT_e > ~ 10eV should thermalize before annihilating. This may not be the case in 'cooler' plasmas, where long-range attractive forces between positrons and electrons become significant enough to enhance mutual localization and hence annihilation.

(ii) Promising Plasmas

Of major interest from the viewpoint of diagnostics is the fact that two potential fusion plasmas are located in the

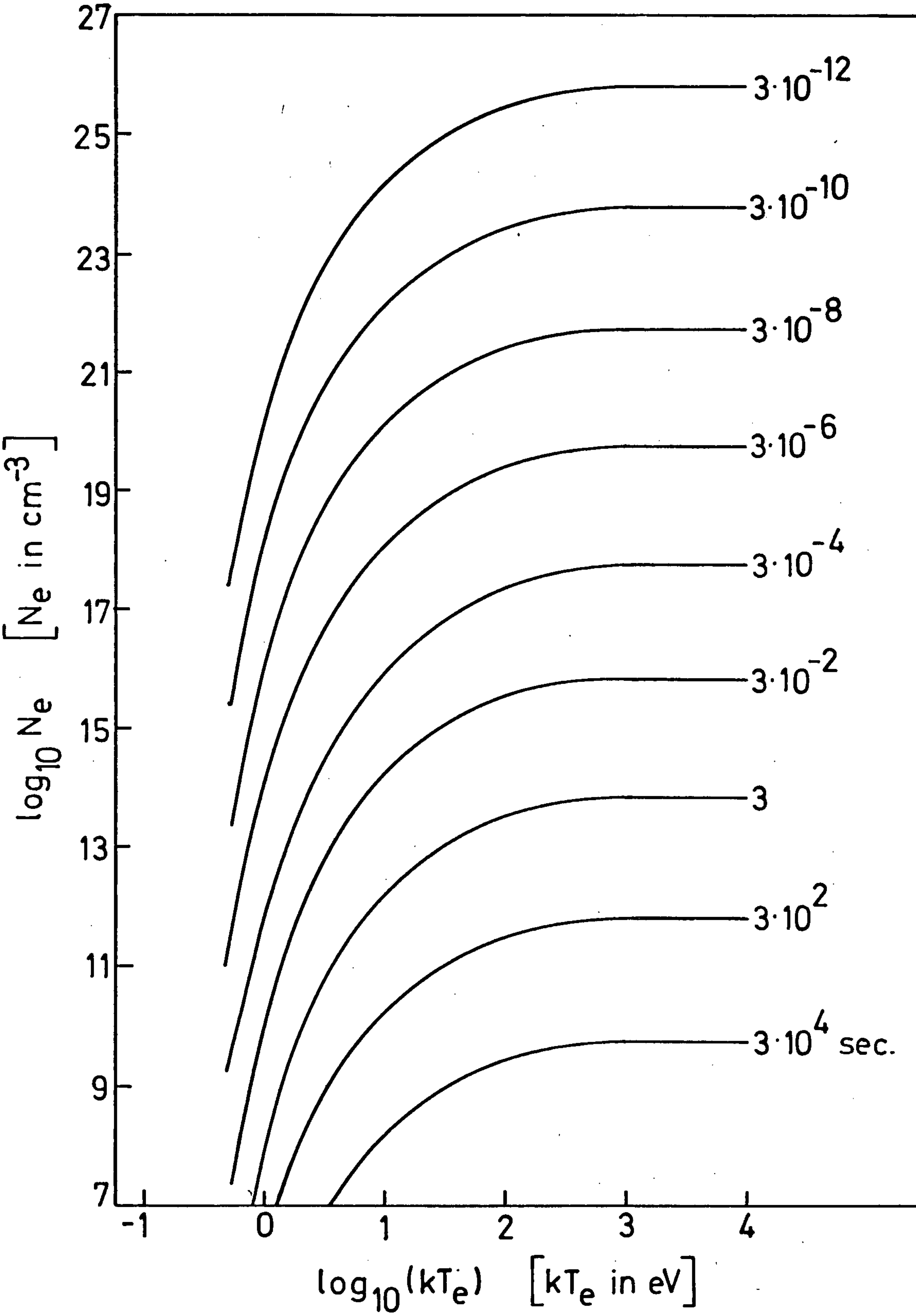

Fig. 10. Equal annihilation time curves (Wolfer - Toptygin) for e^+ in fully ionized H_2.

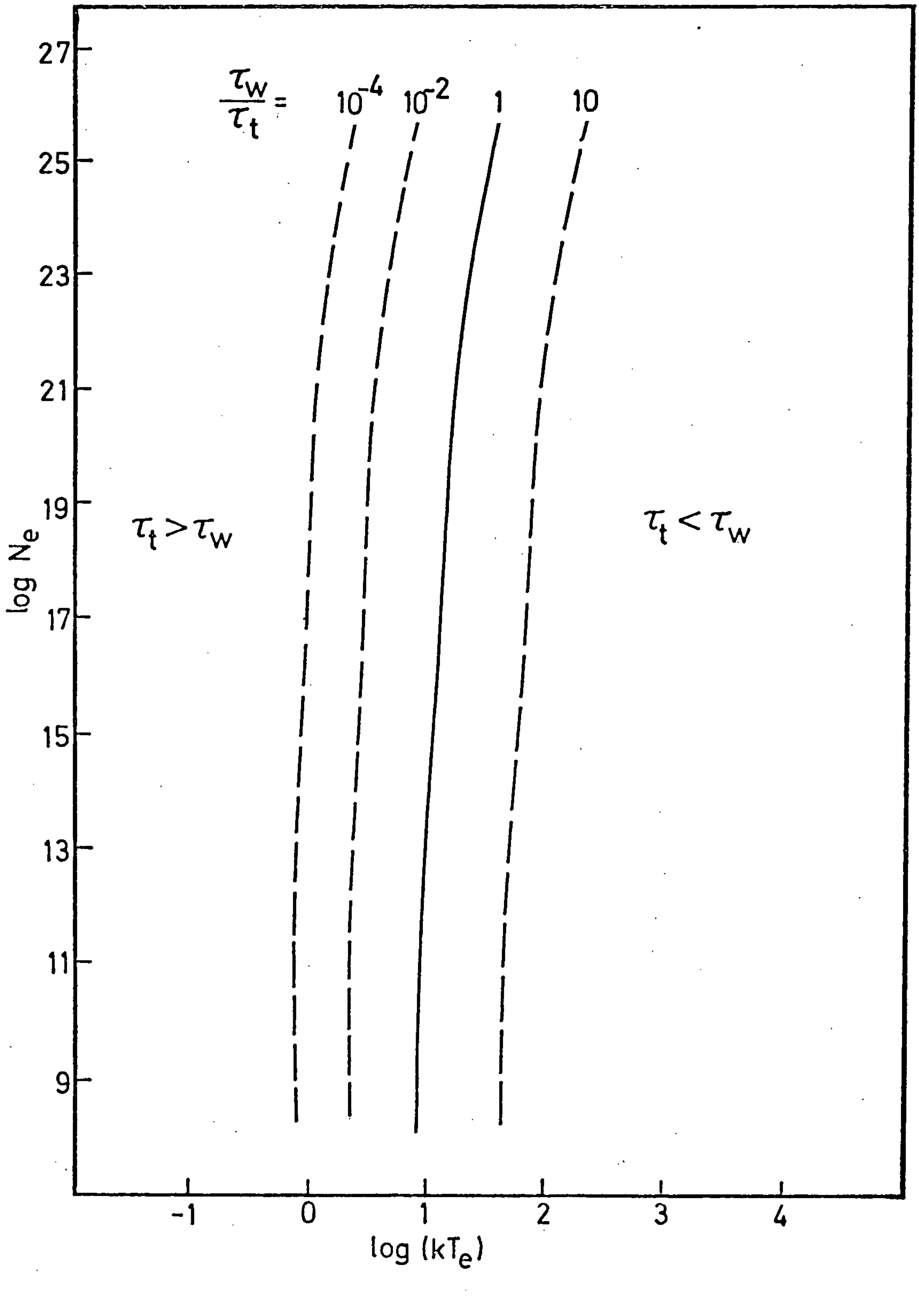

(N_e in cm^{-3} ; kT_e in ev)

Fig. 11. Relative annihilation and thermalization times: 500 KeV e^+ in fully ionized H_2.

favourable $\tau_t < \tau_w$ area: Tokamak or toroidal confinement plasmas: 10^{12} cm^{-3} < n < 10^{16} cm^{-3}; 10^3 eV < kT_e < 10^5 eV and laser compression plasmas: 10^{23} cm^{-3} < n < 10^{26} cm^{-3}; 10^3 eV < kT_e < 10^4 eV. By way of introducing Chapter V, which deals exclusively with these plasmas, a number of preliminary calculations are presented here. These deal with positrons thermalizing in the following hypothetical plasmas:

$$\left.\begin{array}{rl} \text{Tokamak Type:} & n_e = 10^{14}\ \text{cm}^{-3} \\ & kT_e = 10\ \text{KeV} \\ \text{Laser Compression Type:} & n_e = 10^{24}\ \text{cm}^{-3} \end{array}\right\} \qquad (29)$$
$$kT_e = 1\ \text{KeV}$$

Figure 12 is a plot of thermalization time as a function of initial positron energy (i.e. energy of a positron when it first appears in the plasma) under the above conditions. A similar plot of thermalization range as a function of initial positron energy appears in Figure 13. Figures 14 and 15 are logarithmic plots of positron energy loss rate as a function of instantaneous positron energy and positron energy as a function of time respecively, for both sets of parameters defined above.

D. Positron Distributions-Fractional Thermalization

It must be realized that the above plots are meaningful only in terms of single positrons (or perfectly monoenergetic positron distributions) and thus give only a general

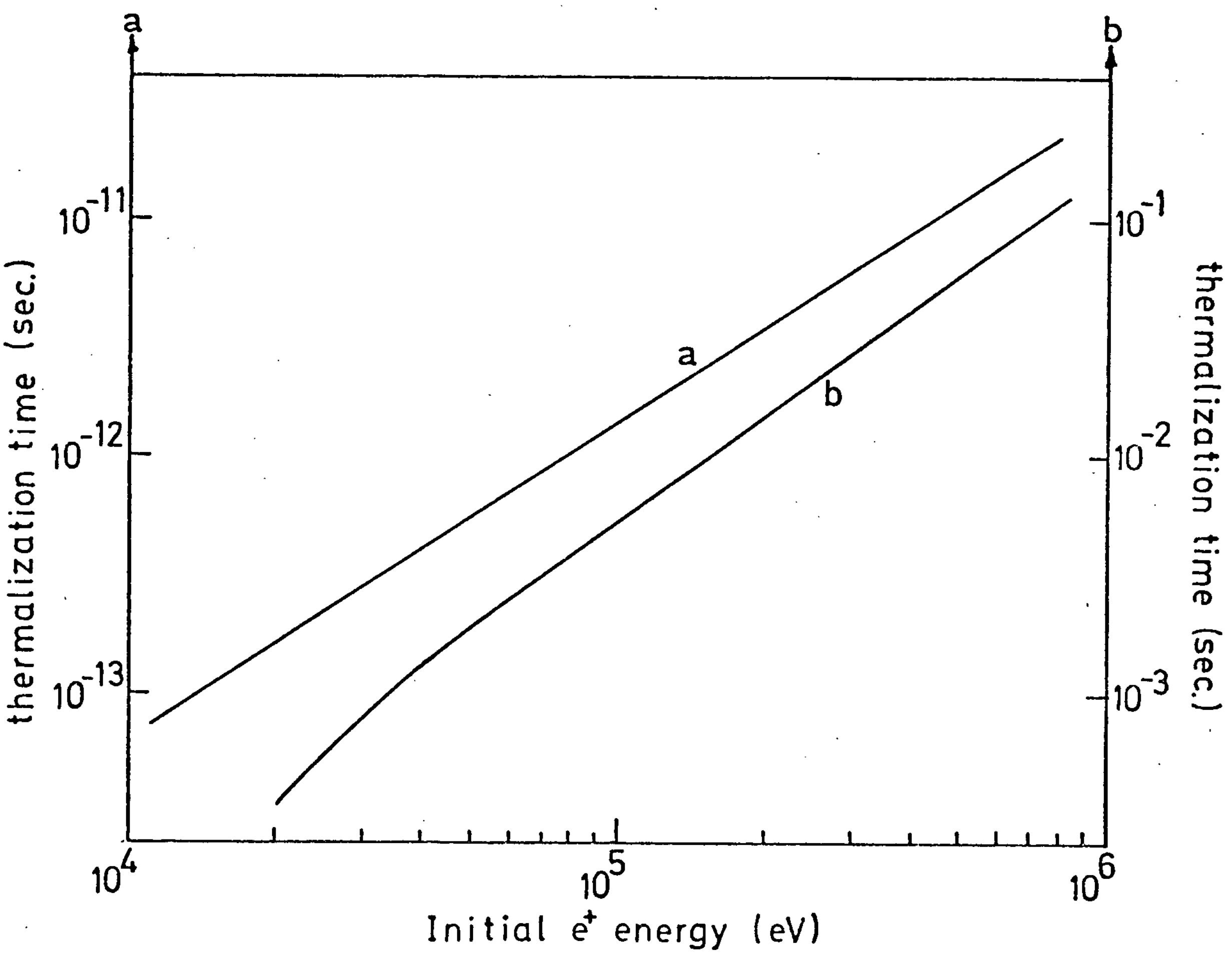

a $\begin{cases} kT_e = 1\ \text{KeV} \\ N_e = 10^{24}\ \text{cm}^{-3} \end{cases}$

b $\begin{cases} kT_e = 10\ \text{KeV} \\ N_e = 10^{14}\ \text{cm}^{-3} \end{cases}$

Fig. 12. Variation of thermalization time with initial e^{+} energy in fully ionized H_2.

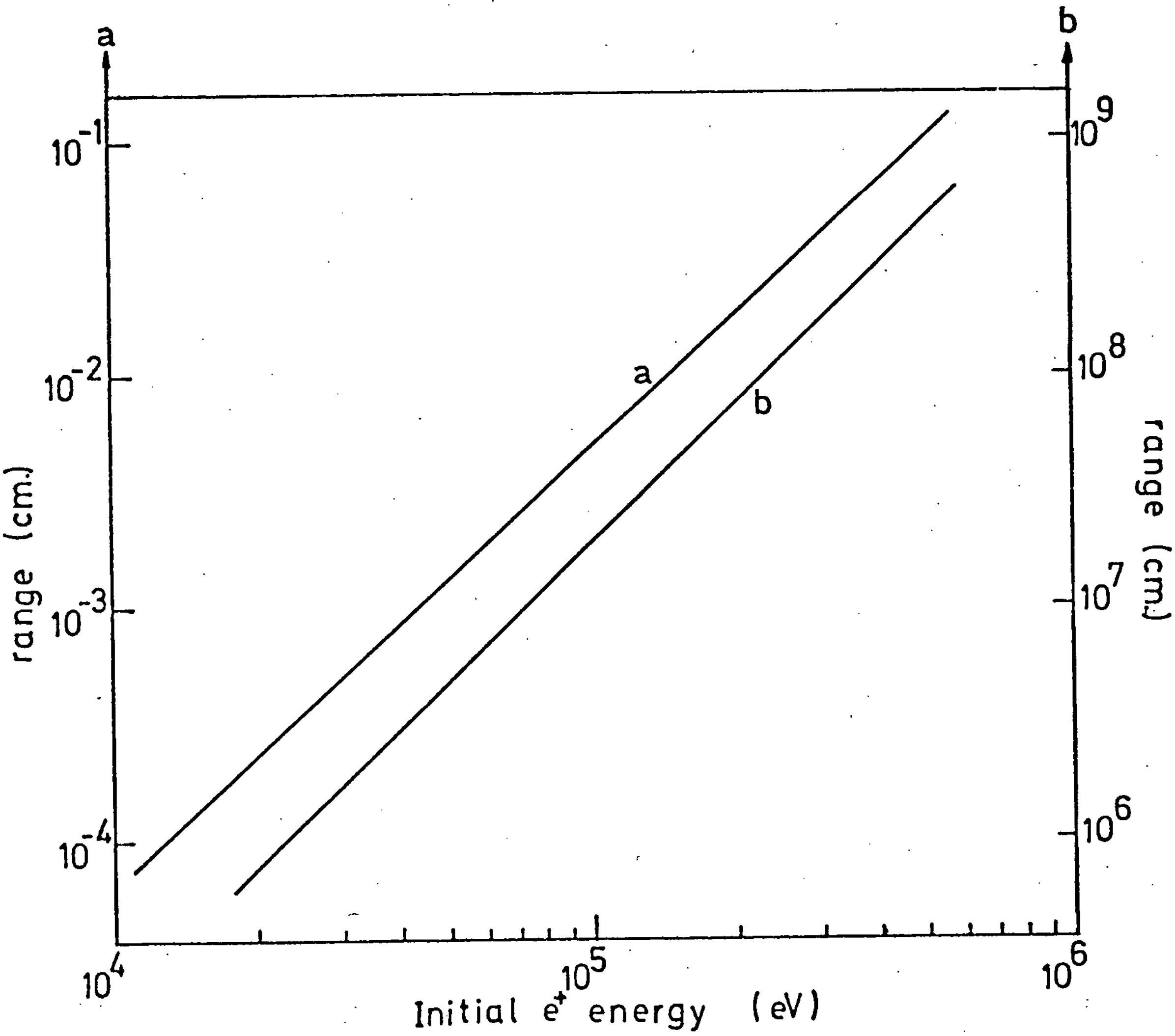

a $\begin{cases} kT_e = 1 \text{ KeV} \\ N_e = 10^{24} \text{ cm}^{-3} \end{cases}$ b $\begin{cases} kT_e = 10 \text{ KeV} \\ N_e = 10^{14} \text{ cm}^{-3} \end{cases}$

Fig. 13. Variation of range with initial e^{+} energy in fully ionized H_2.

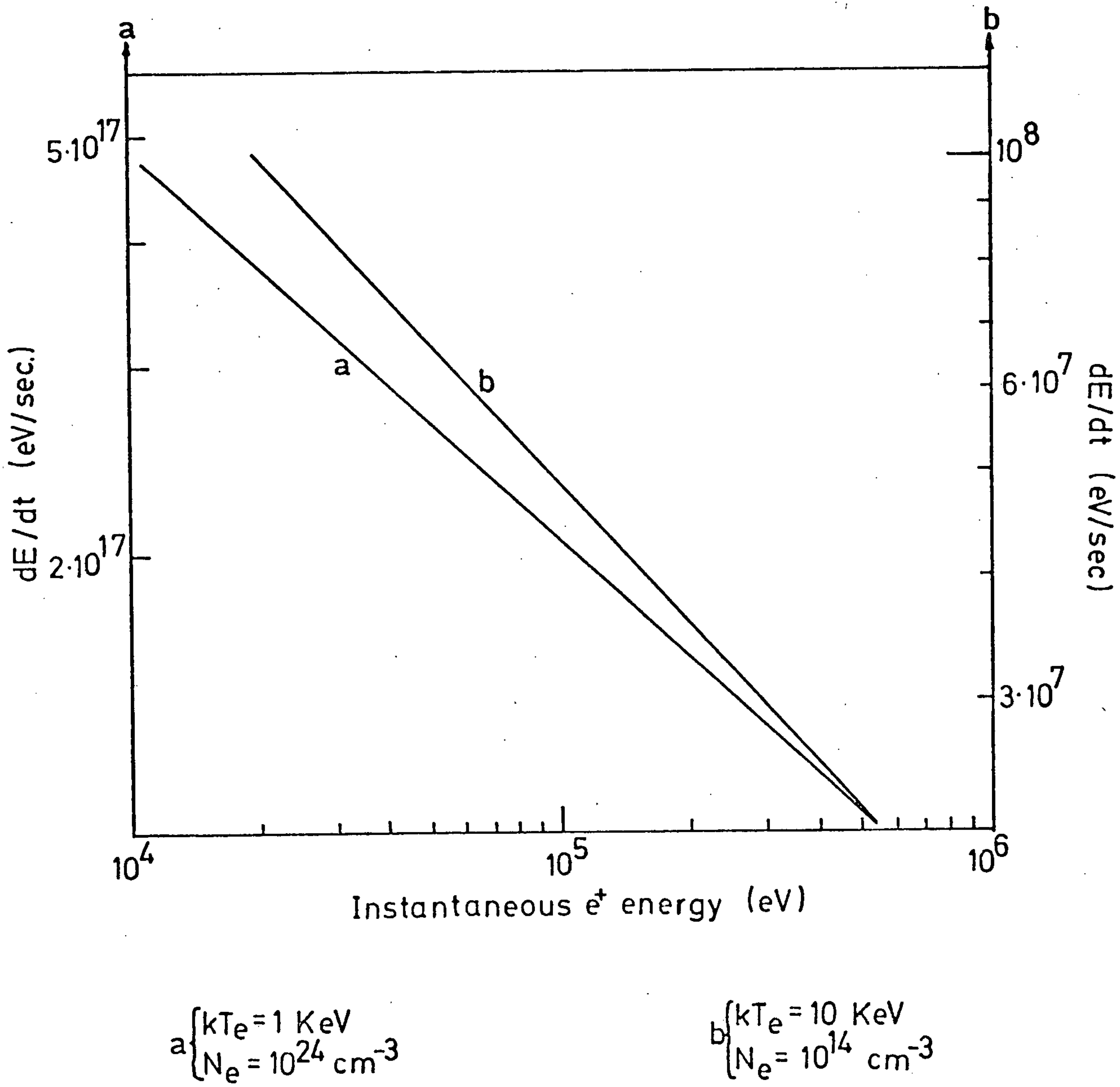

Fig. 14. Variation of dE/dt with e^+ energy in fully ionized H_2.

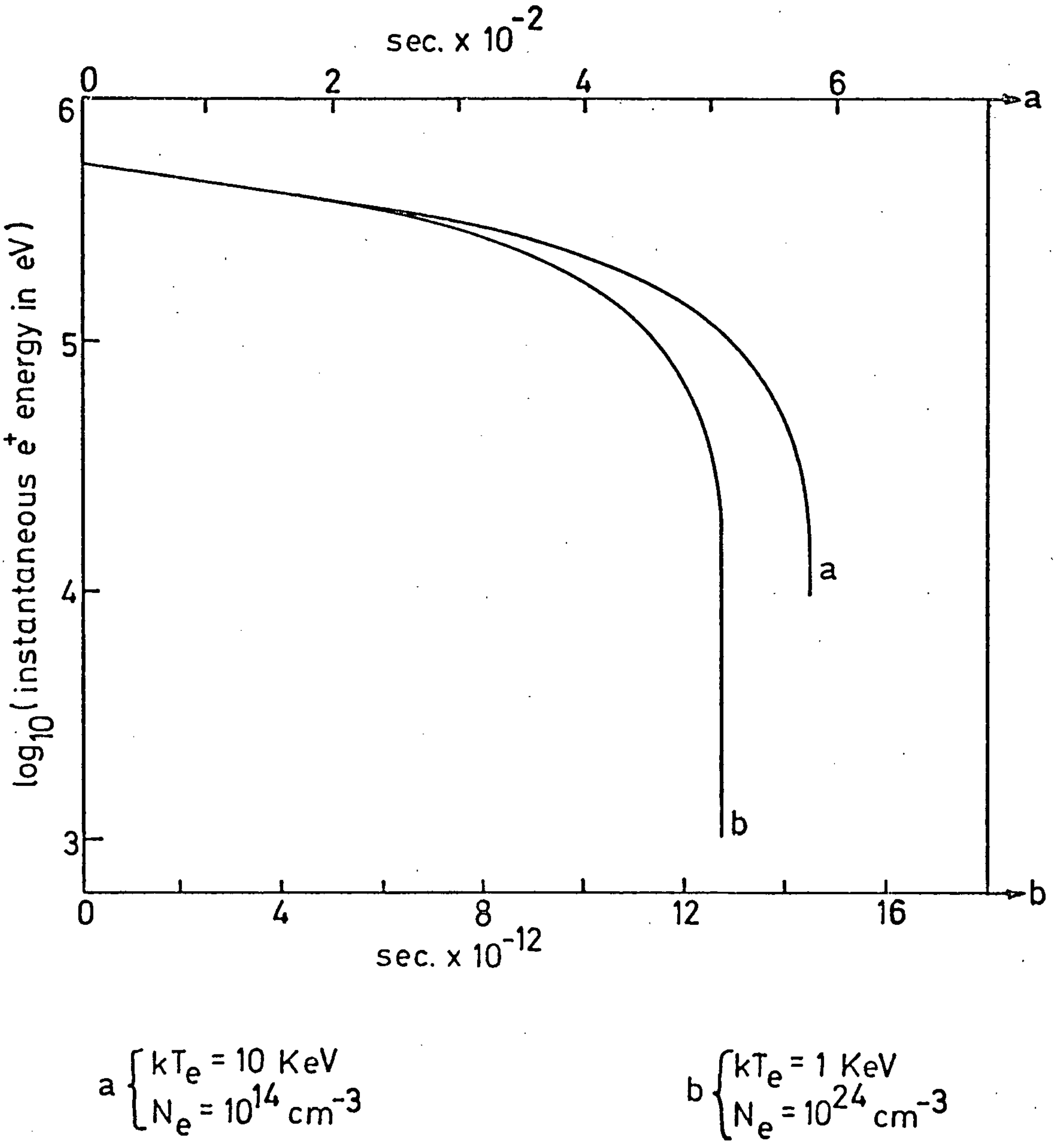

Fig. 15. Variation of e^+ energy with time in fully ionized H_2.

description of the behaviour of positrons from a real source. If the source is a radioactive nucleus undergoing β^+ decay, then the emitted positrons are distributed in energy according to: (see Chapter V, Section C for details)

$$P(E^+)dE^+ = K\ F(Z,E^+)\ (E^{+2} - m^2c^4)^{\frac{1}{2}}\ (E^+_{max} - E^+)^2\ E^+\ dE^+ \qquad (30)$$

where E^+ is the total positron energy, including the rest mass energy

and $P(E^+)dE^+$ is the fraction of all positrons emitted with an energy E^+ in the range dE^+.

Since this is the case, it is useful to define two distribution functions, namely the thermalization time distribution:

$$N(t)dt = \frac{P(E^+)dE^+}{dt} \qquad (31)$$

where $N(t)dt$ is the fraction of all positrons thermalizing in a time t in the range dt

and the thermalization range distribution:

$$M(r)dr = \frac{P(E^+)dE^+}{dr} = \frac{P(E)dE}{dt}\ \frac{1}{v^+} \qquad (32)$$

where $M(r)dr$ is the fraction of all positrons thermalizing in a distance r in the range dr,

v^+ is the instantaneous positron velocity,

and it has been assumed that all emitted positrons eventually thermalize.

The distribution functions N(t) and M(r) have been calculated for the conditions specified by (29) with positrons from a ^{22}Na Source ($E_{max}(e^+) \simeq 542$ KeV). The curves, constructed point by point using expressions (17) and (30), appear in Figure 16 (Tokamak) and Figure 17 (laser compression). Since the area under these curves represents the total number of positrons thermalized, numerical integration of N(t) and M(r) allows the determination of the fraction of positrons that thermalize in a time t and a distance r. Figures 18 and 19 show the results of such calculations: percentage of positrons thermalized as a function of (a) time in the plasma and (b) distance travelled through the plasma (for both plasmas being considered).

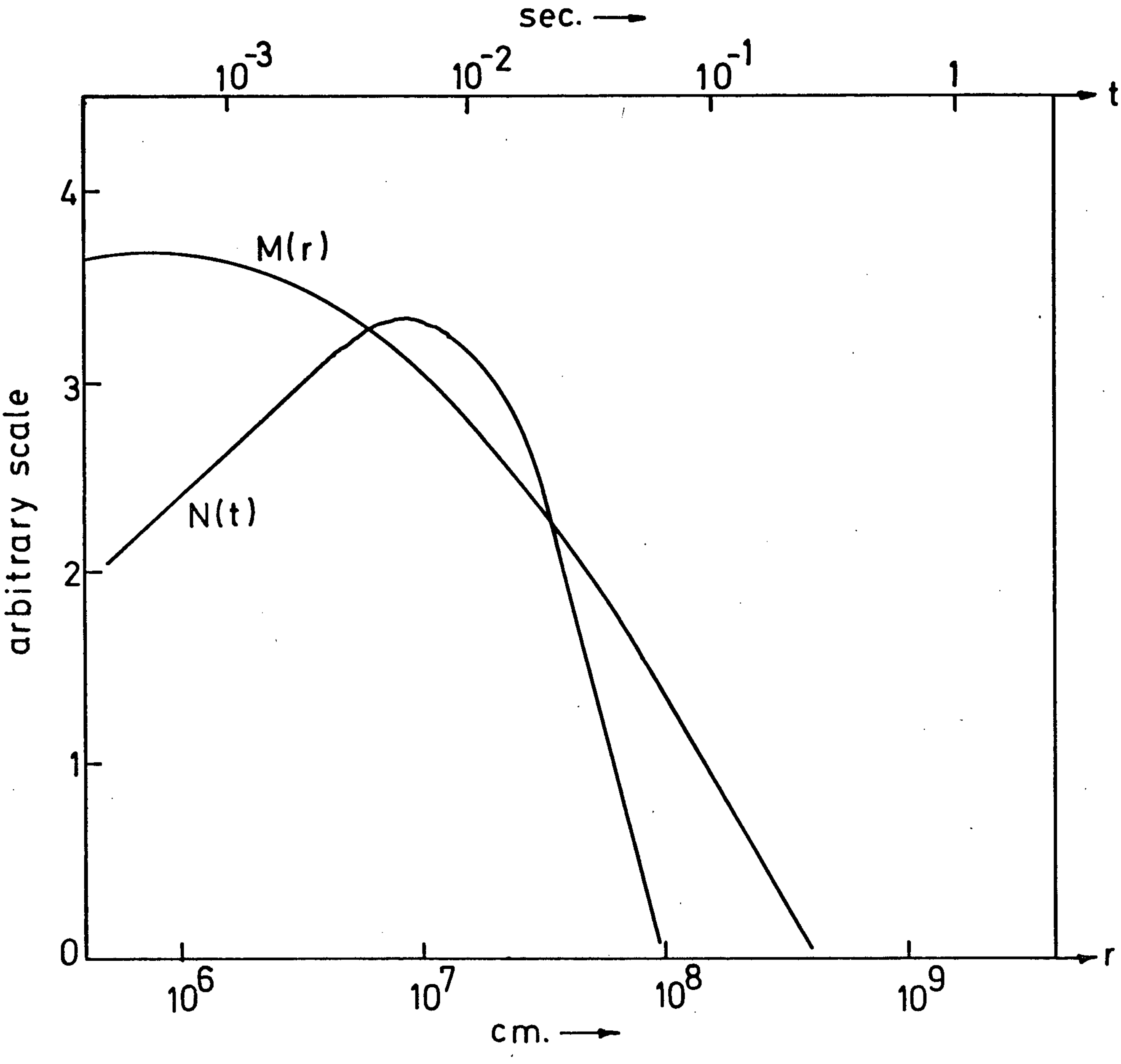

Fig. 16. Distribution functions N(t) and M(r) for ^{22}Na e^+ in fully ionized H_2:
kT_e = 10 KeV
$N_e = 10^{14}$ cm^{-3}

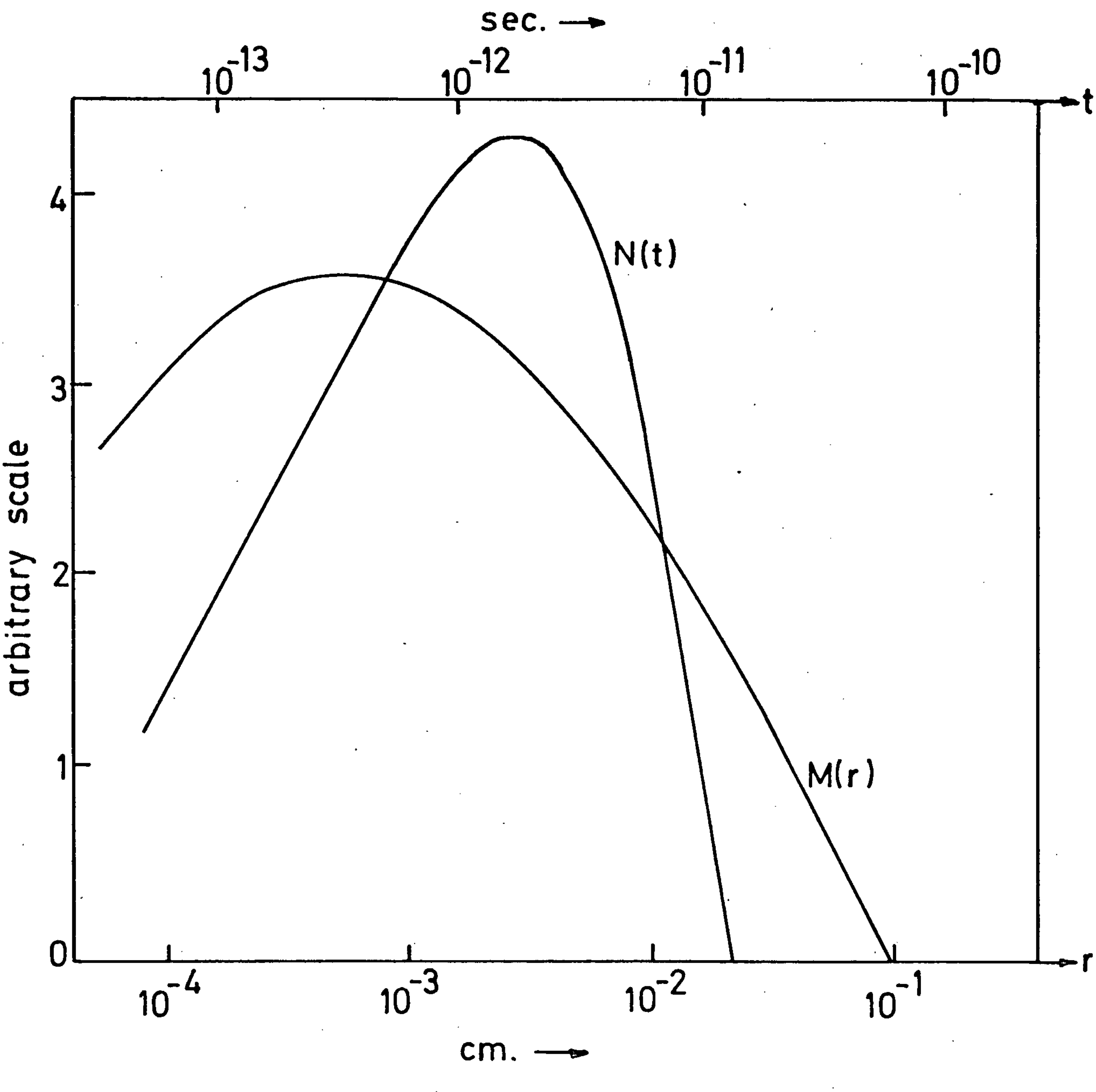

Fig. 17. Distribution functions N(t) and M(r) for ^{22}Na e^+ in fully ionized H_2:

$kT_e = 1$ KeV

$N_e = 10^{24}$ cm^{-3}

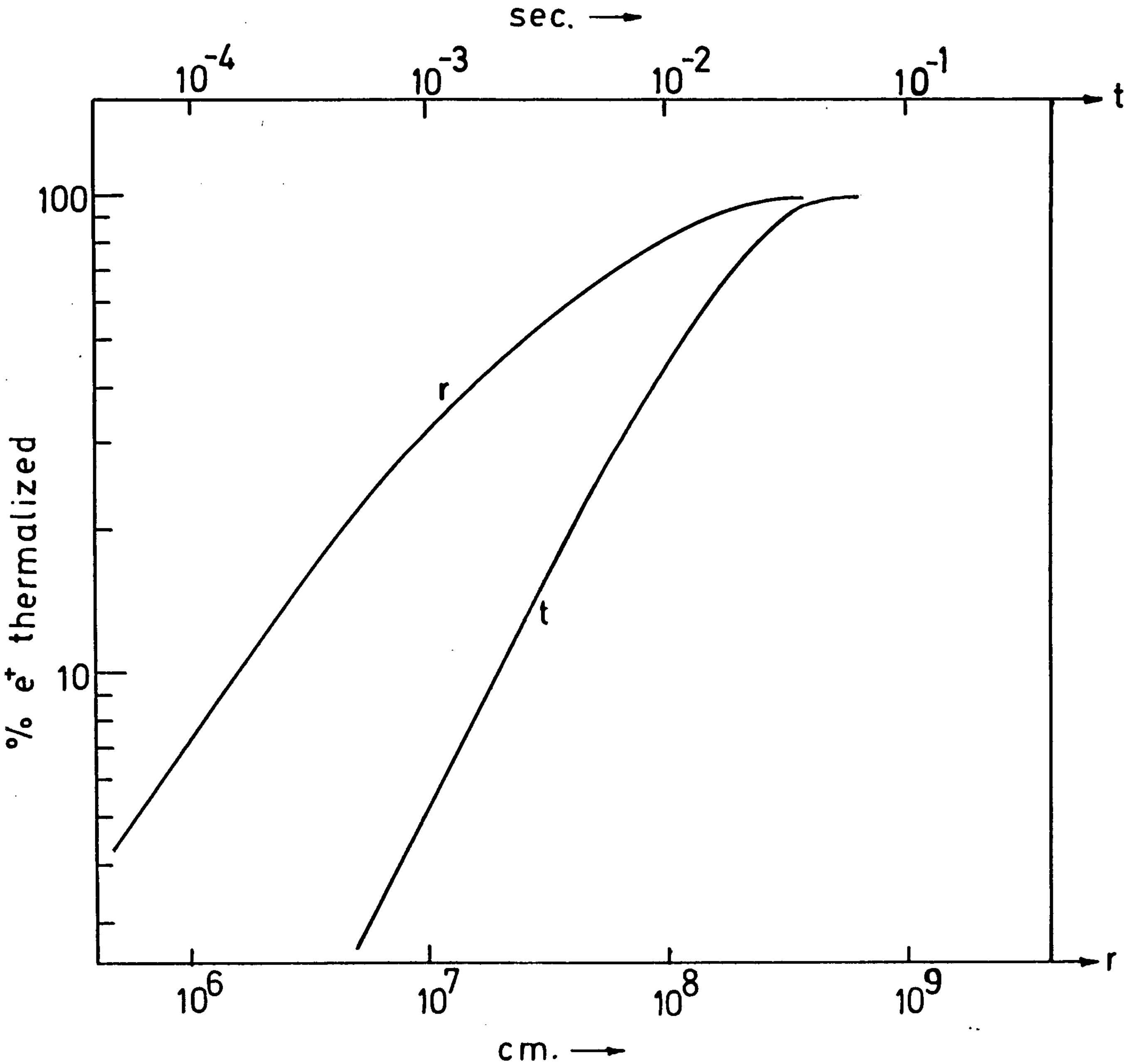

Fig. 18. Thermalization of ^{22}Na e^+ in fully ionized H_2:
$kT_e = 10$ KeV
$N_e = 10^{14}$ cm^{-3}
$\tau_a \sim 1$ sec.

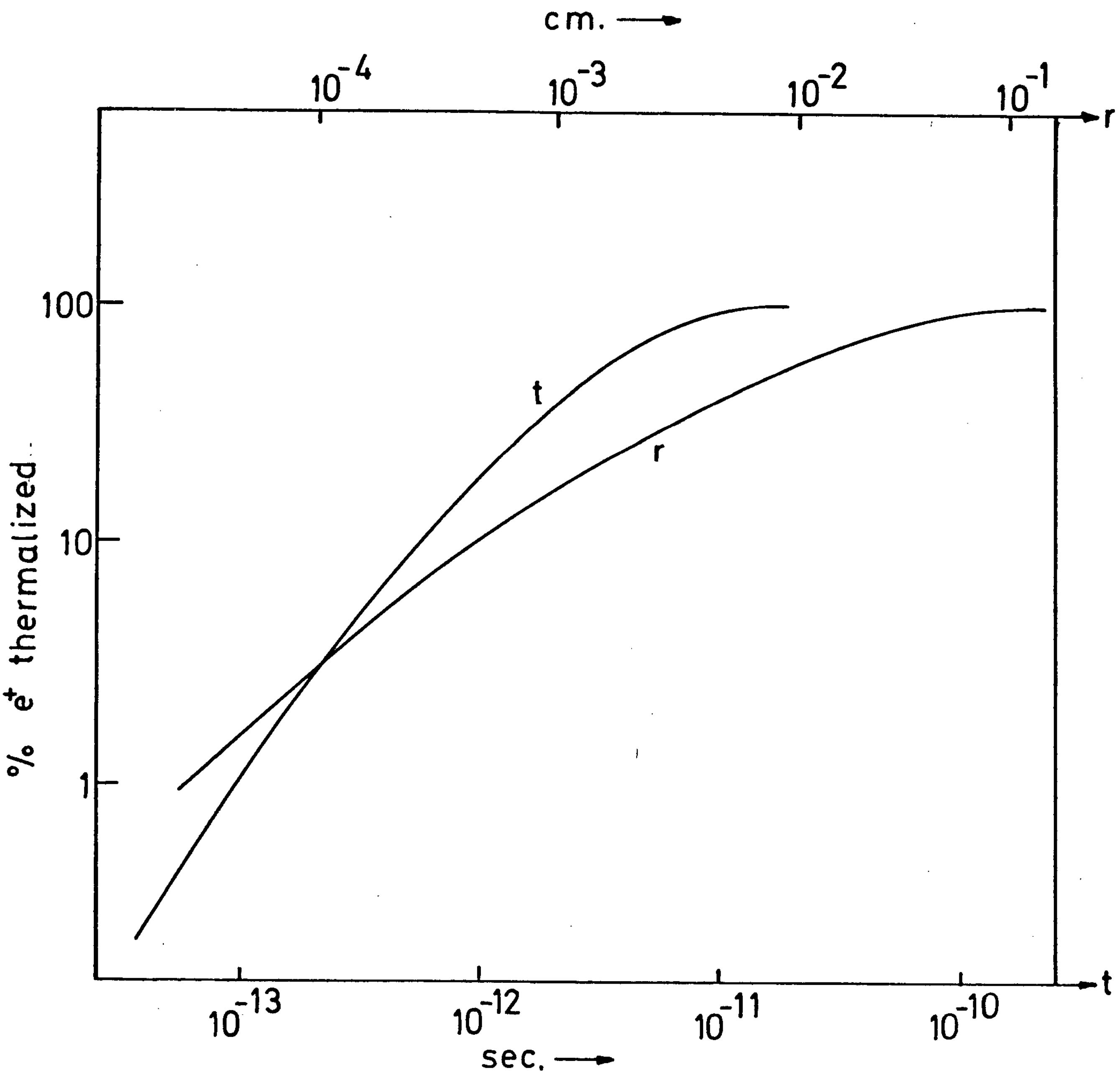

Fig. 19. Thermalization of ^{22}Na e^+ in fully ionized H_2:
$kT_e = 1$ KeV
$N_e = 10^{24}\ cm^{-3}$
$\tau_a \sim 10^{-10}$ sec.

Chapter V

POSITRONS IN TOKAMAK AND LASER COMPRESSION PLASMAS

A. Plasma Parameters

A number of important factors related to the use of positrons to probe plasmas are discussed in this chapter with specific reference to the two hypothetical plasmas introduced in the previous chapter. For the purposes of this chapter a number of additional parameters, to better characterize these plasmas, will be introduced:

Tokamak Type	Laser Compression Type
$n_e = 10^{14}$ cm^{-3}	$n_e = 10^{24}$ cm^{-3}
$kT_e = 10$ KeV	$kT_e = 1$ KeV
$\tau_{p\ell} = 10^{-2} - 10^{-1}$ sec	$\tau_{p\ell} = 10^{-10} - 10^{-9}$ sec
plasma volume: $V \simeq 7 \times 10^6$ cm^3	plasma volume: $V \simeq 9 \times 10^{-7}$ cm^3
(minor radius $\simeq$ 0.5m; major radius $\simeq$ 1.5m)	$d_{plasma} \simeq 120\mu$

The results presented in the previous chapter are discussed and their implications outlined. Positron sources are considered, with special emphasis (qualitative and quantitative) on the unique possibility that some positrons are actually created within the plasmas of interest.

B. Thermalization Times and Ranges

(i) Tokamak: Figure 18 indicates that most of the positrons emitted from a ^{22}Na source would thermalize in a time of ~55 msec and a distance of ~ 2.5 x 10^8 cm. This is consistent with Figures 12 and 13. which confirm that these values correspond to complete thermalization of the most energetic ^{22}Na positrons (542 KeV).* Although an individual positron loses most of its energy during the latter stages of thermalization (during the last 15 msec for a positron with an initial energy of 500 KeV), as indicated by Figures 14 and 15, the majority of positrons thermalize in the 1.6 - 18 msec range, or in terms of distance travelled, in the 4 x 10^5 cm to 7 x 10^6 cm range. This is illustrated by Figure 16 and is a result of the characteristic ^{22}Na positron spectrum (Figure 21).

---

*The effect of the magnetic field on dE^+/dt and hence τ_t and R_t has not been taken into account here. Honda *et al.* (1963) have calculated dE^+/dt, taking into account this effect with the result:

$$\frac{dE^+}{dt} = \frac{e^2\omega_e^{\,2}}{v}\left[\ln\left(\frac{2mv^2}{\hbar\omega_e}\right) - \frac{1}{2}\ln\left(\frac{\omega_e^{\,2} + \omega_B^{\,2}}{\omega_e^{\,2}}\right)\right]$$

where ω_B is the positron gyrofrequency in the existing magnetic field.

The energy loss rate decreases, thus τ_t and R_t increase; but these are not major perturbations.

The calculated thermalization times are less than or of the order of the plasma lifetime, therefore from a time point of view, most of the positrons will thermalize while the plasma is still in existence. The situation from a 'distance travelled' point of view may seem hopeless because of the large positron range at this electron density; however, this is not the case. Any positrons present will be held within the plasma by the same fields which confine the plasma itself. The positrons, like the electrons, will follow helical trajectories (only in opposite directions), rotating around field lines at the positron gyrofrequency:

$$\omega_B = \frac{eB}{mc} \quad , \tag{33}$$

with a rotation radius of

$$r_L = \frac{v_\perp}{\omega_B} \quad , \qquad \text{(Larmour radius)} \tag{34}$$

where B is the toroidal field strength and

$v_\perp$ is the positron velocity perpendicular to the toroidal field.

The Larmour radius of a 500 keV positron, travelling perpendicular to a 10 KG toroidal field is $r_L \approx 2.4$ mm - considerably smaller than mean plasma dimensions. A number of drift motions are also expected to occur, but there is good reason to believe (see discussion on runaway electron drift in ORMAK-Knoepfel *et al.*, 1975) that these will not result in the loss of a large number of positrons.

With these facts in mind it is not unreasonable to expect positrons to be confined within the plasma for the entire duration of their existence (corresponding to a maximum distance travelled of ~ 2.5×10^8 cm for ^{22}Na positrons).

Annihilation times are predicted to be in the range 1-2 sec by both the Dirac (25) and the Wolfer (28) expressions, in the plasma being considered. This is at least one order of magnitude larger than the plasma lifetime and therefore represents some loss of useful gamma ray signal. Although most of the positrons will thermalize within the plasma lifetime, some will annihilate only after the plasma has ceased to exist. This situation could be improved by increasing the plasma density or the plasma lifetime or both.

(ii) Laser Compression: Complete thermalization of ^{22}Na positrons in this hypothetical plasma should occur in a time of ~ 1.3×10^{-11} sec and a distance of ~ 10^{-1} cm (based on Figure 19). Energy loss characteristics are similar to those outlined above and are illustrated in Figures 12-15. The majority of positrons thermalize in the 0.5-5 psec range, or after having travelled between 1.4×10^{-4} cm and 10^{-2} cm. Calculated times for complete thermalization are much less than the 0.1 to 1 nsec plasma lifetime figure. In addition, calculated annihilation times (~ 1.3×10^{-10} sec) are of the right order of magnitude - greater than the thermalization times, but less than the plasma lifetime.

Maximum range values are somewhat larger than the mean plasma dimension, thus some losses are to be expected, however the majority of positrons should thermalize within the plasma. Range losses could be reduced or eliminated by increasing the physical extent and/or density of the plasma.

As will be discussed in the next section, a ^{22}Na source is not the most efficient positron source for use with laser compression type plasmas, thus the calculations cited in this section should be taken only as a general indication of the thermalization characteristics of KeV to MeV positrons in this plasma.

C. Positron Sources

Positron sources for plasma diagnostics work can be classed as extrinsic and intrinsic, an extrinsic source being one that is not inherent to the plasma and an intrinsic source one that is.

(i) Extrinsic Sources: The most common extrinsic sources are radionuclides which undergo β^+ decay. A partial list of some positron emitting radionuclides, specifying half-lives and maximum (cutoff) kinetic energies attained by emitted positrons, is presented in Table II. The source

Table II

Radionuclide e^+ Sources

Radionuclide	Half Life	Max e^+ Energy (KeV)
$^{22}_{11}Na$	2.6 y	542
$^{26}_{13}Al$	7.4×10^5 y	1160
$^{48}_{23}V$	16 d	698
$^{58}_{27}Co$	71 d	510
$^{64}_{29}Cu$	12.8 h	650
$^{65}_{30}Zn$	244 d	325
$^{84}_{37}Rb$	33 d	780
$^{88}_{39}Y$	107 d	760

most commonly used in solid state studies is ^{22}Na, followed by ^{64}Cu.

Copper-64 is short lived (half-life ~ 12.8h), but it has the advantage that intense sources of any configuration can be obtained quickly by thermal neutron irradiation of ^{63}Cu (which is abundant). Sodium-22, due to its chemical properties, is usually available in the form of $^{22}NaCl$ solutions. The use of ^{22}Na has the advantage that the birth of each positron is marked in time, to within less than 10^{-11} sec, by the emission of a 1.28 MeV gamma ray associated with the transition of neon-22 (the product of the β^+ dacay) from the first excited state to the ground state (see Figure 20 - the decay scheme of ^{22}Na).

Positrons emitted by radionuclides have a characteristic energy distribution, represented here by $P(w)dw$, the fraction of all positrons emitted with energy $W = \frac{E^+}{mc^2}$ in the range dw:

$$P(w)dw = K\, F(Z,w)\, (w-1)^{\frac{1}{2}}\, (w_0-w)^2 w\, dw \qquad (35)$$

where $E^+ = mc^2 + E(e^+)$ is the total positron energy: rest mass energy plus kinetic energy,

K is a constant,

$F(Z,w)$ is the Fermi function, a small correction factor to account for the perturbation of the β^+ spectrum by the nucleus,

Z is the atomic number of the product or daughter nucleus,

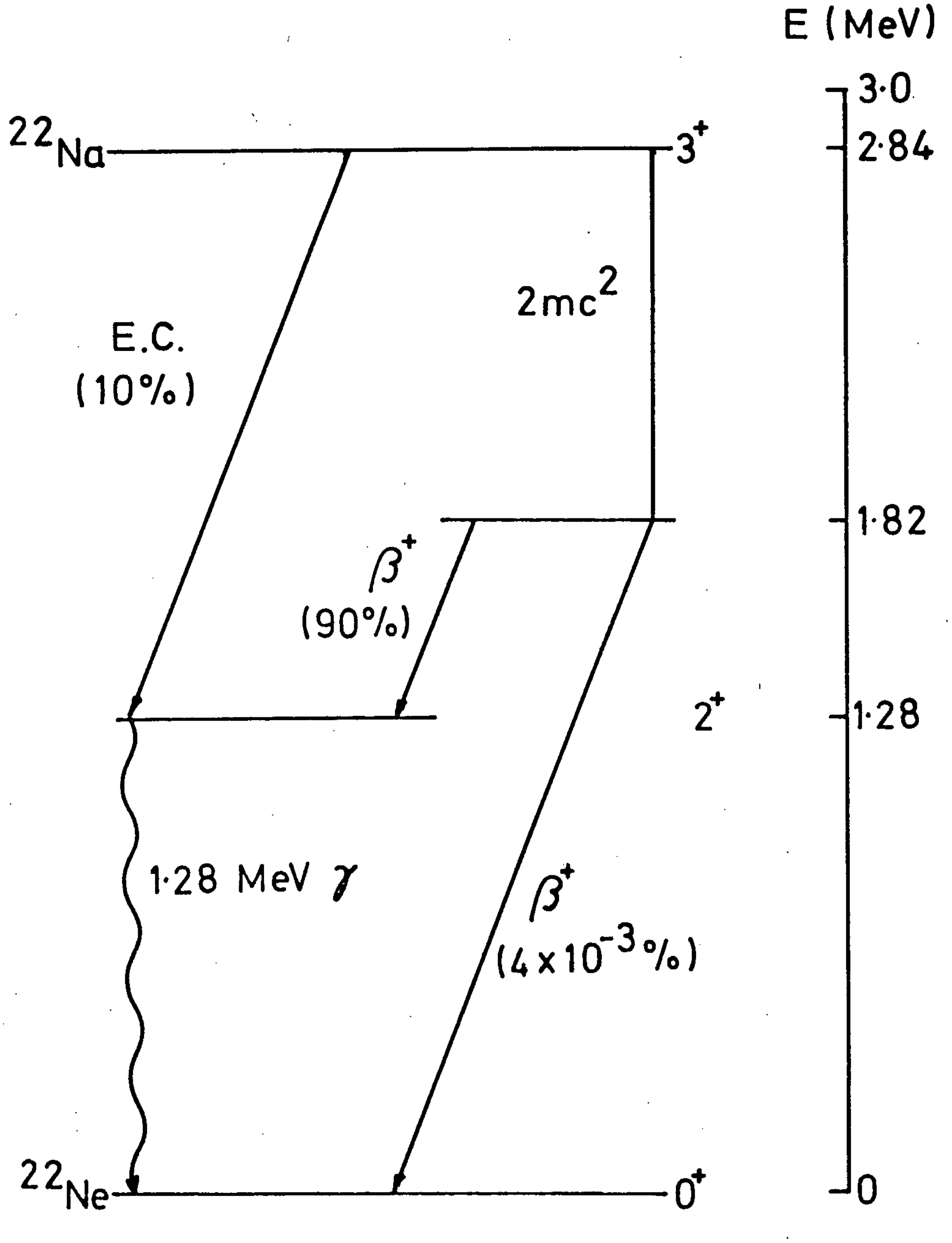

Fig. 20. Decay scheme of ^{22}Na.

and $w_0 = \frac{E^+_{max}}{mc^2}$ is the maximum or cutoff positron energy for a given radionuclide.

A plot of the theoretical β^+ spectrum of ^{22}Na ($E_{max}(e^+)$ = 542 KeV) appears in Figure 21.

Typical $^{22}NaCl$ or ^{64}Cu source strengths range from a few microcuries to hundreds of millicuries (1 Curie (Ci) = 3.7×10^{10} disintegrations per second (dps)). Although stronger sources can be produced, handling and protective shielding become cumbersome.

It is obvious that sources of this nature (extrinsic) will not be very efficient in terms of producing enough positrons to probe laser compression plasmas with lifetimes of the order of 10^{-9} sec or less. If a 1 Ci radionuclide source could somehow be incorporated into a laser compression plasma, only 37 or so positrons would be produced during the lifetime of the plasma. No statistically significant annihilation γ signal could be measured under these circumstances. This is not the case in Tokamak type plasmas, which have lifetimes about seven orders of magnitude longer, allowing for the production of statistically significant numbers of positrons during the existence of the plasma (e.g. $\sim 3.7 \times 10^6$ positrons would be produced by a 10 mCi source during the 10^{-2} sec lifetime of a toroidal plasma).

(ii) Intrinsic Sources: Positron-electron pair production does not occur under normal circumstances in solids, liquids or gases, but it is expected to occur, under

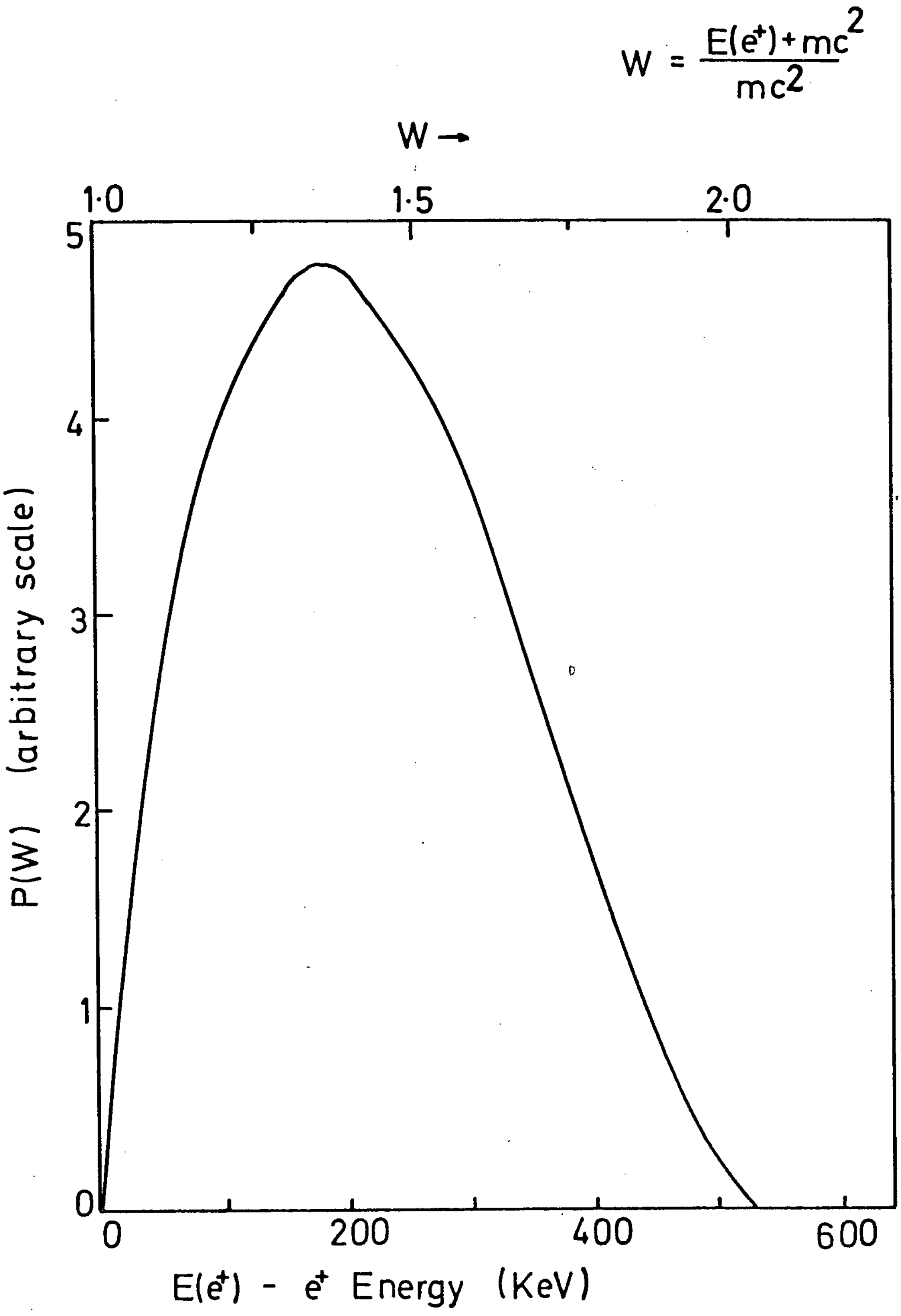

Fig. 21. Energy distribution of ^{22}Na positrons.

normal circumstances, in some plasmas. Such pair production would act as a natural, intrinsic source of positrons - positrons which could then be used for diagnostic purposes.

(a) Tokamak Type Plasmas: Pair production in toroidal plasmas should be mediated by collisions between high energy 'runaway' electrons and 'cooler' electrons, ions or neutrals. In a fully ionized hydrogen plasma of the type being considered, the total cross section for pair production by electron-electron collisions is given approximately by: (Heitler, 1954. Chapter V)

$$\sigma_{pp} \simeq \frac{r_0^2 \ \alpha^2}{\pi} \ \ln^3\left(\frac{\beta E^-}{mc^2}\right) \tag{36}$$

where β is a constant of order one; take $\beta=1$ here,

$r_0 = \frac{e^2}{mc^2}$ is the classical electron radius,

$\alpha = \frac{e^2}{\hbar c}$ is the fine structure constant,

and $E^- = mc^2 + E(e^-)$

The total number of pairs produced per unit time, per unit plasma volume is:

$$N_p \simeq c \ n_r \ n \ \frac{r_0^2 \ \alpha^2}{\pi} \ \ln^3\left(\frac{E^-}{mc^2}\right) , \tag{37}$$

where n is the thermal electron number density

and n_r is the runawy electron density.

Choosing conservative values for n_r(= 10^7 cm^{-3}) and for the runaway electron kinetic energy (~ 10 MeV), based on experiments by Knoepfel *et al.* (1975) with the Oak Ridge Tokamak (ORMAK), N_p can be calculated. These values are deemed conservative because ORMAK is considerably smaller (major radius = 80 cm, minor radius = 23 cm) than the hypothetical toroidal plasma under consideration here and runaway electron densities and energies are expected to increase as plasma dimensions are scaled up. The calculated value, using n = 10^{14} cm^{-3} is: $N_p \simeq 1.1 \times 10^3$ sec^{-1} cm^{-3}. Thus, the total number of pairs produced during the existence of the plasma (runaway electrons exist during most of the plasma lifetime of $\tau_{p\ell} = 10^{-2}$ sec) in a volume of 10^3 cm^3 is ~ 1.1×10^4, or summed over the entire volume of the plasma (~ 7.4×10^6 cm^3): ~ 8.4×10^7 pairs. If all the positrons annihilate in the plasma, this corresponds to an equivalent activity of ~ 30μCi per litre.

(b) Laser Compression Plasmas: Pairs could theoretically be produced by three mechansims in a laser plasma situation: vacuum polarization by intense laser fields, collisionless oscillation of a free electron driven by intense laser fields and collision of electrons accelerated by intense laser fields with other plasma components. The threshold intensities for the first two processes using neodymium glass lasers (λ = 1.06μ) are ~ 10^{26} W cm^{-2} and ~ 3×10^{24} W cm^{-2} respectively (Hora, 1973) - out of the range of existing technology. The third process, however, does not have such a high threshold.

Expression (37) can be used to calculate the total number of pairs produced by this collision process. A calculation of this nature was originally carried out by Bunkin and Kazakov (1970), who wrote E^- as the total (non-relativistic) energy of an electron in the field of a plane monochromatic wave of frequency ω and vacuum amplitude E_v:

$$E^- = mc^2 + \frac{1}{2}\,\frac{e^2\,E_v{}^2}{m\omega^2} \tag{38}$$

The calculation was repeated relativistically by Hora (1973), who considered only the energy associated with the electron oscillation in the laser field, writing:

$$E^- = \frac{ec\,E_v}{\omega\,\eta^{\frac{1}{2}}} \tag{39}$$

In this way, he was able to consistently take into account the enhancement of electron energies due to the variation of the complex refractive index of the plasma, η, with electron collision frequency. The results of N_p calculations using (38) and (39) do not differ by more than an order of magnitude because E^- appears in the logarithmic term of expression (37).

Using the expression for total electron energy (38), the total pair production cross section can be written in terms of laser intensity, I, as:

$$\sigma_{pp} \simeq \frac{r_0^2\ \alpha^2}{\pi}\ \ln^3\left[1 + \left(\frac{2\pi\ r_0}{mc}\right)\frac{I}{\omega^2}\right], \tag{40}$$

where ω is the laser frequency. The total number of pairs produced per unit time, per unit plasma volume is then:

$$N_p = c\ n^2\ \frac{r_0^2\ \alpha^2}{\pi}\ \ln^3\left[1 + \left(\frac{2\pi\ r_0}{mc}\right)\frac{I}{\omega^2}\right], \tag{41}$$

where n is the electron number density of the plasma. This calculation has been carried out for a Nd glass laser produced plasma with $n = 10^{21}\ cm^{-3}$. The value of n chosen for this calculation is approximately the critical density, above which the refractive index of the plasma for 1.06μ light becomes imaginary and the light no longer penetrates the plasma.*

Resulting N_p values are: ~ $1.4 \times 10^{22}\ sec^{-1}\ cm^{-3}$ with $I = 5 \times 10^{18}\ W\ cm^{-2}$ and ~ $5.6 \times 10^{23}\ sec^{-1}\ cm^{-3}$ with $I = 5 \times 10^{19}\ W\ cm^{-2}$. In terms of pairs produced within the finite plasma being considered, this translates into:

---

*Higher density plasmas are predicted, however energy transfer by some method other than by electromagnetic fields is expected to take place from the outer 'laser interaction shell' to the inner, high density core. The high energy particles in the field-free cores of such plasmas should make some contribution to pair production by collisions, however, this contribution is not being considered quantitatively here. Such considerations are complicated by the fact that the 'shell' to 'core' energy transfer process is not well understood.

$$\text{and} \quad \begin{array}{l} \sim 1.4 \times 10^5 \text{ with } I = 5 \times 10^{18}\ \mathrm{W\ cm^{-2}} \\ \sim 5.6 \times 10^6 \text{ with } I = 5 \times 10^{19}\ \mathrm{W\ cm^{-2}} \end{array}$$

for a plasma with a volume $V = 10^{-6}\mathrm{cm}^3$ and a laser pulse length $\tau_\ell = 10^{-11}$ sec. Note that the relevant time parameter here is τ_ℓ (which defines how long the laser fields are present) and not $\tau_{p\ell}$, the plasma lifetime, which is somewhat longer.

Chapter VI

GAMMA RAY DETECTORS

An assortment of detectors can be used to measure the annihilation radiation which escapes from the plasma. Each type has its advantages and disadvantages and is usually suited for use with a specific analysis technique (see Chapter VII).

A. Scintillation Counters

Counters of this type consist of a scintillant (phosphor) which is optically coupled to a photomultiplier (Figure 22a, Ouseph, 1975). An annihilation gamma which enters the scintillant can lose energy to it via the photoelectric effect and the Compton effect, leaving behind a trail of ion pairs. Recombination occurs (although energy transfer mechanisms associated with it differ from one phosphor to another) with the emission of visible light photons. Since the phosphors are chosen to be transparent to their own radiation, some fraction of the emitted photons is detected by the photomultiplier, which amplifies the signal

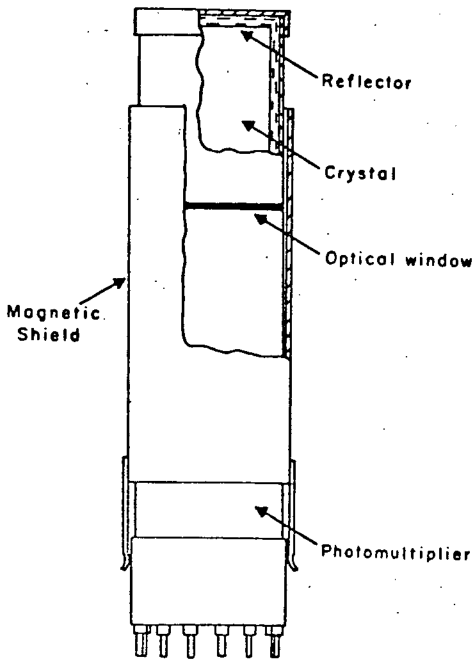

Fig. 22 a.

Scintillation type detector.

Fig. 22 b.

Semiconductor type detector.

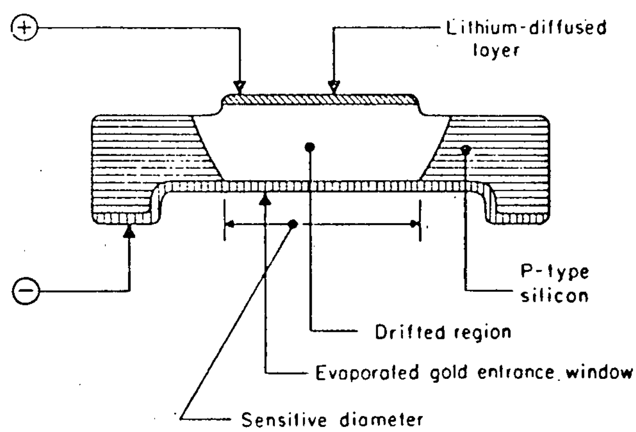

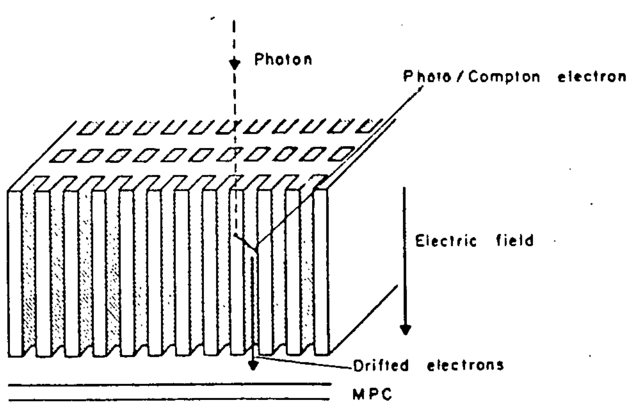

Fig. 22c.

Multiwire drift type detector.

and triggers a counter. The main scintillants suitable for γ ray detection are listed in Table III.

Sodium iodide activated with thallium (the activator defines the emission wavelength) is the most common scintillation type gamma ray detector. The efficiency of these detectors varies with the energy of the incoming gamma radiation and with the physical size of the crystal. A cylindrical crystal of NaI ($T\ell$), 4 cm in diameter and 2.5 cm in length has an efficiency* of $\varepsilon \simeq 50\%$ for 500 KeV gamma photons. The energy resolution is limited by statistical fluctuations associated with the detection and amplification processes. A detector utilizing a NaI ($T\ell$) crystal with the dimensions quoted is capable of $\rho \simeq 8\%$ energy resolution** at gamma ray energies of $E(\gamma) \simeq 600$ KeV, which corresponds to a gamma ray linewidth of $\Delta E_{FWHM} \simeq 48$ KeV (Burcham, 1973, Chapter 6). Average response times of the common scintillants are indicated in Table III.

---

*Efficiency, ε, is defined as the percentage of γ rays entering the detector which are detected in (contribute to) the 'full energy' or annihilation photopeak (Figure 27).

**Percentage resolution, ρ, is defined as:

$$\rho = \frac{\Delta E_{FWHM}}{E(\gamma)} \times 100\%$$

where ΔE_{FWHM} is the full width at half maximum of the gamma ray 'line' corresponding to a gamma ray of energy $E(\gamma)$ (see Chapter VII, Section D for more details).

Table III

γ Ray Scintillants

Material	Form	Main Emission λ (Å)	Response Time (nsec)
NaI(Tℓ)	Hygroscopic Crystal	4100	250
Anthracene/ Stilbene	Organic Crystal	4000 - 4450	8-30
Organic Plastics	Geometry as Required	4250	2

(after Burcham, 1973, Chapter 6)

B. Semiconductor Counters

A number of methods exist to produce semiconductors with regions of low (or zero) conductivity (no electrons in the conduction band). A high electric field can be placed across such regions of low conductivity without significant current flow. Gamma rays passing through these regions elevate electrons into the conduction band creating free electron-hole pairs. The energy required to accomplish this is low: 3.6 eV and 0.67 eV per electron-hole pair in silicon and germanium respectively. Under the influence of the electric field, the electrons and holes migrate in opposite directions, the net result being a small current which can be detected and amplified externally and used to trigger a counter.

Lithium drifted germanium detectors (the lithium compensates the acceptor centres in the germanium to create regions of low conductivity) are the most suitable for high resolution gamma ray work (Figure 22b, Coche and Siffert, 1968). Although this type of detector must be cooled to liquid nitrogen temperatures to minimize thermal excitation of electrons to the conduction band, the energy resolution is excellent because the unwanted 'noise' due to statistical fluctuations is significantly lower. An energy resolution of $\rho \simeq 0.6\%$ at gamma energies of 500 KeV is typical.* This

*Higher resolution (narrower response function) is possible if preamplifier noise (the resolution limiting factor at gamma ray energies of this order) can be reduced. For example, a resolution of $\rho \simeq 0.25\%$ at $E(\gamma) = 500$ KeV has been reported (Heath *et al.*, 1966).

corresponds to a linewidth of $\Delta E_{FWHM} \simeq 3$ KeV and is more than an order of magnitude improvement over scintillation counters. Figure 23 (Hollander, 1966) is a comparison of a number of typical detection systems in terms of attainable resolution (width of the response function). The crystal diffraction curve is included for completeness only - this is not a useful technique where weak sources are involved, due to its inherent inefficiency (counting rates of the order of 5×10^{-9} of the source strength for 500 KeV γ rays).

The efficiency of semiconductor detectors is lower than that of scintillation type detectors because of the difference in stopping power (which varies with atomic number) and because the physical size of useable semiconductors is limited by fabrication procedures. Depending primarily on the volume of the detector, the efficiency varies from $\varepsilon \simeq 1\%$ to $\varepsilon \simeq 10\%$ for 500 KeV gamma rays, as shown in Figure 24 (Cappellani and Restelli, 1968). One NaI (Tℓ) curve is plotted for comparison. The response time of semiconductor detectors is in the nanosecond range.

C. Multi-Wire Proportional Counters

Recently, an ingenious gamma ray detector with spatial resolution in two dimensions has been developed (Jeavons *et al.*, 1975). Some preliminary work with annihilation radiation has been carried out and Stewart (Queen's

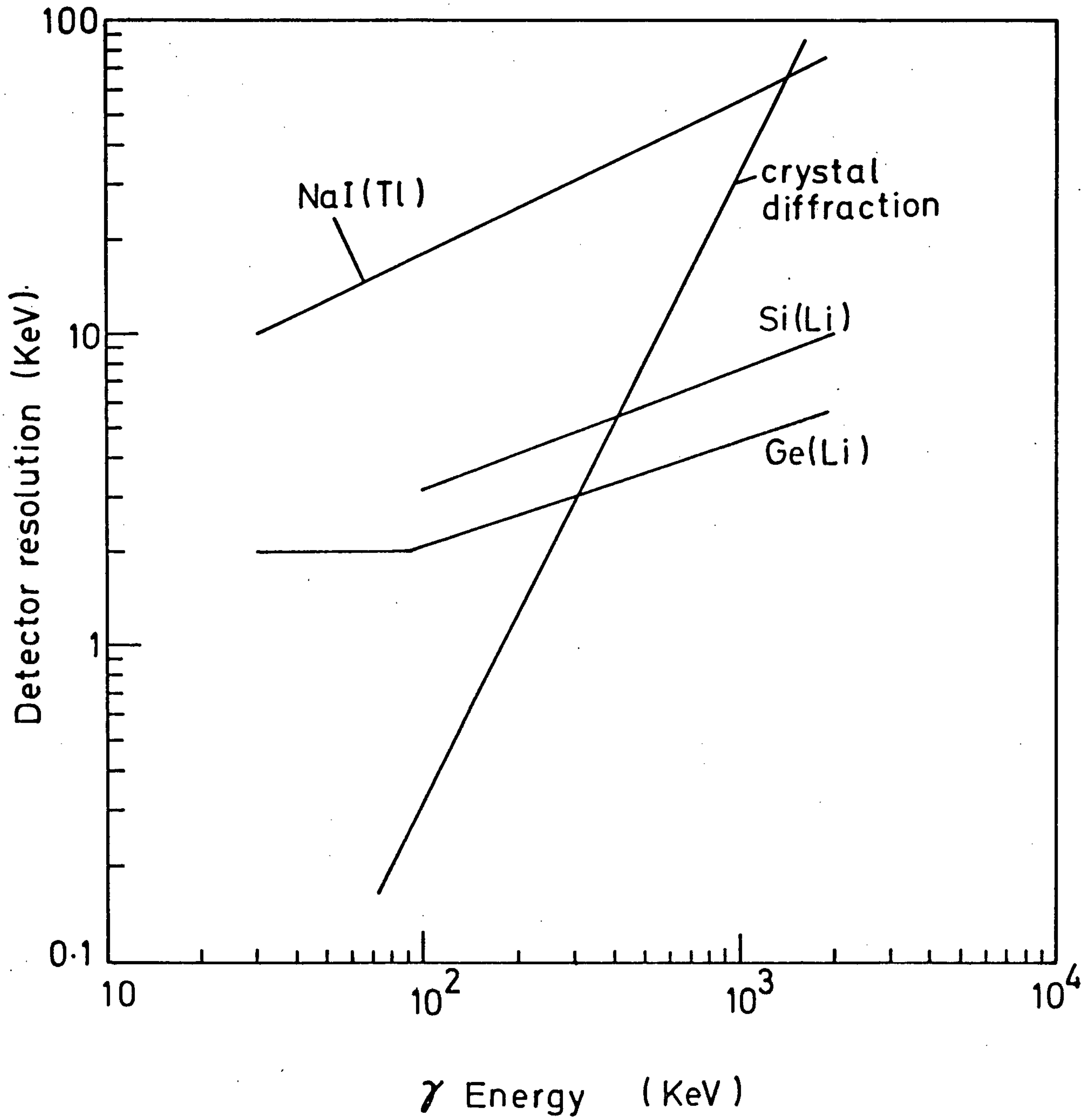

Fig. 23. Variation of detector resolution with γ energy.

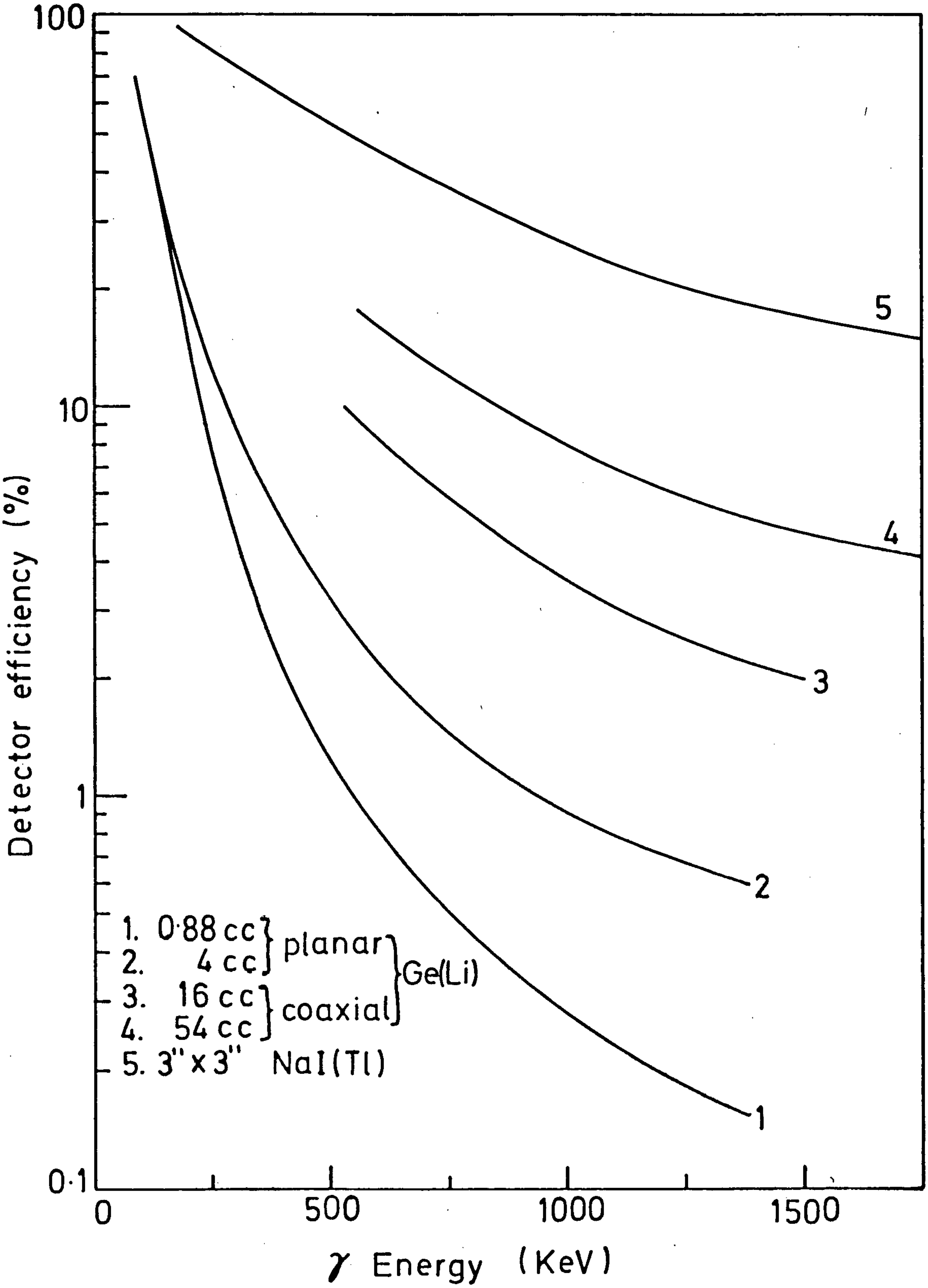

Fig. 24. Variation of detector efficiency with γ energy.

University) is incorporating this type of detector in an angular correlation system which is to have an angular resolution of 0.1 mrad x 0.1 mrad. This is equivalent to an energy resolution of $\rho \simeq 0.01\%$ at $E(\gamma) = 511$ KeV (corresponding to a linewidth of ~ 50 eV).

The device converts incoming gamma photons to electrons via the photoelectric interaction. These electrons escape into one of many parallel holes drilled through the converter and drift out of the converter (guided by the holes) under the influence of an external electric field. Having left the converter the electrons are counted by a multi-wire proportional counter. The latter is essentially a grid of individual, closely spaced proportional counters.

Using a gas-solid hybrid converter (Figure 22c, Jeavons *et al.*, 1975), 60% of the gamma photons (at 1.8 MeV) that interact are counted. This efficiency is projected for the entire 0.1 MeV to 2.0 MeV range of incoming gamma ray energies. Although the single-event energy resolution is poor, the spatial resolution (which is the important factor in angular correlation experiments) is good. The latter is ~ 1.3 mm, approximately equal to the hole size (1.0 mm) for incident gamma ray energies less than about 1.0 MeV. Response times are of the order of 500 nsec.

Chapter VII

ANALYSIS TECHNIQUES

A. Technique Survey

As a final gauge of the common annihilation radiation analysis techniques, and in light of the preceding discussions concerning sources (strengths) and detectors (resolutions; efficiency), gamma ray counting rate calculations are carried out. The initial calculations for both Tokamak and laser compression plasmas are general in nature, however subsequent calculations relate to specific techniques. The four techniques considered (measurements of: 2γ angular correlation, annihilation line width, positron lifetime and slow positron beam spread) are illustrated schematically in Figure 25. In each case, a schematic raw data curve is shown and deriveable functions or parameters indicated. Here, c is the count rate, N_{e^-} is the electron number density and $f_{e^-}(v)$ is the electron velocity distribution.

B. General Counting Rate Calculations

Considering only positrons produced in a plasma and assuming that nearly all these positrons annihilate in

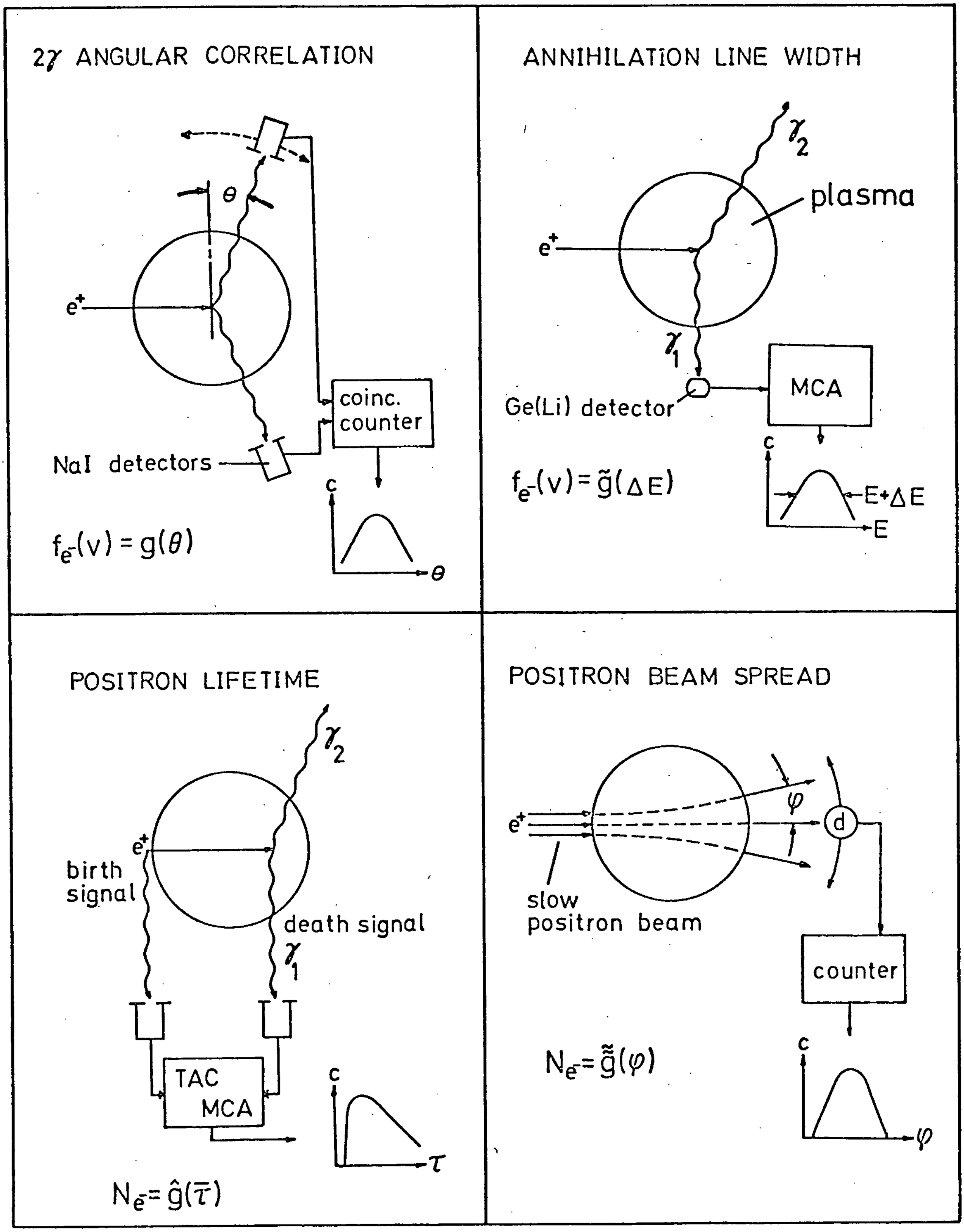

Fig. 25. Analysis techniques.

this plasma, the number of counts (gamma photons) registered during one plasma lifetime can be written as:

$$C = 2A \varepsilon GM_a \tag{42}$$

where A is the number of positrons produced during the plasma lifetime in the volume being considered,

ε is the detector efficiency,

G is the solid angle factor that indicates what percentage of gamma rays produced in the plasma volume being considered enters the detector,

and M_a is a miscellaneous attenuation factor that is meant to account for:*

(a) positrons escaping from the plasma,

(b) positrons annihilating after the plasma has ceased to exist,

(c) absorption of gamma rays by intervening material,

(d) various gamma ray scattering corrections.

The factor of 2 accounts for the fact that each annihilation event creates two gamma photons.

---

*For the purpose of these order of magnitude calculations M_a values of 0.1 (Tokamak) and 0.5 (laser compression) have been chosen, assuming that miscellaneous losses associated with the well localized laser compression plasma are less than those associated with the more diffuse Tokamak plasma. Exact M_a values can be determined only when the complete experimental layout is known.

(i) Tokamak Plasma

C is calculated for the following hypothetical arrangement:

Detector Efficiency	ε = 10%
Plasma Volume Visible to Detector	50 cm x 50 cm x 50 cm = 1.25×10^5 cm^3 (~ 1.7% of total volume)
Total number of Annihilations in this Volume during Plasma lifetime (10^{-2} sec)	A = 1.4×10^6 (from Chapter V, Section C)
Detector Distance from Centre of Plasma	100 cm
Solid Angle Factor	G $\simeq$ 2%
Miscellaneous Attenuation Factor	$M_a \simeq 0.1$
Detector Dimensions << Plasma Dimensions	
Calculated Counting Rate	C $\simeq$ 560 counts per discharge

This count rate is sufficiently high, that of the analysis techniques outlined in this chapter, at least the annihilation line broadening technique should be feasible.

(ii) Laser Compression Plasma

The parameters used to calculate C are:

Detector Efficiency	ε = 10%
Detector Surface Area	7 cm^2

Plasma-Detector Distance	20 cm
Solid Angle Factor	$G \simeq 0.14\%$
Total Number of Annihilations in Entire Plasma Volume during Plasma Lifetime (10^{-9} sec)	$A = 1.4 \times 10^5$ (for $I = 5 \times 10^{18}$ W cm^{-2}, Chapter V, Section C)
Miscellaneous Attenuation Factor	$M = 0.5$

Plasma Dimensions << Detector Dimensions

$C \simeq 20$ counts per plasma detonation

The counting rate increases linearly with the surface area of the detector, thus the use of a number of detectors in parallel would significantly enhance the counting rate. For a 2π detector ($G = 50\%$), with the plasma at the centre, $C \simeq$ 7,000 counts per plasma detonation. Any increase in laser power and hence A will also increase C. Annihilation gamma radiation from laser compression plasmas should be detectable and intense enough to facilitate at least one type of analysis.

C. 2γ Angular Correlation

The theory of this technique has been outlined in Chapter II, Section (C)(i), thus it remains to evaluate its applicability to the Tokamak or laser compression systems.

(i) TOKAMAK Plasma

If two detectors are used, and only γ coincidences are counted, then the coincidence counting rate is approximately:

$$C_c = 4A\ \varepsilon_1\varepsilon_2\ G_1G_2 \quad , \tag{43}$$

where the subscripts identify the detectors. No spatial (or angular) resolution is possible with the detector arrangement quoted in Section (B)(i) of this chapter. In order to measure angles in the milliradian range, the geometrical resolution of the system must be at least of this order. This implies: (a) a detector with slit width: ~ 1 mm sampling a plasma characterized by linear dimensions of the order of mm, from a distance of 100 cm or (b) a slit width of ~ 1 cm at a distance of 10 m sampling a plasma characterized by centimetre dimensions. (Recall that source and detector need be well defined in only one dimension since only one component of the electron-positron centre of mass is being measured.) For a detector 10 cm long, the solid angle factors are $G_{1,2} \simeq 10^{-3}\%$ and $G_{1,2} \simeq 10^{-4}\%$ respectively for geometries (a) and (b) mentioned above. In case (a), $A \simeq 10^1$; thus, even choosing $\varepsilon_1 = \varepsilon_2 = 100\%$, the total number of coincidence counts per Tokamak discharge is $C \simeq 10^{-8}$ (miscellaneous attenuation ignored). Clearly, angular correlation measurements of the type described here are not feasible at the positron density calculated to exist during a typical Tokamak discharge. This density could be increased by somehow injecting positrons into the plasma from outside, or doping the discharge gas with a β^+ decay radionuclide, however it is doubtful whether it could be increased by the requisite eight or so orders of magnitude to yield a reasonable number of coincidence counts per discharge.

(ii) Laser Compression Plasma

Replacing the extended Tokamak source by the laser compression point source ($A = 5.6 \times 10^6$ corresponding to a Nd laser intensity: $I \simeq 5 \times 10^{19}$ W cm^{-2}), but retaining the ε and G factors of the previous calculation (same angular resolution required), expression (43) indicates $C \simeq 2 \times 10^{-3}$ coincidence counts per detonation. This is the optimum count rate which would in practice be reduced by the less than perfect detector efficiencies and by miscellaneous losses.

As pointed out in Chapter V, Section (C)(i), it is not possible to significantly increase the positron density in the plasma by any conventional means (e.g. radionuclide doping), due to the short time scales involved.

Since it is not practical (at this time) to sum over the order of thousands of detonations, one dimensional angular correlation analysis of laser compression plasmas must be ruled out.

The exact situation with respect to two-dimensional angular correlations using multi-wire proportional counters is not clear, since such a system does not yet exist. One of the advantages of using two-dimensional multi-wire proportional counters is that the counting rate increases significantly due to their inherent sensitivity and the increase in the solid angle factor. If an efficient 2D angular correlation system can be developed to replace the current 1D, 'long slit' systems, angular correlation studies may be possible with some fusion plasmas. An additional advantage of the 2D technique is the fact that it would make available information about two components of the positron-electron centre of mass momentum simultaneously.* In plasmas (unlike solids) the individual positron and electron contributions to the centre of mass momentum would be roughly equal, necessitating the application of some type of unfolding procedure to separate the contributions (more details in the next section).

D. Doppler Broadening and Shift of the Annihilation Line

Perhaps the most promising positron technique that could be used to study plasmas involves the analysis of the Doppler broadening of the 511 KeV annihilation line. A number of "line-broadening" studies have been carried out with positrons annihilating in metals (Du Mond *et al.*, 1949; Murray, 1967). Although Doppler broadening was measured in these experiments, excessively high source activity (Du Mond *et al.*) and low detector resolution (Murray) limit the usefulness of these techniques for solid-state diagnostic purposes.** This is not the case in many plasmas, where the resolution problem does not exist.

---

*This is an advantage only in cases where the momentum distribution is expected to be anisotropic. In isotropic situations a parallel wire proportional counter (multi-slit system) would suffice.

**Nonetheless, some work of this nature has been attempted; see, for example, Hotz *et al.* (1968) and MacKenzie (1969).

(i) Theory

The total energy of one annihilation gamma photon, as measured by an observer at rest with respect to the plasma, is given by expression (61) (Appendix B). It is possible to analyze this energy in terms of three effects contributing to its magnitude. Its approximate magnitude is determined by $E_0 = mc^2$, one half of the pair rest mass energy. The thermal motion of the pre-annihilation pair manifests itself in two different ways: (a) it causes an absolute shift in the energy of each gamma photon (away from $E_0 = mc^2$) of the order of:

$$\delta E \simeq \frac{E_0}{2}\left(\frac{\bar{v}_{cm}}{c}\right)^2 = \frac{1}{2}\, m\bar{v}_{cm}^2 \quad , \tag{44}$$

(see expression (63), Appendix B) where $\bar{v}_{cm}$ is the mean centre of mass velocity of the pre-annihilation pair; and (b) it introduces a Doppler shift in the energy of a given gamma photon which depends on the magnitude of the velocity component of the pre-annihilation pair in the direction of emission of that gamma photon ($\hat{v}_{cm}$). The magnitude of this shift is:

$$\Delta E_D = E_0 \frac{\hat{v}_{cm}}{c} \quad , \tag{45}$$

where $\hat{v}_{cm}$ is taken relative to a fixed detector (see expression (64), Appendix B).

The E_0 term locates the 'annihilation line' at an energy of about 511 KeV, while δE (expression (44)) manifests itself as a shift of the entire line to a higher energy. The mean absolute shift, as a function of the mean plasma electron energy (kT_e) is plotted in Figure 26 as the 'shift' curve (details in part (ii) of this section). Clearly, it is impossible to measure the shift at low plasma temperatures and at electron temperatures characteristic of solids (e.g. the fractional shift $\delta E/E_0$ is ~ 4 x 10^{-3}% at a mean plasma temperature of ~ 10^5°K or ~ 10 eV). Although it may be possible to measure absolute shifts in more energetic plasmas and thus determine mean plasma temperatures, this is not the most promising approach.

The ΔE_D term (expression (45)) describes the broadening of the $\hat{v}_{cm}$ = 0 delta function profile. Writing the fractional line broadening as:

$$\frac{\Delta E_D}{E_0} = \frac{\hat{v}_{cm}}{c} , \qquad (46)$$

it is evident that in solids, where mean electron energies are of the order of electron volts, the mean annihilation line broadening will be less than 1% (ΔE_D of the order of a few KeV).* The resolution of the present day semiconductor

*Figure 26, which is a plot of $2\sqrt{\ln 2}\, \Delta E_D$ against kT_e (broadening curve), gives an indication of how ΔE_D varies with electron temperature, T_e (see part (ii) of this section for more details).

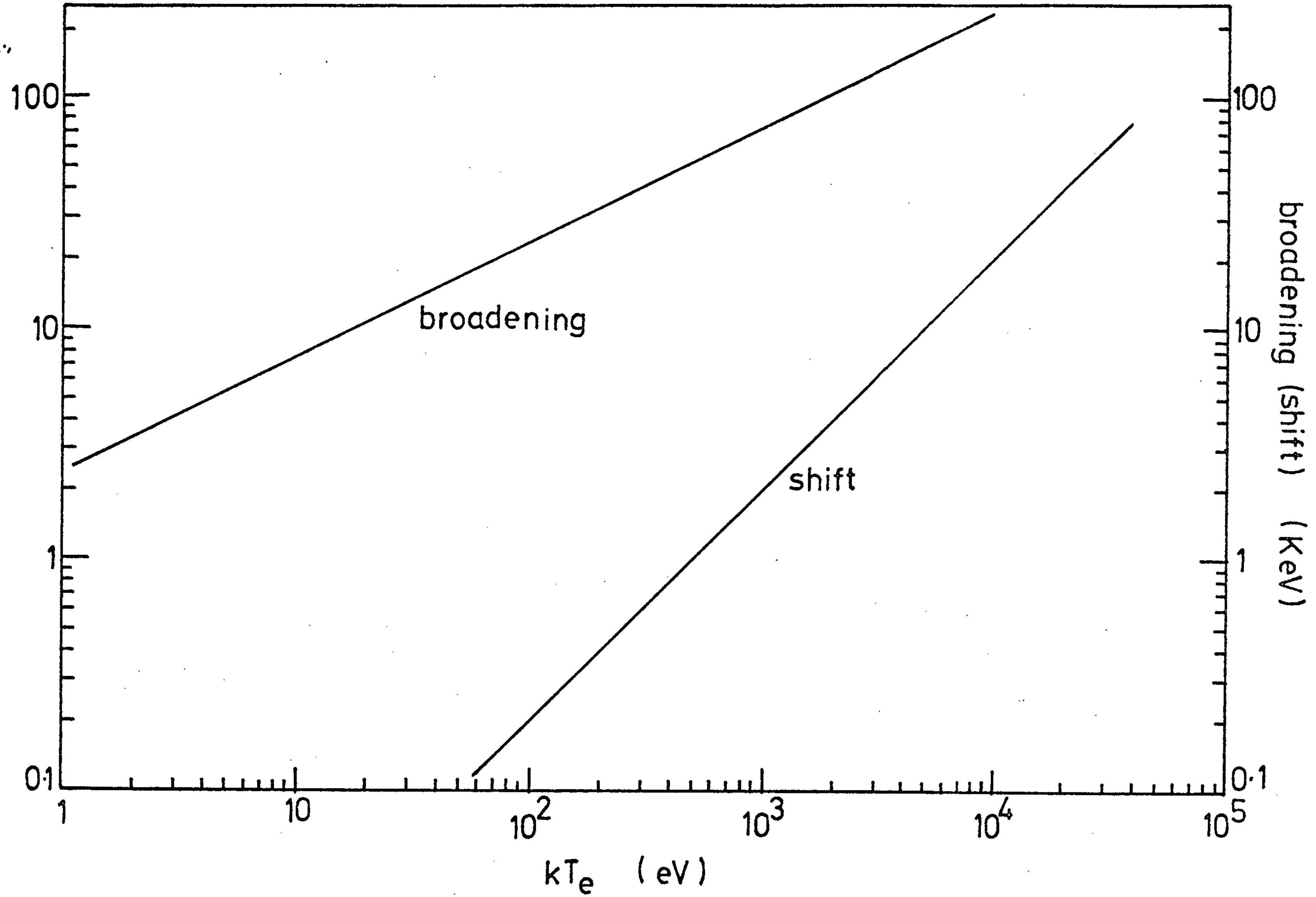

Fig. 26. Variation of Doppler broadening and shift with plasma kT_e.

detectors which could be used to measure annihilation line profiles is of the same order of magnitude, making exact determination of broadening and line profiles difficult. The situation in plasmas is much more favourable, because mean electron temperatures are considerably higher than in solids; in fact, in some fusion plasmas electron temperatures may reach 10^{8}°K (mean electron energies of the order of 10 KeV). At these temperatures, the mean fractional line broadening, $\Delta E_D/E_0$ amounts to ~ 20% - easily detectable. Even at electron temperatures as low as 10^{6}°K ($kT_e \simeq 100$ eV) the line broadening is easily detectable.

In addition to the annihilation line width, the shape is also of interest. When the 1γ contributions can be ignored (low probability - see Appendix A), the theoretical 2γ annihilation spectrum for positrons and electrons annihilating at rest is a delta function at $E(\gamma) = mc^2$. If such static situations exist (it seems this may be the case in ice, deZafra and Joyner, 1958), then the measured width of the annihilation line in these cases is entirely a result of instrument broadening (i.e. it is just the instrument response function). In the usual situation where the positron-electron centre of mass velocity is not zero, the measured profile is a convolution of the instrument profile and the Doppler broadened delta function profile.* Since the Doppler profile

*Practically speaking, the annihilation spectrum (Figure 27) consists of a Compton continuum (which results because some of the annihilation gammas suffer Compton scattering and the associated energy loss before being detected)

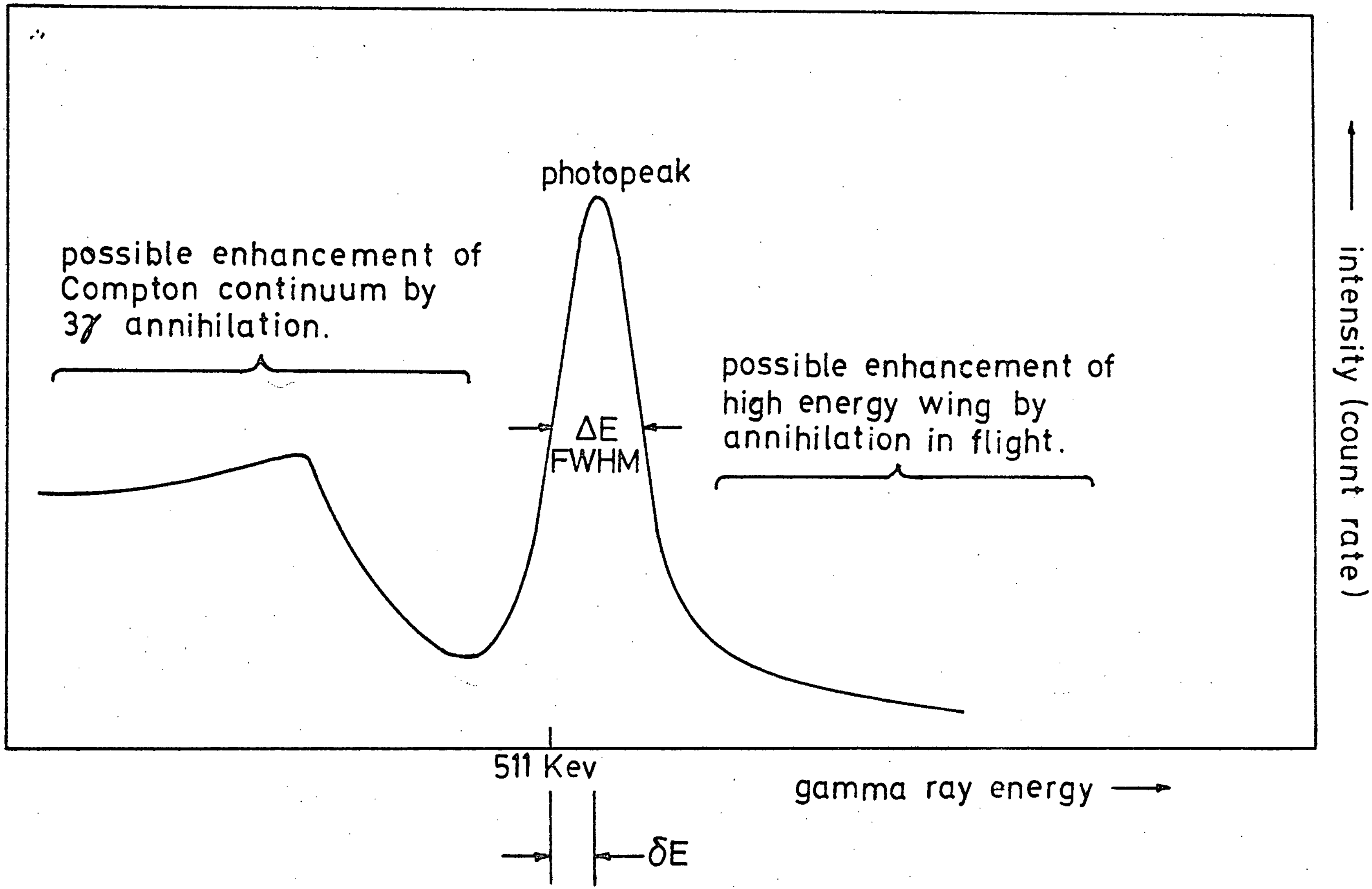

Fig. 27. Annihilation gamma ray spectrum.

results from the positron-electron centre of mass motion, it is essentially a record of the positron-electron centre of mass velocity distribution and therefore implicitly of the electron velocity distribution.

(ii) Analysis

Aside from the scale factor E_0/c, the annihilation line Doppler profile, $I_D(E)$, is just $w_{cm}(\hat{v})$, the positron-electron centre of mass velocity distribution in one component (defined by the detector location). If w_{cm} is isotropic, then $f_{cm}(v)$, the distribution in magnitude of centre of mass velocity, follows by integration over velocity space.

It is important to note that both $w_{cm}(\hat{v})$ and $f_{cm}(v)$ are actually convolutions of the two corresponding positron and electron functions: $w_{e^+}(\hat{v})$, $w_{e^-}(\hat{v})$ or $f_{e^+}(v)$, $f_{e^-}(v)$. If f_{e^+} and f_{e^-} are identical, as one would expect them to be after complete positron thermalization, deconvolution or unfolding to determine $f_{e^-}(v)$, the electron velocity distribution of interest is straightforward. Otherwise, the functional form of f_{e^+} must be known in order to find f_{e^-}.

---

and the photopeak (the annihilation line itself), separated by a well defined valley. Any gamma photons resulting from 3γ annihilation (energies distributed from 0 to 511 KeV, Figure 2) will increase the intensity of the Compton distribution and the valley relative to that of the photopeak. Annihilation of positrons in flight (prior to thermalization) would be signalled by an intensity increase of the high energy wing of the annihilation line. The latter effect is expected to be negligible in plasmas.

The following is an outline of the complete procedure to determine $f_{e^-}(v)$:

(a) Measure the annihilation profile: $I_m(E)$. This can be written as:

$$I_m(E) = \int_{-\infty}^{\infty} I_i(E - E')\, I_D(E')\, dE' \tag{47}$$

where I_i is the instrument response function and I_D is the true Doppler profile.

(b) Unfold $I_m(E)$ to determine $I_D(e)$. This is straightforward using Fourier techniques.

(c) Make the appropriate scale change to convert $I_D(E)$ to $w_{cm}(\hat{v})$.

(d) Calculate $f_{cm}(v)$ from $w_{cm}(\hat{v})$ by integrating over velocity space. The function $f_{cm}(v)$ can now be written as:

$$f_{cm}(v) = \int_{-\infty}^{\infty} f_{e^+}(v - v')\, f_{e^-}(v')\, dv' \ , \tag{48}$$

where f_{e^+} and f_{e^-} are individual positron and electron velocity (magnitude) distributions respectively.

(e) Unfold $f_{cm}(v)$ to determine $f_{e^-}(v)$. Unless $f_{e^+} = f_{e^-}$, f_{e^+} must be known.

A somewhat less detailed analysis can be carried out by looking at line widths only. The HWHM of $I_D(E)$ or $w_{cm}(\hat{v})$ can be taken as an indication of the mean kinetic energy associated with the centre of mass motion of the positron electron pairs. This is in turn related to the mean kinetic energy associated with electron motions and hence to the mean electron temperature.

For example, if $w_{cm}(\hat{v})$ is a Gaussian with a FWHM of Δv_{cm} and both f_{e^+} and f_{e^-} are Gaussians with FWHM of Δv_{e^+} and Δv_{e^-}, then

$$\Delta v_{cm} = \Delta v_{e^+}{}^2 + \Delta v_{e^-}{}^2 \tag{49}$$

If $f_{e^+} = f_{e^-}$ then

$$\Delta v_{e^-}{}^2 = \frac{\Delta v_{cm}{}^2}{2} \tag{50}$$

The FWHM of $I_D(E)$ is usually written in terms of the Doppler width as:

$$\Delta E_{FWHM} = 2\sqrt{\ln 2}\; \Delta E_D \tag{51}$$

Using expression (46) for ΔE_D, expression (50) to link pair centre of mass and individual electron velocities, and writing:

$$v_{e^-} = \frac{\Delta v_{e^-}}{2} = \sqrt{\frac{2k\,T_{e^-}}{m}} \tag{52}$$

for the HWHM velocity associated with $f_{e^-}(v)$, expression (51) can be solved for T_{e^-}:

$$T_{e^-} = \frac{\Delta E^2_{FWHM}}{(4\ \ln 2)\ 4k\ mc^2} \tag{53}$$

where k is Boltzman's constant.

The 'broadening' curve of Figure 26 is a plot of ΔE_{FWHM} against kT_{e^-} - it specifies how the annihilation line width changes with plasma electron temperature. The variation of the absolute shift of the annihilation line with kT_{e^-} has also been plotted in Figure 26, with the aid of expressions (44), (50) and (52), which indicate (if $\bar{v}_{cm}$ is taken to be $\Delta v_{cm}/2$) that for a given value of T_{e^-}, the approximate shift is just $2kT_{e^-}$.

(iii) Assessment

The success of the line-broadening technique depends on being able to accurately measure the annihilation line shape, or at least its width. Detectors with the required resolution of 1 to 3 KeV at FWHM exist. The calculations of Chapter VII, Section B, indicate that currently available Ge(Li) detectors should be senstive enough to detect statistically significant amounts of annihilation radiation from positrons created in Tokamak and laser compression plasmas. It should be possible to measure accurate line profiles by integrating over a few cycles of either of these plasmas or by counting with more than one detector simultaneously (based on calculated counting rates). The line-broadening technique appears feasible.

E. Positron Lifetime Measurements

The essentials of measuring positron lifetimes have been outlined in Chapter II, Section (C)(ii). Measurements of positron lifetimes in plasmas of known electron density could resolve an important theoretical question: how large is the Coulomb correction to the annihilation cross section (and hence to the annihilation time) of positrons interacting with a 'sea' of unbound electrons, themselves exhibiting binary and collective interactions? Is Wolfer's theoretical prediction of the Coulomb correction accurate? (Chapter IV, Section C). Positron lifetime measurements could be used to ascertain plasma electron densities once these questions have been answered, that is, once the correct functional relationship between annihilation times and plasma electron densities has been determined.

Although the measurement of lifetimes involves delayed coincidence counting (counting positron creation and annihilation pulses in coincidence and keeping track of the electronically introduced delay times to obtain coincidence), it does not require the extreme spatial resolution demanded by angular correlation methods, thus, counting rates are higher. An accurate time mark signalling the creation of each positron is necessary for the success of this method. Since this is difficult to arrange in a laser plasma system (size and time scales being what they are), positron lifetime measurements in such a system do not seem feasible.

In a Tokamak plasma, positrons from extrinsic sources could be used, creation pulses being supplied by a thin scintillator placed between the source and the plasma or by the natural 1.28 MeV gamma ray which signals the β^+ decay of ^{22}Na (Chapter V, Section (C)(i)). The expected count rate can be calculated approximately using expression (43) with:

$\varepsilon_1 = \varepsilon_2 = 50\%$ (high efficiency NaI(Tℓ) detectors: the relatively slow time response is not a deterrent here because annihilation times should be orders of magnitude longer)

$G_1 \simeq 2\%$ (the solid angle factor for the detector generating positron creation pulses can vary greatly depending on the exact detection method and geometry chosen; for example $G_1 \simeq 50\%$ for a source next to the detector - a common arrangement)

$G_2 \simeq 2\%$ (solid angle factor for the detector generating positron annihilation pulses - same as in first calculation)

$A \simeq 3 \times 10^6$ (number of positrons annihilating in a 50 cm x 50 cm x 50 cm volume during the plasma lifetime, assuming that all the positrons from a 500 mCi extrinsic source are retained by the plasma and homogeneously distributed therein)

$M_a \tilde{\simeq} 0.1$ (assume a one order of magnitude signal loss due to miscellaneous causes as in first calculation).

These values give a coincidence count rate of $C_c \simeq 120$ counts per discharge. If this situation is realizeable, positron lifetime measurements in this type of plasma are feasible; however, important technical problems remain. Before measurements of this nature can be conducted, the following problems must be solved:

(a) introducing the positrons into the plasma without major losses* (it might be possible to dope the plasma 'fuel' with the appropriate amount of a β^+ radionuclide before the discharge - but this complicates (b) below)

(b) differentiating with certainty between positron creation and annihilation pulses (the degree of difficulty here depends on the solution to (a) above)

(c) arranging the experiment so that the random coincidence counting rate (noise) is at an acceptable low level

---

*The positrons created in the plasma by collisions are of no use in this case because there is no detectable signal to mark their births in time - they only add to the random coincidence count rate.

F. Positron Beam Broadening ('Slow' Positrons)

It is possible to pass a collimated beam of 'slow' positrons through a plasma and deduce the electron density from the angular broadening of the beam (which is due to the cumulative effect of small angle positron scattering). This type of experiment has been carried out by Lohnert and Schneider (1971) who designed a slow positron 'gun' capable of producing ~ 1850 'slow' ($kT_{e^+} \simeq 3$ KeV) positron per second at a beam radius of 1.9 mm. A 2 mCi ^{22}Na source supplied the positrons, which were decelerated, focussed and collimated to produce the beam. After passing through a 6" slab of plasma and an iris and annihilating in a target, individual positrons were detected by 'coincidence counting' the annihilation radiation. The radial positron intensity and hence the beam spread angle could be calculated, knowing the coincidence count rate at various iris diameters.

Electron density measurements were carried out in a glow discharge plasma (n variable from ~ 10^{11} cm^{-3} to ~ 10^{13} cm^{-3}). Beam spread results agreed reasonably well with spectroscopic and probe measurements, although a systematic error of 12-15% was evident. The advantage of using a positron beam instead of an electron beam for this type of measurement is not evident. (Intense electron beams are readily available and electron detection is much less complicated than the method used by Lohnert and Schneider to detect positrons).

Although the unique properties of positrons were not directly exploited in this work, it makes a valuable contribution, in that it suggests the idea of using 'slow' positrons to probe plasmas. If an efficient slow positron source could be developed, positrons could be introduced into plasmas already 'thermalized' to the mean energy of the plasma electrons. They would annihilate almost immediately (during the first or second collision with an electron), thus defining an 'active' plasma volume from which high count rates could be expected. Losses associated with long thermalization times and ranges in some plasmas would be eliminated. Except for finite plasma lifetimes, the situation would be similar to that in solids and liquids, viz., all positrons annihilating very soon after entering the material and near the point of entry.*

Unfortunately, high intensity slow positron sources do not, as yet, exist. The Lohnert-Schneider device yields one slow (3 KeV) positron for every 4 x 10^4 fast positrons emitted by the ^{22}Na source. Other slow positron sources have been constructed (see for example Canter, *et al.*, 1972) and although their conversion efficiencies are no better, they do yield lower energy 'slow' positrons (about two 1 eV positrons for every 10^5 fast positrons emitted by a ^{22}Na source). Until high intensity slow positron sources are developed, experiments taking full advantage of the unique properties of slow positrons are difficult.

---

*No significant annihilation occurs in the Lohnert-Schneider experiment because the 'slow', 3 KeV positrons are still considerably 'faster' than the average plasma electrons (by about 3 orders of magnitude in energy).

Chapter VIII

CONCLUSION

A. Summary and Results

This thesis has discussed the positron and its behaviour in a plasma with the view of evaluating the feasibility of using positrons to probe plasmas and measure characteristic plasma parameters. Outlines of (a) the basic physical properties of the positron and (b) the objectives of plasma diagnostics were presented as necessary background material. After a discussion of the criteria that must be satisfied if positron probes are to be feasible, the life of a positron in partially ionized and fully ionized plasmas was considered qualitatively. A quantitative analysis of positron behaviour in a fully ionized hydrogen plasma followed. Based on this, it was ascertained that positron techniques may be applicable to two potential fusion plasmas: the Tokamak type and the laser compression type. Positron thermalization calculations for these two hypothetical plasmas were carried out. A discussion of gamma ray detectors and positron sources (including calculations of pair production in the two plasmas being considered) was necessary before counting rate calculations could be carried out. Four gamma ray analysis techniques were described, and based partly on counting rate calculations, evaluated as to their suitability for use in potential 'positron plasma probe' systems. The results of this evaluation, along with characteristic time and distance scales are summarized in Table IV. These results can be taken as a general indication of the usefulness of positron techniques (at this point in time) to probe plasmas where $kT_{e^-} > \sim 10$ eV. Some of these techniques could be adapted for use with lower temperature plasmas when high intensity, slow positron sources become available.

B. Suggestions for Future Work

The following research (development) projects are suggested on the basis of material presented in this thesis:

(a) A search for annihilation radiation in current fuel pellet detonation experiments to determine if pair production occurs in laser produced plasmas, followed by a detailed analysis of the annihilation line width and shape to ascertain if the positrons have thermalized prior to annihilating.

(b) A search for annihilation gamma rays in the radiation flux exiting from existing Tokamak devices to

Table IV

Summary of Conclusions

	Tokamak Plasma	Laser Compression Plasma
Time Scales	$\tau_t < \tau_a \gtrsim \tau_{p\ell}$ (0.002-0.018) (1) (0.01-1.0) (sec)	$\tau_t < \tau_a < \tau_{p\ell}$ (0.0005-0.005) (0.13) (0.1-1.0) (nsec)
Distance Scales	$R_t < d_{p\ell}$ $((0.4\text{-}7) \times 10^6)$ (∞, orbiting) (m)	$R_t \simeq d_{p\ell}$ (1-100) (120) (μm)
2γ Angular Correlation	Not Feasible at This Time (Counting Rate Too Low)	Not Feasible at This Time (Counting Rate Too Low)
Energy Shift & Line Broadening Measurements	Feasible	Feasible
Positron Lifetime Measurements	Marginal at This Time	Not Feasible (Plasma Dimensions Too Small)
Slow Positron Probing	Feasible (Depending on Intense Slow Positron Source Development)	Marginal (Depending on Intense Slow Positron Source Development)

τ_t : Positron Thermalization Time

R_t : Positron Thermalization Range

$d_{p\ell}$: Characteristic Plasma Dimension

τ_a : Positron Annihilation Time

$\tau_{p\ell}$: Plasma Lifetime

NOTE: τ_t and R_t figures denote ranges in which most ^{22}Na positrons would thermalize.

determine if pair production occurs in high temperature, high density toroidal plasmas, followed by a line analysis as in (a) above; also, a check for correlation between positrons and runaway electrons to test the pair creation by collision hypothesis.

(c) Development of intense, slow positron sources (i.e. development of efficient fast to slow positron con verters) to improve the effectiveness of most positron diagnostic techniques and extend the n and T_e ranges over which they are useful.

(d) Development of a complete theory of positron behaviour in plasmas to complement the experimental work.

It seems that yet another area of application has opened to Anderson's 'positively charged electron'. To the list of states of matter which the positron is helping to elucidate: solids, liquids and gases, one may soon be able to add the fourth state of matter: the plasma.

BIBLIOGRAPHY

Bethe, H.A. (1930). Ann. Physik 5, 325.

Bunkin, F.V. and Kazakov, A.E. (1970). Dokl. Akad. Nauk SSSR 193, 1274. [Sov. Phys.-Dokl. 15, 758 (1971)].

Burcham, W.E. (1973). *Nuclear Physics an Introduction*, Longman, London.

Canter, K.F., Coleman, P.G., Griffith, T.C. and Heyland, G.R. (1972). J. Phys. B 5, L167.

Cappellani, F. and Restelli, G. (1968). In *Semiconductor Detectors*. (G. Bertolini and A. Coche, eds.), p. 365. North-Holland Publ. Co., Amsterdam.

Coche, A., and Siffert, P. (1968). In *Semiconductor Detectors*. (G. Bertolini and A. Coche, eds.), p. 149. North-Holland Publ. Co., Amsterdam.

DeBenedetti, S. (1956). Nuovo Cimento [10] 4, Suppl. 3, 1209.

Deutsch, M. (1951). Phys. Rev. 82, 455.

Deutsch, M. (1953). Progr. Nucl. Phys. 3, 131.

deZafra, R.L. and Joyner, W.T. (1958). Phys. Rev. 112, 19.

Dirac, P.A.M. (1930). Proc. Cambridge Phil. Soc. 26, 361.

DuMond, J.W.M., Lind, D.A. and Watson, B.B. (1949). Phys. Rev. 75, 1226.

Goldanskii, V.I. (1961). Referenced in a paper by: B.G. Egiazarov, L.A. Maksimov and A.A. Sazykin in *Scientific and Technical Symposium: Certain Problems in the Technology of Gas Discharge Experiments*, p. 120. Gosatomizdat, Moscow. [In Russian]

Goldanskii, V.I. (1968). Atomic Energy Rev. 6, 3.

Hanson, N.R. (1963). *The Concept of the Positron*, p. 135. Cambridge Univ. Press, London.

Heath, R.L., Black, W.W. and Cline, J.E. (1966). IEEE Trans. Nucl. Sci. NS-13, 445.

Heitler, W. (1954). *The Quantum Theory of Radiation* (third ed.). Oxford Univ. Press, London.

Hogg, B.G., Laidlaw, G.M., Goldanskii, V.I. and Shantarovich, V.P. (1968). Atomic Energy Rev. 6, 149.

Hollander, J.M. (1966). Nucl. Instr. Meth. 43, 65.

Honda, N., Aono, O. and Kihara, T. (1963). J. Phys. Soc. Japan 18, 256.

Hora, H. (1973). Opto-electronics 5, 491.

Hotz, H.P., Mathiesen, J.M. and Hurley, J.P. (1968). Phys. Rev. 170, 351.

Husseiny, A.A. and Forsen, H.K. (1970). Phys. Rev. A 1, 1483.

Husseiny, A.A. and Sabri, Z.A. (1974). Phys. Rev. A 10, 644.

Jeavons, A.P., Charpak, G. and Stubbs, R.J. (1975). Nucl. Instr. Meth. 124, 491.

Knoepfel, H., Spong, D.A. and Zweben, S.J. (1975). Dynamics of High Energy Runaway Electrons in ORMAK. O.R.N.L. publication.
See also:
Knoepfel, H., and Zweben, S.J. Phys. Rev. Lett. 35, 1340 (1975).

Krall, N.A. and Trivelpiece, A.W. (1973). *Principles of Plasma Physics*, McGraw-Hill Book Co., New York.

Lang, G. and DeBenedetti, S. (1957). Phys. Rev. 108, 914.

Larkin, A.I. (1959). Zhur. Eksperim. i Teoret. Fiz. 37, 264. [Sov. Phys. - JETP 10, 186 (1960).]

Lohnert, G.H. and Schneider, R.T. (1971). J. Appl. Phys. 42, 4799.

MacKenzie, I.K. (1969). Phys. Lett. A 30, 115.

Mohorovicic, S. (1934). Astron. Nachr. 253, 94.

Murray, G. (1967). Phys. Lett. B 24, 268.

Ore, A. and Powell, J.L. (1949). Phys. Rev. 75, 1696.

Ouseph, P.J. (1975). *Introduction to Nuclear Radiation Detectors*, Plenum Press, New York.

Ruark, A.E. (1945). Phys. Rev. 68, 278.

Shearer, J.W. and Deutsch, M. (1949). Phys. Rev. 76, 462.

Stewart, A.T. (1957). Can. J. Phys. 35, 168.
see also reviews in:
Positron Annihilation. (A.T. Stewart and L.O. Roellig, eds.). Academic Press, New York (1967).

Toptygin, I.N. (1962). Zhur. Eksperim. i Teoret. Fiz. 43, 1031. [Sov. Phys. - JETP 16, 728 (1963).]

Toptygin, I.N. (1964). Zhur. Tekh. Fiz. 34, 645. [Sov. Phys. - Tech. Phys. 9, 499 (1964).]

West, R.N. (1973). Advances in Physics 22, 263.

Wolfer, W.G. (1969). Ph.D. Thesis, University of Florida, Department of Nuclear Engineering Sciences.

APPENDIX A

ANNIHILATION MODES

1γ Free Annihilation

In the 1γ case, the annihilation cross section is related to the atomic number (Z) of the recoil-absorbing nucleus. If the relative positron-electron velocity is small ($v \ll c$), the annihilation cross section can be written as (Heitler, 1954; Chapter V):

$$\sigma_{1\gamma} \simeq \frac{4}{3} \pi r_0^{\,2} \; Z^5 \; \alpha^4 \left(\frac{v}{c}\right) \tag{54}$$

This is approximately eight orders of magnitude less than the corresponding 2γ cross section, and indicates that 1γ annihilations do not contribute significantly to the annihilation radiation flux. The strong Z dependence does enhance the 1γ contribution somewhat, however even at $Z = 82$, three orders of magnitude still separate the 1γ, 2γ annihilation cross sections.

$2\gamma, 3\gamma$ Free Annihilation

The annihilation cross section for positrons ($v << c$) in a medium with electron density n can be written in terms of a compound annihilation rate ν', which includes both 2γ and 3γ contributions.

$$\sigma_{2\gamma+3\gamma} = \frac{\nu'}{nv} \tag{55}$$

with

$$\nu' = \frac{1}{\tau'} = C_{2\gamma}\ \psi^2_{2\gamma} + C_{3\gamma}\ \psi^2_{3\gamma}\ , \tag{56}$$

where $\psi^2_{2\gamma}$ is the density of electrons with antiparallel spins (w.r.t. the positron) at the average position of the positron and $\psi^2_{3\gamma}$ is the density of electrons with parallel spins at the average position of the positron. $C_{2\gamma}$ and $C_{3\gamma}$ describe fundamental interaction rates:

$$C_{2\gamma} = 4\pi C\left(\frac{e^2}{mc^2}\right)^2 \tag{57}$$

$$C_{3\gamma} = 4\pi C\left(\frac{e^2}{mc^2}\right)^2 \frac{4\alpha}{9\pi}\left(\pi^2 - 9\right) = \frac{C_{2\gamma}}{1115} \tag{58}$$

In the ideal free annihilation case, $\psi^2_{2\gamma} = \frac{1}{4}$ n and $\psi^2_{3\gamma} = \frac{3}{4}$ n. The factor of three reflects the fact that a J = 1 configuration can occur in three ways: $m_s = -1, 0, +1$, where m_s is the spin angular momentum of the electron-positron system, as opposed to the one possible J = 0 configuration ($m_s = 0$). Expression (56) can now be written as:

$$\nu' = \pi r_0{}^2 \; cn\left[1 + \frac{4\alpha}{3\pi}\left(\pi^2 - 9\right)\right] \quad , \tag{59}$$

the second term indicating the 3γ contribution. The first term is just the Dirac result quoted in Chapter II (equation 3).

2γ-3γ Bound Annihilation

Bound annihilation corresponds to annihilation of positronium. The expression for the annihilation rate (and the lifetime) is identical to (56), however $\psi_{2\gamma}$ and $\psi_{3\gamma}$ must now express the appropriate bound state wave functions. In the most stable configuration, $\psi_{2\gamma}$ and $\psi_{3\gamma}$ are hydrogen-like, S state wave functions. Calculation of annihilation times yields the results: (DeBenedetti, 1956)

$$\left.\begin{aligned} \tau_{2\gamma} &= 1.25 \times 10^{-10} \text{ sec} \\ \tau_{3\gamma} &= 1.41 \times 10^{-7} \text{ sec} \end{aligned}\right\} \tag{60}$$

Unlike the free positron that experiences the influence of a large number of electrons, the bound positron interacts essentially with one particular electron, hence no electron density term appears in the expression for the lifetime (annihilation time) τ_a.

APPENDIX B

ENERGY AND MOMENTUM BALANCE IN ANNIHILATION

The positron-electron centre of mass momentum ($\underset{\sim}{p}_{cm}$) manifests itself in two different ways after the pair has annihilated. The component of momentum perpendicular to the direction of γ ray emission ($\underset{\sim}{p}_{\perp}$) causes a slight deviation from collinear trajectories (and a small shift in the γ ray energies) and the component of momentum parallel to the direction of γ ray emission ($\underset{\sim}{p}_{||}$) causes unequal distribution of energy to the annihilation gamma photons (the geometry of a typical annihilation is illustrated in Figure 28a). These effects are summarized by the energy partitioning expression (see, for example, Goldanskii, 1968):

$$E(\gamma_{1,2}) = \frac{\varepsilon_t}{2}\left[\frac{1 - \left(\frac{v_{cm}}{c}\right)^2}{1 - \frac{v_{cm}}{c}\cos\alpha_{1,2}}\right] \qquad (61)$$

where ε_t = $2mc^2 + E(e^-) + E(e^+)$, the total energy of the pair,

v_{cm} is the magnitude of the velocity of the centre of mass of the annihilating pair,

Fig. 28. Annihilation dynamics.

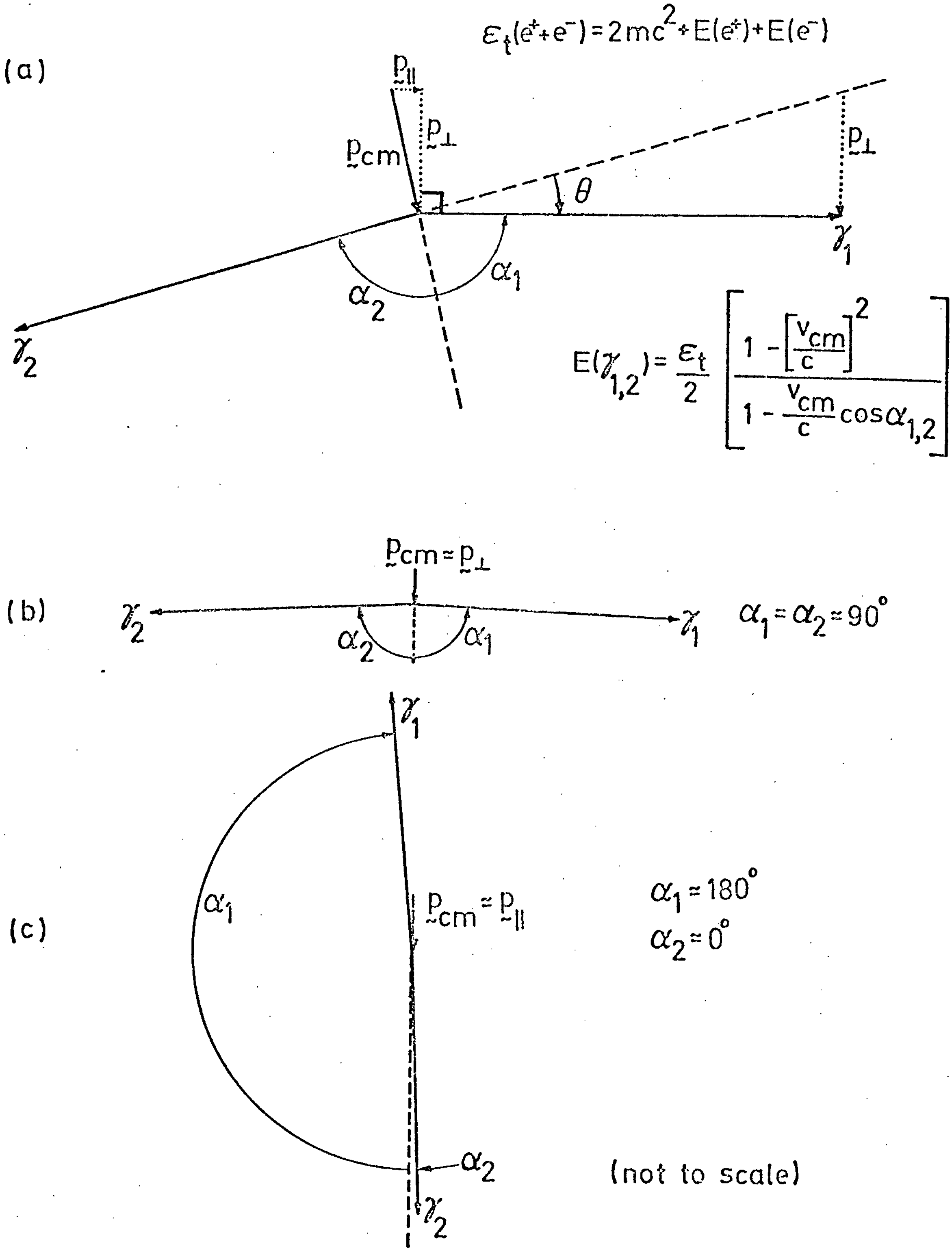

and α_1, α_2 are the angles between the directions of γ ray emission and the direction defined by $\underset{\sim}{p}_{cm}$.

The magnitudes of the annihilation γ ray momenta are just:

$$p(\gamma_{1,2}) = \frac{E(\gamma_{1,2})}{c} \tag{62}$$

A look at the limiting cases (components) is informative. When γ ray emission occurs almost perpendicular to $\underset{\sim}{p}_{cm}$, $\alpha_1 = \alpha_2 \simeq 90°$, expression (61) reduces to:*

$$E(\gamma_1) = E(\gamma_2) \cong mc^2\left(1 - \frac{1}{2}\,\frac{v_{cm}^{\;2}}{c^2}\right) . \tag{63}$$

This corresponds to the equal partitioning situation pictured in Figure 28b. The second term represents the kinetic energy of the pre-annihilation pair. If the γ rays are emitted almost parallel to $\underset{\sim}{p}_{cm}$, then $\alpha_1 \cong 180° \neq \alpha_2 \cong 0°$ and expression (61) indicates:

$$\left.\begin{aligned} E(\gamma_1) &\simeq \frac{\varepsilon_t}{2}\left(1 + \frac{v_{cm}}{c}\right) \\ E(\gamma_2) &\simeq \frac{\varepsilon_t}{2}\left(1 - \frac{v_{cm}}{c}\right) , \end{aligned}\right\} \tag{64}$$

---

*This expression is meant only to indicate the approximate magnitude of the small shift in $E(\gamma_{1,2})$ away from mc^2 when $\alpha_{1,2} \simeq 90°$. The minus sign is a result of the approximation procedure used (of course, $v_{cm} = 0$ when $\alpha_{1,2}$ is exactly equal to 90°). In fact the sign of the shift in energy is positive.

corresponding to the unequal partitioning situation illustrated in Figure 28c. The second terms here represent Doppler shifts.

Thus, although the energy of any annihilation γ ray is given by expression (61), it is useful to keep in mind the component makeup of $\underset{\sim}{p}_{cm}$ (and hence of $\underset{\sim}{p}(\gamma_{1,2})$) and what this means (i.e. that perturbations in γ ray energies - away from mc^2 - can be thought of as arising from two different motions). The magnitudes of γ ray energy shifts associated with $\underset{\sim}{p}_{\perp}$ and $\underset{\sim}{p}_{||}$ (values in terms of v_{cm} appear in expressions (63) and (64)) are approximately:

$$\left.\begin{aligned} \Delta E_{||} &\approx \frac{1}{2}\, p_{||}\, c \\ \Delta E_{\perp} &\approx \frac{1}{2}\, p_{\perp}\, c \;, \end{aligned}\right\} \qquad (65)$$

where $p_{||}$ and $p_{\perp}$ are the magnitudes of $\underset{\sim}{p}_{||}$ and $\underset{\sim}{p}_{\perp}$ respectively.

Only $\underset{\sim}{p}_{\perp}$ plays a role in perturbing collinear γ ray emission, thus it is $\underset{\sim}{p}_{\perp}$ that appears in expressions (4) and (5) which describe the magnitude of this perturbation.

APPENDIX C

POSITRONIUM FORMATION

Positronium formation is expected to take place between free plasma electrons and positrons ranging in energy from about 50 eV down to and including the mean plasma electron energy. Positronium formation involving previously bound electrons would be limited by a threshold positron energy, V_p: (lower limit)

$$V_p = V_i - I_p \quad , \tag{66}$$

where I_p = 6.8 eV is the positronium binding (or ionization) energy. A positron with V_p would have just enough energy to ionize (and capture) the most weakly bound electron and still maintain the energy balance (since the positron-electron system releases 6.8 eV upon forming positronium). By analogy with the situation in gases, most of the positronium formation involving a previously bound electron might be expected to occur in the energy gap between V_e and V_p (see Figure 6a). This energy range is known as the 'Ore gap'.

Positronium formation in a fully ionized medium could occur only with free electrons, as indicated in Figure 6b. The important question is: will the P_s, once formed remain bound long enough to annihilate? It is natural to take $kT_e = I_p$ as a dividing energy as did Toptygin (1964) in discussing a similar question. In plasmas where $kT_e >$ I_p (the majority of fully ionized plasmas), P_s would be scarce, because even if it did form, it would be broken up (ionized) immediately by collisions. Toptygin indicates that even P_s formed in plasmas where $kT_e < I_p$ (the majority would be partially ionized plasmas) would not exist much longer than about 10^{-10} sec, the lifetime of the singlet P_s state, due to (a) straightforward singlet annihilation, (b) collisions resulting in triplet to singlet conversion followed by singlet annihilation and (c) collisions resulting in P_s breakup (ionization).

It should be noted that collisional breakup may play an even more significant role than suggested by Toptygin - at all values of kT_e, but especially for $kT_e < I_p$. The electrons in the high energy tail of the thermal Maxwell distribution (whatever the mean temperature) should enhance noticeably P_s ionization, as they enhance conventional ionization. In H_2 gas, for example, complete dissociation and ionization has occurred when $kT_e \simeq 1.5$ eV, however the dissocation-ionization potential corresponds to $kT_e \simeq 15$ eV. The factor of ten reflects the ionizing power of the fast electrons associated with a thermal distribution with a relatively low mean energy (1.5 eV).

Although its exact magnitude is difficult to predict, it does seem that there will be a bound state contribution (mostly from 2γ decay of singlet P_s) to the overall annihilation radiation spectrum of cool ($kT_e < \sim I_p$) plasmas. This contribution has not been considered in detail in this study because the majority of plasmas of interest fall into the region where P_s is expected to be scarce, if at all present - that is, the region where the mean thermal plasma temperatures are such that: $kT_e > \sim I_p$.

APPENDIX D

POSITRON ENERGY LOSS RATE IN A PLASMA

The stopping power (and energy loss rate) of a single component (electron) plasma can be written as an integral over the product of the energy transfer, ΔE (positron to electron) and the differential Coulomb scattering cross section, $d\sigma$ as:

$$- \frac{dE}{dx} = - \frac{1}{v} \frac{dE}{dt} = n \int \Delta E \, d\sigma \tag{67}$$

where E is the positron kinetic energy and v its velocity

and n is the plasma electron number density.

Writing ΔE in terms of Δp, the momentum transferred in a given collision, and $d\sigma$ in terms of Δp as:*

---

*This is just Rutherford's Coulomb scattering formula written in terms of Δp (in the Born approximation limit). It is usually written in terms of the centre of mass scattering angle θ_c as

$$d\sigma = 2\pi \left(\frac{e^2}{mv^2}\right)^2 \csc^4(\tfrac{1}{2}\theta_c) \sin\theta_c \, d\theta_c$$

$$d\sigma = 8\pi \left(\frac{e^2}{v}\right)^2 \frac{d(\Delta p)}{(\Delta p)^3} \quad , \tag{68}$$

it follows that:

$$-\frac{dE}{dt} = \frac{4\pi\ n\ e^4}{mv} \int \frac{d(\Delta p)}{\Delta p} \quad , \tag{69}$$

where the integration is carried out over all possible values of Δp in the range Δp_{min} to Δp_{max}. The largest possible momentum transfer, Δp_{max}, occurs during head-on collisions and has a value:

$$\Delta p_{max} = 2\ mv \tag{70}$$

The smallest possible momentum transfer, Δp_{min}, corresponds to the generation of a single plasma wave of energy $\hbar\omega_e$:*

No exchange terms appear because the positron is distinct from the electron. Expression (68) follows from the above if the fractional energy transfer (for a given collision) is written as $\frac{\Delta E}{E} = \sin\ (\frac{1}{2}\ \theta_c)$.

*If energy is written as $E = \frac{p^2}{2m}$, then momentum transfer can be written as:

$$\Delta p = \frac{m\ \Delta E}{p} \ ,$$ which yields, with

$\Delta E_{min} = \hbar\omega_e$, a Δp_{min} value of

$$\Delta p_{min} = \frac{\hbar\omega_e}{v} \quad .$$

$$\Delta p_{min} = \frac{\hbar \omega_e}{v} \tag{71}$$

Recall that the momentum transfer value that separates 'hard' and 'soft' collisions is: $\Delta p_D = \frac{\hbar}{\lambda_D}$, where λ_D is the Debye length:

$$\lambda_D = \left(\frac{k\ T_e}{4\pi\ n\ e^2}\right)^{\frac{1}{2}} \tag{72}$$

where k is Boltzman's constant,

and e, n, T_e are the electron charge, number density and temperature respectively.

The contribution from 'soft' collisions ($\Delta p_{min} < \Delta p < \Delta p_D$) follows from (69) upon integration from Δp_{min} to Δp_D:

$$-\left.\frac{dE}{dt}\right|_{SOFT} = \frac{4\pi\ n\ e^4}{mv} \ln\left(\frac{\Delta p_D}{\Delta p_{min}}\right)$$

$$= \frac{4\pi\ n\ e^4}{mv} \ln\left(\frac{\sqrt{2}v}{v_e}\right) \tag{73}$$

Integration of (69) from Δp_D to Δp_{max} yields the 'hard' collision contribution:

$$-\left.\frac{dE}{dt}\right|_{HARD} = \frac{4\pi\ n\ e^4}{mv} \ln\left(\frac{\Delta p_{max}}{\Delta p_D}\right)$$

$$= \frac{4\pi\ n\ e^4}{mv} \ln\left(\frac{\sqrt{2}\ m\ v\ v_e}{\hbar\ \omega_e}\right) \tag{74}$$

Note that 'soft' and 'hard' collision contributions are separated only to logarithmic accuracy.

The total energy loss rate is the sum of these contributions (essentially the result of integrating (69) from Δp_{min} to Δp_{max}):

$$- \left.\frac{dE}{dt}\right|_{TOTAL} = \frac{4\pi\ n\ e^4}{mv} \ln\left(\frac{\Delta p_{max}}{\Delta p_{min}}\right)$$

$$= \frac{e^2\ \omega_e^{\ 2}}{v} \ln\left(\frac{2\ mv^2}{\hbar\ \omega_e}\right) \qquad (75)$$

The contribution to dE/dt from positron-ion collisions has been ignored here since it is smaller than the contribution from positron-electron collisions by a factor of m/m_i, where m_i is the ion mass.

Relativistic effects have not been considered in this derivation since their magnitudes are small in the energy range of interest ($E(e^+) < \sim 500$ KeV).

The approach of Husseiny and Sabri (1974) is similar, but differs in one essential respect. They define the 'soft' collision cross section using a Debye length shielded potential and use the pure inverse Coulomb potential to define only the 'hard' collision cross section. The general result is complicated, but in the slowing down range ($v > v_e$) it reduces to:

$$-\left.\frac{dE}{dt}\right|_{TOTAL} = \frac{1}{(4\pi\ \varepsilon_0)^2}\ \frac{e^2\ \omega_e^{\ 2}}{2\ \pi\ v}\ \ln\left[(4\pi\ \varepsilon_0)^{\frac{1}{2}}\ \frac{m\ v\ v_e}{2\ \hbar\ \omega_e}\right] , \qquad (76)$$

an expression derived by Husseiny and Forsen in 1970. Note that, aside from units, this expression is similar to the 'hard' collision contribution (74), in the sense that dE/dt is functionally related to v and v_e in a similar manner. It is, as yet, unclear which expression (75 or 76) yields the most accurate value for dE/dt and hence for the thermalization time.